Republic of Iraq
Ministry of Higher Education and Scientific Research
University of Babylon / College of Science
Department of Physics

Synthesis and Photoresistance Characteristics of ZnO/TiO_2 nanomaterials Heterojunction

A Thesis

Submitted to the Council of College of Science, University of Babylon in Partial Fulfillment of the Requirements of the Degree of Doctor of Philosophy in Physics

by

Ahmed Abdulla Auda Ali

B.Sc. in Physics 1994

M.Sc. in Physics 1997

Supervised by

Prof. Dr.
Hikmat Adnan Jawad

Asst. Prof. Dr.
Burak Yahya Kadem

2023 A.D.

1445 A.H.

بِسۡمِ ٱللَّهِ ٱلرَّحۡمَٰنِ ٱلرَّحِيمِ

﴿قَالَتۡ لَهُمۡ رُسُلُهُمۡ إِن نَّحۡنُ إِلَّا بَشَرٞ مِّثۡلُكُمۡ وَلَٰكِنَّ ٱللَّهَ يَمُنُّ عَلَىٰ مَن يَشَآءُ مِنۡ عِبَادِهِۦۖ وَمَا كَانَ لَنَآ أَن نَّأۡتِيَكُم بِسُلۡطَٰنٍ إِلَّا بِإِذۡنِ ٱللَّهِۚ وَعَلَى ٱللَّهِ فَلۡيَتَوَكَّلِ ٱلۡمُؤۡمِنُونَ ١١﴾

صدق الله العلي العظيم

سُورَةُ إِبْرَاهِيمَ (الاية 11)

Supervisor's Certification

We certify that this thesis entitled (**Synthesis and Photoresistance Characteristics of ZnO/TiO_2 Nanomaterials Heterojunction**) has been written by (**Ahmed Abdulla Auda Ali**) under our supervision at the department of Physics, College of Science, University of Babylon, in partial fulfillment of the requirements for the Doctorate of Philosophy in Material Science.

Signature:
Supervisor : Dr. Hikmat Adnan Jawad
Title : Professor
Address : Department of Physics,
College of Science
University of Babylon.
Date : / / 2023

Signature:
Supervisor : Dr. Burak Yahya Kadem
Title : Assistant Professor
Address: Department of Physics,
College of Science
Al-Karkh University of Science
Date : / / 2023

Certification of the Head of the Department

In view of the available recommendation , I forward this thesis for debate by the examination committee.

Signature:
Name: Dr. Samira Adnan Mahdi
Title: Assistant Professor
Address : Head of the Department of Physics, College of Science
University of Babylon
Date : / / 2023

Examination Committee Certification

We certify that we have read the thesis entitled "**Synthesis and Photoresistance Characteristics of ZnO/TiO_2 Nanomaterials Heterojunction**". As the examining committee, we have thoroughly examined the contents of the thesis submitted by the student, "**Ahmed Abdulla Auda Ali**". In our opinion, it meets the requirements for the degree of Doctor of Philosophy in Physics.

Signature
Name: **Dr. Mohammed Hadi Shinen Alshammeri**
Title: **Professor**
Address: **College of Science / University of Babylon**
Date : / /2023
(Chairman)

Signature
Name: **Dr. Ehssan Dhiaa Jawad Al- Bermany**
Title: **Professor**
Address: **College of Education for Pure Sciences /University of Babylon**
Date: / /2023
(Member)

Signature
Name: **Dr. Mohammed Kadhim Hamad**
Title: **Professor**
Address: **College of Education for Pure Sciences /University of Misan**
Date: / /2023
(Member)

Signature
Name: **Dr. .Maan Abd-Alameer Salih**
Title: **Asst. Professor**
Address: **College of Science / University of Babylon**
Date: / /2023
(Member)

Signature
Name: **Dr. Raed Kadhum Fakher Alfahed**
Title: **Asst. Professor**
Address: **Al-Nahrain Research Center for Renewable Energy / Al-Nahrain University**
Date: / /2023
(Member)

Signature
Name: **Dr. Hikmat Adnan Jawad**
Title: **Professor**
Address: **College of Science / University of Babylon**
Date: / /2023
(Member and Supervisor)

Signature
Name: **Dr. Burak Yahya Kadem**
Title: **Asst. Professor**
Address: **College of Science/ Al-Karkh University of Science**
Date: / /2023
(Member and Supervisor)

Approved by the Council of the College of Science

Signature
Name: **Dr. Mohammed Hadi Shinen Alshammeri**
Title: **Professor**
Address: **Dean of College of Science / University of Babylon**
Data: / /2023

Acknowledgments

Praise be to Almighty Allah, Lord of the Worlds, for His graces that are not counted and peace be upon our Prophet Mohammed and his infallible progeny.

I would like to extend my sincere thanks to Asst. Prof. Samira Adnan Mahdi (Ph. D.), the Head of the Department of Physics, as well as all my professors and the dedicated staff who have gracefully guided me throughout my (Ph. D.) study.

My heartfelt gratitude goes to my supervisors, Prof. Hikmat Adnan Jawad (Ph. D.) and Asst. Prof. Burak Yahea Kadim (Ph. D.), for their unwavering guidance and support throughout the process of writing this work.

I also want to express my special thanks and appreciation to Prof. Iman Mingher Obied (Ph.D.) for her invaluable support and meticulous proofreading.

Summary

Heterojunction of titanium dioxide (TiO_2) and zinc oxide (ZnO) thin film devices were prepared and characterized for the applications of photoresistivity. It was synthesized using solution-gelation methods and spraying on different substrates to study the effect of the substrate on the of synthesized devices.

Complementary examinations were also carried out including ; X-ray diffraction, energy band gap measurements, carrier concentrations, mobility of charge carriers, morphological properties, and the first derivative of current with respect to time (dI/dt) values of ON-OFF states.

The results of the XRD examination show distinct crystalline patterns, the presence of TiO_2(anatase) and ZnO(wurtzite) phases in the thin films. Energy band gap measurements show fluctuations in band gap values, revealing information about the materials' optoelectronic properties. The energy band gap range of all samples between (3.23-3.75eV).

Scanning electron microscope (SEM) images reveal considerable advances in the shape and particle size management of TiO_2 and ZnO thin films. The nanomaterials were tailored to certain shapes and sizes through careful manipulation of production procedures and annealing temperatures, ranging from spherical-like structures in ZnO to nanoribbon-like forms in TiO_2. The hybrid structure displays an unusual overlap of the two materials, implying the establishment of a heterojunction with a well-defined interface.

When deposited on indium tin oxide (ITO) substrates, TiO_2 demonstrates reduced in resistance and moderate switching behavior. Conversely, Si/SiO_2 substrates display higher resistance and more pronounced switching behavior. Moreover, TiO_2 showcases very high resistance, while ZnO exhibits lower resistance with strong switching behavior on interdigitated electrodes (IDEs) substrates.

Hybrid ($ZnO:TiO_2$) exhibits a relatively moderate switching behavior on ITO substrates, as indicated by its low ratio of resistance when the light is off to when the light is on (R_{OFF}/R_{ON}) ratio of 1.06. On Si/SiO_2 substrates, the hybrid thin film demonstrates a significantly higher R_{OFF}/R_{ON} ratio of 5.28, suggesting a stronger resistance and more pronounced switching behavior. Likewise, the R_{OFF}/R_{ON} ratio for the Hybrid thin film on IDEs substrates is 2.46, indicating a moderate yet distinctive response to light.

Similarly, the bilayer thin film displays a moderate switching behavior on ITO substrates, with a RO_{FF}/R_{ON} ratio of 1.36. On Si/SiO_2 substrates, the bilayer thin film exhibits a substantial resistance and strong switching behavior, as indicated by its R_{OFF}/R_{ON} ratio of 4.72. When applied to IDEs substrates, the R_{OFF}/R_{ON} ratio for the bilayer thin film is 3.9, demonstrating a moderate yet significant reaction to light.

The study also includes a thorough examination of photoresistance properties. TiO_2 has the highest photoresistivity values, which range from 1.57×10^9 (Ω.m) on ITO to 123×10^7 (Ω.m) on Si/SiO_2, while no response on IDE substrate . ZnO has lower photoresistivity values ranging from 0.436×10^9 (Ω.m) to 9.89×10^7 (Ω.m) and 0.254×10^3 (Ω.m). The photoresistivity of the hybrid thin film ranges from 0.801×10^9 (Ω.m) to 7.1×10^7 (Ω.m) and 7.03×10^3 (Ω.m), whereas the photoresistivity of the bilayer thin film ranges from $0.064\ 10^9$ (Ω.m) to 7.02×10^7 (Ω.m) and 2.09×10^3 (Ω.m).

A positive value suggested movement during light exposure, while a negative value denoted acceleration from the conduction band to the valence band. This relationship underscores the critical role of dI/dt in understanding the kinetics of charge transport and resistance in photoresistive materials, where the lowest value signifies the highest photoresistance and vice versa.

The values of dI/dt were indicative of the optimal performance of the hybrid and bilayer thin film types on different substrates. In particular, when deposited on an

ITO substrate, the hybrid thin film demonstrates highly favorable characteristics, with dI/dt values of 0.065 μA s^{-1} (ON) and -0.23 μA.s^{-1} (OFF). On the Si/SiO_2 substrate, both the hybrid and bilayer thin films exhibited comparable optimal values. The hybrid thin film displays dI/dt values of 508 μA.s^{-1} (ON) and -521 μA.s^{-1} (OFF), while the bilayer thin film shows dI/dt values of 190 μA s^{-1} (ON) and -422 μA.s^{-1} (OFF). Notably, the bilayer thin film performed better on the IDEs substrate, with dI/dt values of 9.95 A.s^{-1} (ON) and -44 A.s^{-1} (OFF). The results showed the varying current rate dynamics of different thin films on diverse substrates, offering valuable insights into their photoresistive behaviors and electrical characteristics.

List of Abbreviations

Abbreviation	Definition
λ_{max}	Maximum Wavelength
ρ_{ph}	Photoresistivity
$\sigma_{\circ}$	Pre-exponential Factor of Conductivity
B	Edge Width Parameter
C.B.	Conduction Band
dI/dt	Time Rate of Current
E_a	Activation Energy
E_g	Energy Band Gap
F.T.	Fall Time (Recovery Time)
h	Planck's Constant
HCl	Hydrochloric acid
I.P.	Time Period of Current
IDEs	Interdigitated Electrodes
I_{ph}	Photocurrent
ITO	Indium Tin Oxide
I-V	Current- Voltage Characteristics
K_B	Boltzmann Constant
MEA	Mono Ethanolamine
MONPs	Metal Oxide Nano Particles
R.T.	Rise Time (Response Time)
R_{ph}	Photoresistance
S.T.	Starting Point
SEM	Scanning Electron Microscope
Si/SiO_2	Silicon/Silicon Dioxide
Sol-Gel	Solution-Gelatin
t	Thickness
TiO_2	Titanium Dioxide
TTIP	Titanium Tetra Isopropoxide
V.B.	Valance Band
XRD	X-Ray Diffraction
ZnAc	Zinc Acetate
ZnO	Zinc Oxide

M	Mobility
μ_o	Pre-exponential Factor of Mobility
α	Absorption Coefficient
β	Full Width of Halve Maximum (FWHM)
θ	Position Angle
λ	Wavelength
σ	Conductivity
$\boldsymbol{\nu}$	Frequency

Table of Contents

List of Figures

List of Tables

Chapter One

Introduction

1.1 Background

The domain of materials science encompasses a multidisciplinary exploration of intrinsic material properties to meet the ever-evolving demands of modern society. From understanding fundamental principles to designing materials with tailored characteristics, it plays a pivotal role in technological advancements that impact various industries. One transformative area within materials science is semiconductor research, which has led to a technological revolution with profound implications in contemporary life [1-3].

Semiconductor research focuses on controlling electron flow within materials, enabling the creation of essential electronic components such as transistors [4] and integrated circuits [5]. Semiconducting materials possess distinctive characteristics, allowing them to toggle between conductive and non-conductive states, forming the foundation of modern electronics. These semiconductors are indispensable building blocks powering everything from handheld devices to cutting-edge renewable energy systems [6].

To amplify the capabilities of semiconductors, scientists and engineers delve into the captivating world of nano-materials [7]. Engineered at the nanoscale, nano-materials exhibit intriguing properties distinct from their bulk counterparts. With dimensions typically ranging from one to a few hundred nanometers, these nanostructures offer enhanced electrical [8], optical, and mechanical attributes [9], opening new opportunities to optimize device performance. Precise manipulation of nano-features has propelled the development of more efficient and powerful electronic devices like advanced transistors, high-density memory storage units, and ultra-sensitive sensors, shaping the future of electronics [10].

Among the diverse array of nano-materials, thin films hold a paramount position due to their significance in cutting-edge technologies [11]. Thin films are exceedingly thin layers, often a few nanometers to micrometers in thickness, deposited onto surfaces to confer specific functionalities [12]. They are crucial in

microelectronics, photonics, optoelectronics, and more. Thin films facilitate the creation of intricate device structures, and their versatility is evident in applications such as solar cells, sensors, and advanced display technologies [13-15].

In this context, photocurrent response and photoresistance are central themes of interest. Photocurrent response refers to the material's ability to generate an electric current when exposed to light [16].

Understanding and enhancing this response in nano-materials and thin films offer opportunities for novel photodetectors and energy-harvesting devices. On the other hand, photoresistance relates to the change in material's electrical resistance under light illumination, providing a means to design light-sensitive electronic elements [17].

The continuous progress in materials science, semiconductor research, and nano-materials has significantly impacted multiple industries. Advancements in these domains have fueled the development of faster, more compact, and energy-efficient electronic devices, paving the way for the next generation of computing and communication technologies. In the pursuit of novel materials and their tailored properties, research in photocurrent response and photoresistance promises ground breaking technologies that will reshape our world, driving human prosperity and addressing the demands of our society [18].

This study sets the stage for a comprehensive exploration of materials science, semiconductor research, nano-materials, and thin films, with a significant focus on photocurrent response and photoresistance. By delving into the unique properties of nano-structured materials, it aims to advance our understanding of materials at the nanoscale, offering potential for innovative and sustainable solutions in light-sensitive electronic applications. Through rigorous investigation and scientific inquiry, this study seeks to pave the way for a brighter and more technology-driven future.

The motivation for this thesis is to explore novel nanomaterials, specifically the ZnO:TiO_2 heterojunction, which holds the potential for improved properties and functionalities compared to individual materials. The synergistic effects between the constituent materials of heterojunctions, where two different materials meet, often give rise to enhanced properties.

Therefore, this thesis seeks to investigate how the combination of ZnO and TiO_2, both known for their semiconducting properties, could result in improved performance characteristics, particularly in terms of photoresistance. Photoresistance, the change in electrical resistance of a material upon exposure to light, holds immense promise for various sensing applications such as environmental monitoring, light sensing, and other sensor-based technologies.

Developing efficient and sensitive photoresistive materials are of utmost interest, and this thesis aims to explore the potential of ZnO:TiO_2 heterojunctions as photoresistive materials and understand the underlying mechanisms. The tunable properties of nanomaterials based on size, composition, and structure make them highly advantageous.

Therefore, the purpose behind this research is likely to explore how the synthesis methods and parameters can be manipulated to tailor the properties of ZnO:TiO_2 heterojunctions, enabling their use in specific applications such as optoelectronics, photodetectors, or gas sensors.

Investigating the synthesis and characteristics of ZnO:TiO_2 heterojunctions contribute significantly to the fundamental understanding of materials science and nanotechnology and may lead to uncovering new insights into the interactions between these materials at the nanoscale, leading to discoveries that advance the broader field of nanomaterials.

The objective for this thesis could also stem from identified research gaps or unanswered questions in the field. Prior studies might have focused on individual

ZnO or TiO_2 materials, but there may be limited understanding of their combined behavior as a heterojunction. This thesis could aim to bridge this gap in knowledge.

1.2 Semiconductors

Semiconductors are a class of materials that play a pivotal role in modern technology, powering a vast array of electronic devices we use in our daily lives. These materials exhibit a unique property that sets them apart from conductors (like metals) and insulators (like plastics and ceramics) - their ability to conduct electricity selectively. In other words, they can behave as both conductors and insulators under different circumstances, making them essential components in the field of electronics [19].

The key characteristic of semiconductors is their electrical conductivity, which lies between that of conductors and insulators. When subjected to certain conditions, such as temperature, light, or an electric field, they can either increase or decrease their conductivity. This property is the foundation for the operation of electronic devices like transistors, diodes, integrated circuits, and more [20].

Semiconductors have revolutionized the world of electronics, allowing for the development of powerful computers, smartphones, communication systems, renewable energy technologies, and much more. Their ability to control the flow of electricity precisely and reliably has transformed society, leading to the digital age we currently live in [21].

Throughout the years, advancements in semiconductor manufacturing processes have led to smaller, faster, and more efficient devices, driving the constant evolution of technology. Moore's Law, an observation made by Gordon Moore in 1965 [22], predicted that the number of transistors on a semiconductor chip would double approximately every two years. This prediction has largely held true, and the ongoing miniaturization of semiconductor components continues to shape the progress of electronics and computing.

1.3 Photovoltaic technology

Photovoltaic (PV) technology is a branch of renewable energy that harnesses the power of sunlight to generate electricity. It involves the use of solar cells, also known as photovoltaic cells, to convert sunlight directly into electrical energy. These solar cells are made of semiconductor materials, usually silicon, and exploit the photovoltaic effect to produce a flow of electrons when exposed to sunlight [23].

The photovoltaic effect occurs when photons strike the surface of the solar cell, causing an excited electron from the semiconductor material. By connecting multiple solar cells together in an arrangement known as a solar panel or module, a significant amount of electricity can be generated. Figure 1.1 shows a graphic illustration of how a photovoltaic cell works.

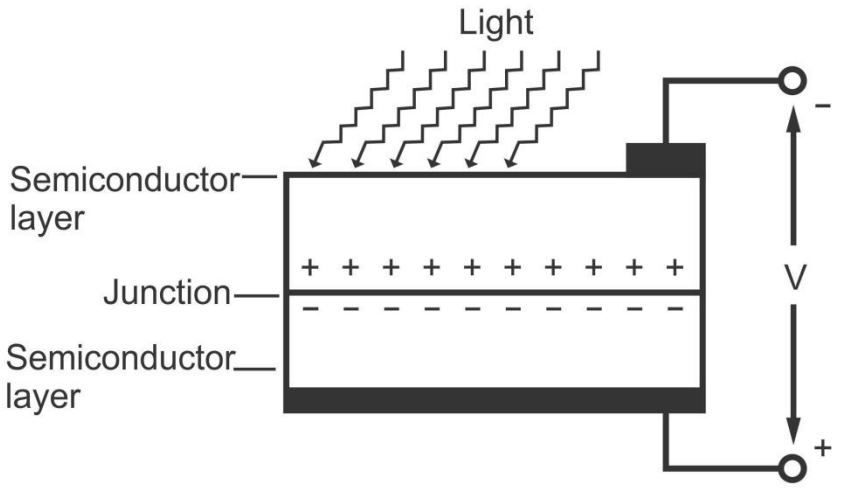

Figure 1.1 Principle mechanism of the operation of photovoltaic cell.

Photovoltaic technology has demonstrated rapid advancements over years, leading to improve efficiency and lower production costs. As a result, solar power has become an increasingly viable and attractive alternative to conventional fossil-fuel-based energy sources. Some key features and benefits of photovoltaic systems include: Firstly, renewable energy, solar power is an abundant and

inexhaustible renewable energy source. The sun's energy is virtually limitless, making solar an attractive option for sustainable electricity generation. Secondly, environmentally friendly, solar energy produces no harmful greenhouse gases or air pollutants during operation, helping to reduce carbon emissions and combat climate change. Thirdly, distributed generation, PV systems can be deployed at various scales, from small residential installations to large utility-scale solar farms.

This distributed generation approach can reduce strain on centralized power grids and increase energy independence. Fourthly, off-grid applications, photovoltaic systems are particularly valuable in remote areas where connecting to a traditional power grid may be impractical or expensive.

Solar power allows for off-grid electricity generation, providing power to isolated communities and facilities. Fifthly, low operating costs, once installed, solar panels require minimal maintenance and have low operating costs, making them cost-effective over the long term. Sixthly, technology integration, solar panels can be integrated into buildings' designs, providing both energy generation and structural benefits, such as shade and weather protection. Finally, sustainable energy transition, the widespread adoption of photovoltaic technology plays a crucial role in the global transition to a sustainable and clean energy future [24].

Despite its advantages, some challenges remain for photovoltaic technology, such as energy storage for times when sunlight is unavailable and the need for continued advancements in efficiency and affordability. However, ongoing research and development efforts continue to address these issues and drive the growth of solar power as a key component of the renewable energy landscape.

1.4 Photodetectors

Photodetectors, also known as photosensors or light sensors, are devices designed to detect and measure light or other electromagnetic radiation across a broad range of wavelengths. These devices convert light signals into electrical signals, enabling the detection and analysis of light for various applications. They play a critical role in diverse fields, ranging from simple everyday applications to highly advanced scientific and industrial uses [25].

The basic principle behind photodetectors is the photoelectric effect (Figure 1.2), where incident photons of light interact with the detector material, leading to the generation of electron-hole pairs. The subsequent movement of these charge carriers creates an electrical current or voltage proportional to the intensity of the incident light [26].

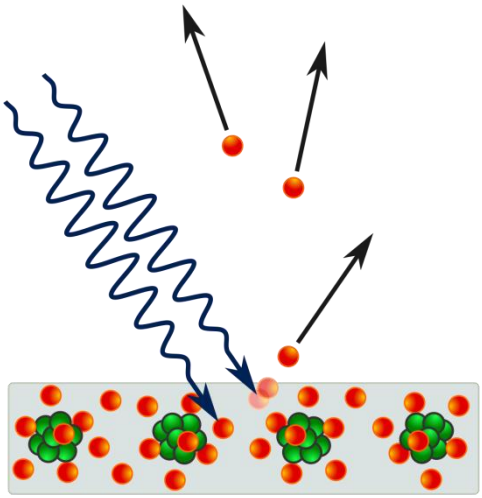

Figure1.2 Photoelectric effect.

Different types of photodetectors exist, each with its own specific characteristics and applications: First of all, photodiodes are one of the most common types of photodetectors [27]. They are semiconductor devices that operate in reverse bias, meaning they allow current flow when light is incident on their surface. Photodiodes are widely used in optical communication systems, light meters, and

various proximity sensors [28]. Additionally, they are similar to photodiodes but have an additional amplification stage, providing higher sensitivity to light. They are often used in low-light applications, such as light detection in electronic devices and optical switches [29].

photodetectors are fundamental components in modern technology, contributing to fields as diverse as communication, imaging, scientific research, and environmental monitoring. Their continuous development and integration into various applications drive progress in numerous industries [30].

Photoresistance, also known as a light-dependent resistor (LDR) or photocell, is a type of passive electronic component whose electrical resistance changes in response to the intensity of light falling on its surface [31]. It belongs to the class of light-sensitive devices and is widely used in various applications to control or measure light levels.

The basic construction of a photoresistor involves a semiconductor material that exhibits a property called the photoelectric effect. When light photons strike the surface of the photoresistor, they excite electrons within the semiconductor material, causing an increase in the number of free charge carriers (electron-hole pairs). This results in a decrease in the resistivity of the material, causing its electrical resistance to decrease as well. Conversely, in the absence of light or under low-light conditions, the number of free charge carriers reduces, and the photoresistor exhibits higher resistivity, leading to an increase in its electrical resistance [32].

Key characteristics and applications of photoresistors include:

1- Photoresistors are primarily used as light sensors or light detectors. They respond to changes in light intensity, making them suitable for applications like streetlight control, outdoor lighting, and automatic brightness adjustment in displays and cameras [33].

2- Photoresistors have a simple construction, making them cost-effective and easy to use in various electronic circuits [34].

3- Photoresistors are often used in combination with other electronic components, such as operational amplifiers or microcontrollers, to create more sophisticated light sensing and control systems. While they are not suitable for precise measurements or high-speed applications, their simplicity, cost-effectiveness, and versatility make them valuable tools for various light-dependent projects and applications [35].

1.5 Metal oxide semiconductors

The most common and widely described semiconductors in photo-electronic applications are metal oxides and semiconductors such as titanium dioxide (TiO_2), and zinc oxide (ZnO) [36].

Titanium dioxide (TiO_2) is the most active of the compounds that have been tested. It is relatively cheap, photochemically stable, non-toxic, easily UV-activated, and insoluble in most reaction environments. However, its application is limited because of its narrow photocatalytic region ($\alpha < 400$ nm) and its ability to absorb only a small fraction (5%) of incident solar irradiation, which results from its relatively large bandgap energy (anatase, ~3.2 eV) [37].

Many recent studies have focused on modifying the morphology and crystalline structure of TiO_2 to improve its optoelectronic activity. Using hybrid semiconductors such as TiO_2:ZnO, TiO_2:SiO_2, etc. [38]. To increase the response of TiO_2 to solar radiation, it is modified with ZnO, [39]. It has been proven that the formation of oxide hybrids is an appropriate tool for improving the photocatalytic ability of TiO_2 materials. The selection of an appropriate modifier and its compatibility with the material are important for the hybrid's physicochemical and optical properties. Each of the modifiers substantially affect

the surface charge of the material and, therefore, enhance or weaken its photocatalytic capacity [40].

Zinc oxide (ZnO), on the other hand, is one of the metal oxide semiconductors that have drawn great attention due to its noticeable combination of physical properties. ZnO has wide bandgap energy of about 3.3 eV at 300K, high excitation binding energy of 60 mV, the n-type semiconductor has wurtzite structure and varied growth morphology, all of these properties makes ZnO a majority material in the broad-band semiconductors and nanotechnology fields. Also, ZnO exhibited unique electrical properties which makes it useful for different applications such as in ultraviolet light emitting diodes (LEDs), photovoltaic devices , optical waveguides, gas sensors, etc. [41].

Titanium dioxide and zinc oxide have very similar physicochemical properties including nontoxicity, biocompatibility, thermal and chemical stability, insolubility in water, resistance to chemical breakdown and photo corrosion, and mechanical strength [42].

Many methods for the production of TiO_2:ZnO oxide systems have been proposed using different precursors of titania and zinc oxide. These methods include an electrospinning technique, a chemical co-precipitation method, the sol-gel technique, or solvothermal and hydrothermal methods [43]. These methods enable precise control of the synthesis to obtain materials with useful properties. The process can be controlled by temperature changes, sequence and type of reagent dosage, rate of stirring, pH, the ratio of water to precursors, and calcination conditions [44].

Depending on the process parameters, the products exhibit different physicochemical properties and structure. The physicochemical properties of TiO_2:ZnO oxide systems depend on their morphology, the size of crystallites, and the crystallographic structure [45]. Moreover, ZnO has a band gape energy of 3.3 eV, which is slightly more negative than that of TiO_2. Therefore, the synthesis of

TiO_2:ZnO oxide systems can result in the injection of conduction band electrons from ZnO to TiO_2, which is favorable to electron-hole separation. Therefore, the incorporation of these two materials into an integrated structure is of great significance because the resulting products may possess improved specific and well-defined physical and chemical properties, which were determined during their synthesis [46].

The spray pyrolysis method exhibits relatively low costs, suitability for large-scale applications, and ease of manipulation. Furthermore, this technique finds utility in the deposition of thin film solutions on substrates, as well as in the deposition of multi-layer thin films. [47].

The present work studies the photoresistance performance of the TiO_2:ZnO heterojunction that prepared by sol-gel technique and deposited using spray pyrolysis method. Complementary characteristics such as morphology, structure, optical properties and electrical properties are also investigated.

1.6 Literature review

Metal oxides play a crucial role in the field of optoelectronics due to their widespread availability, cost-effectiveness, and exceptional photoconversion capabilities. Specifically, they function as active components in photovoltaic systems, leveraging their optical characteristics and electrical conductivity to enhance the efficiency of photovoltaic cells [48]. Moreover, metal oxides find applications in heterogeneous photocatalysis, a treatment technology employed for various pollutants in water treatment, air depollution, hydrogen production, hydrocarbon generation, and the transformation of specific compounds [49].

In the realm of flexible electronics and optoelectronics, transparent and conductive oxide/metal/oxide nanolaminate structures have been developed. These structures provide a low-temperature coating suitable for organic materials, contributing to advancements in this field [50]. Hybrid metal oxide photocatalysts are being explored for highly efficient photoanodes in photoelectrochemical cells,

with a focus on achieving sustainable hydrogen production. Various metal oxides, including TiO_2, Fe-Ti-O, ZnO, and Zn_2TiO_4, are under investigation for their photocatalytic properties [51].

To enhance the stability and electrical properties of graphene for transparent electrodes, multilayered electrodes consisting of metal oxides overcoated with graphene have been developed [52]. ZnO, a wide-band semiconductor, emerges as a notable candidate for photoconduction in optoelectronic devices operating in the visible and ultraviolet spectral regions [53]. ZnO-based photodetectors exhibit an exceptionally high photoconductive gain, indicating significant potential for efficient photoresponse [54]. Additionally, ZnO nanocrystals serve as model systems for studying the generation and properties of excess charge carriers in semiconductor nanocrystals, with the maximum number of excess electrons per nanocrystal in ZnO photodoping found to be size-dependent [55, 56].

TiO_2, renowned for its efficient photoactivity, high stability, and low cost, is extensively utilized as a photoconductor. It is commonly employed as a semiconductor substrate for water photo-dissociation and is considered an ideal solid-state photocatalyst for academic study [57, 58]. However, the industrial application of pristine TiO_2 is hindered by its limited absorption of visible light due to its bandgap [59]. To overcome this limitation, TiO_2 can be doped or co-doped with elements such as Se and Zr, reducing the bandgap and enhancing the photo-response under visible light irradiation [60]. Furthermore, the fabrication of TiO_2 p-n homojunctions improves charge separation and transfer, leading to significantly higher photoactivity in photoelectrochemical and photocatalytic hydrogen generation [61].

Extensive research has been conducted on ZnO:TiO_2 heterostructures, revealing their favorable photoelectrochemical properties and potential as photoconductors. These heterostructures exhibit intercalated valence and conduction bands, resulting in a decreased band gap, reduced recombination rate, and increased light absorption range [62]. The addition of ZnO to TiO_2 enhances the electrical

conductivity, charge separation, and photoresponse ability of the photoelectrodes [63]. Incorporating ZnO nanoparticles into TiO_2-based photoanodes increases the specific surface area and pore volume, thereby improving dye sensitizer capacity [64]. Additionally, ZnO:TiO_2 heterostructures are employed in the fabrication of visible-light phototransistors, demonstrating high photoresponsivity and photosensitivity under illumination [65].

The recent literature further delves into the photocurrent response of TiO_2:ZnO hybrid heterojunctions, showcasing varying values based on specific compositions and structures. Notably, TiO_2/ZnO heterojunctions have demonstrated high photoresponsivity and photosensitivity under 520 nm wavelength light, emphasizing their potential for visible-light photocurrent response applications [66]. In comparative studies, ZnO/TiO_2 heterojunction photoelectrodes achieved significantly higher photocurrent density compared to pure TiO_2, indicating the effectiveness of the hybrid structure [67].

ZnO-TiO_2 core-shell nanotubes exhibit a high UV response and improved performance under heating, demonstrating a promising photo/dark current ratio and responsivity [68]. TiO_2/ZnO nanotube layers with varying ZnO coatings exhibit considerable enhancement in photocurrent density and incident photon to current conversion efficiency [69].

The application scope of ZnO:TiO_2 heterostructures is extended to visible-light photocurrent response applications, showcasing high photoresponsivity and photosensitivity. The optimized TiO_2/ZnO heterostructure, in particular, exhibits impressive performance under 520 nm wavelength light illumination [70]. This underscores the potential of ZnO:TiO_2 heterostructures in enhancing the performance of phototransistors based on oxide semiconductors. In solar cell applications, TiO_2/ZnO double-layer coatings prove effective in reducing substrate reflectivity and minimizing spectral mismatch, resulting in a substantial increase in average photocurrent [71].

Additionally, TiO_2/ZnO hybrid nano-sponges, when employed as photoanodes in photoelectrochemical water splitting tests, demonstrate a significant increase in the photoelectrochemical response [72]. Titanium dioxide-nitrogen doped graphene quantum dot (TiO_2-NGQD) composites exhibit superior photocurrent generation and photocatalytic degradation of phenol compared to commercial standard TiO_2, particularly under visible light illumination [73]. Furthermore, TiO_2 conjugated with zinc oxide thin films achieves notable efficiency in dye-sensitized solar cells [74].

1.7 Aims

The main goals of this study are to:

1. Explore the synthesis of a ZnO:TiO2 heterojunction using the sol-gel technique and spray pyrolysis deposition method on different substrates.
2. Investigate the influence of different precursor materials, solvents, catalysts, and annealing temperatures on the overall properties of both TiO_2 and ZnO thin films.
3. Conduct a comprehensive analysis of the optical properties of the synthesized materials, including their absorption characteristics and measurements of the optical band gap. Then, test the morphology of the prepared thin film samples using scanning electron microscopy (SEM), and evaluate the structural properties of the materials through advanced techniques such as X-ray diffraction (XRD).
4. Study the electrical characteristics of the ZnO:TiO_2 heterojunction by analyzing its IV characteristics. Assess the thermal dependence of the heterojunction's conductivity to elucidate its performance under varying temperature conditions.
5. Examine the photoresistance characteristics of the ZnO:TiO_2 heterojunction to provide insights into its photoresponse behavior.

Chapter Two

Theoretical Background

2.1 Structural Properties

The crystallite size (D) was calculated using the Scherer equation [75] as follows:

$$\boldsymbol{D = \frac{k\lambda}{\beta cos\theta}} \qquad 2.1$$

where $\boldsymbol{\theta}$ is Bragg angle, $\boldsymbol{\lambda}$ is the incident X-ray wavelength (0.15406 nm), $\boldsymbol{(k)}$ is a dimensionless shape factor, with a value close to unity (0.9) and $\boldsymbol{\beta}$ is the full-width at half maximum (FWHM) of the diffraction peak.

The lattice strain (ε) can be calculated using the equation 4.2 [76]:

$$\boldsymbol{\varepsilon = \frac{\beta}{4tan\theta}} \qquad 2.2$$

The crystallite size (D) is an essential parameter that provides information about the size of the individual crystalline domains within the material[77]. The equation considers the X-ray wavelength, the shape factor, and the diffraction angle. The angle at which the X-ray beams strike the crystal lattice, leading to constructive interference and diffraction, is called the Bragg angle [78].

Lattice strain is a measure of the distortion or deformation in the crystal lattice of a material, which can arise from various factors such as lattice defects, dislocations, and external stresses. Lattice strain affects the diffraction peak positions and shapes, leading to peak broadening. The observed FWHM of the peaks is influenced by both the crystallite size and lattice strain. An increase in lattice strain results in a broader peak [79-80].

2.2 Optical Properties

The process of generating electron-hole pairs and initiating the photo-current response is essential for moving from the valence band to the conduction band. Direct and indirect transitions are the two types of transitions [81]. In direct

transitions, the energy of an absorbed photon matches the energy difference between the valence band and the conduction band. When a photon with the correct energy is absorbed by the material, an electron in the valence band is directly excited to the conduction band. Direct transitions are more probable and efficient, resulting in a stronger absorption of light and higher photo-current response [82].

On the other hand, in an indirect transition, the energy of the absorbed photon does not exactly match the energy difference between the valence band and the conduction band. Instead, the absorbed photon interacts with phonons (quantized lattice vibrations) to assist the electron in overcoming the energy difference. Indirect transitions are less probable and less efficient compared to direct transitions, leading to weaker absorption of light and lower photo-current response [83].

Semiconductor nanoparticles, zinc oxide (ZnO) and titanium dioxide (TiO_2), offer unique properties that can improve absorbance in photoresistance devices [84]. These nanoparticles can be engineered to have a specific bandgap energy, allowing them to absorb light at different wavelengths. By tuning the bandgap energy, nanoparticles can be designed to match the visible spectrum more effectively, leading to enhanced light absorption and increased photo-current response [85].

Furthermore, heterojunction composites made from these semiconductor nanoparticles provide further opportunities to enhance absorbance. Combining different semiconductor materials with complementary bandgap energies can widen the absorbance spectrum. This enables the composite to harvest a broader range of wavelengths from the solar spectrum, improving the overall efficiency of photovoltaic devices[86]. The bandgap energy of a semiconductor material is a critical factor influencing the photo-current process and photo-resistance [87].

Narrow bandgap materials can absorb a wider range of light energies, including lower energy photons. This leads to more efficient generation of electron-hole pairs and a stronger photo-current response. On the other hand, wider bandgap materials can only absorb higher energy photons, limiting their ability to generate electron-hole pairs from the lower-energy end of the solar spectrum. This results in a weaker photo-current response compared to narrow bandgap materials [88].

Concerning photo-resistance, materials with narrower bandgaps generally exhibit lower photo-resistance due to their enhanced absorption of light and efficient generation of electron-hole pairs. Higher photo-resistance indicates a stronger change in electrical resistance when exposed to light, making these materials more suitable for light-sensitive applications like photoresistors [88-89].

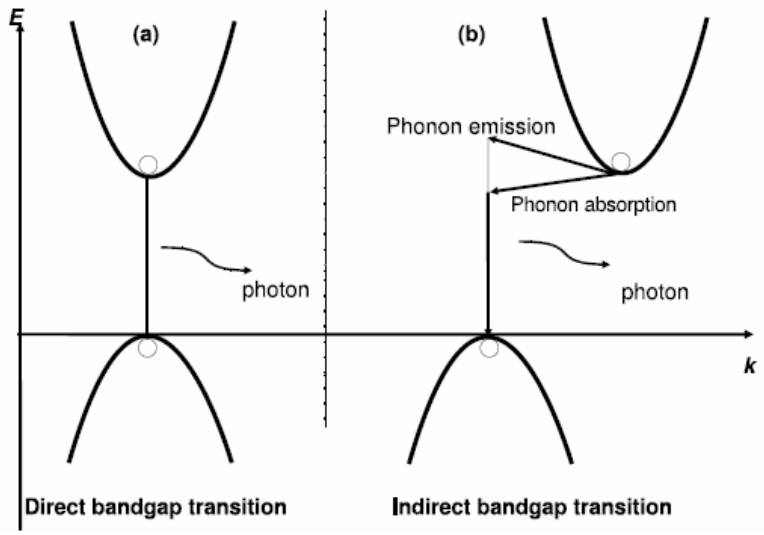

Figure 2.1 Scheme of optical transition in semiconductor with a (a) direct bandgap and (b) indirect bandgap [90].

Photons are absorbed by the semiconductor from the incident beam; The rate of absorption is proportional to the photon energy $(h\upsilon)$, where (h) is Plank's constant, (υ) is the incident photon frequency, The electronic transition is connected with absorption between the valance and conduction bands in the material starting at the absorption edge which corresponds to minimum energy

difference (E_g) between the V.B. and the C.B. [91]. If the energy of the photon (E) is greater than or equal to the energy gap (E_g), the interaction between the photon and a valence electron occurs, resulting in the promotion of the electron to the conduction band and the formation of an electron-hole pair. The wavelength (λ) of the incident photon that leads to the creation of the electron-hole pair is referred to as the maximum wavelength (λ_{max}) [92]:

$$\lambda_{max} = \frac{hc}{E_g} = \frac{1.24}{E_{g(eV)}} \quad (2.3)$$

The photon flux diminishes exponentially in its magnitude as it traverses the semiconductor, in accordance with Beer's law [93].

$$I_T = I_o e^{-\alpha t} \quad (2.4)$$

Where (I_o, I_T) photons absorbed per unit distance of the semiconductor. Additionally, the thickness of the film is denoted as (t) [93]:

$$\alpha = 2.303 \frac{A_b}{t} \quad (2.5)$$

Where (A_b) is the absorption.

The phenomenon of radiation absorption, which results in the occurrence of electronic transitions between the valence and conduction bands, can be classified into two distinct categories: direct transitions and indirect transitions. The mathematical representation of these transitions is provided by the Tauc equation [94]:

$$(\alpha h\nu) = B(h\nu - E_g)^r \quad (2.6)$$

where $(h\nu)$is the incident photon energy, (r) is constant which takes the values (1/2, 3/2, 2, and 3) depending on the material and the type of the optical transition whether it is direct or indirect, where (r) equal to 1/2, 2, 1/3 or 2/3 for direct allowed, indirect allowed, direct forbidden and indirect forbidden transitions,

respectively. In the present study of TiO_2 and ZnO the value of (r) of Eq. (2.6) was taken as 1/2. and (B) is the edge width parameter [95].

The optical constants hold significant importance as they elucidate the optical characteristics of the substances. The absorption coefficient of the substance exhibits a profound dependency on both the photon energy and the energy of the band gap. As it is possible to know the nature of electronic transfers from knowing the value of the absorption coefficient, if the value of the absorption coefficient is high (α>10^4), then this means the possibility of a direct electronic transmission [96].

In summary, optimizing absorbance through the use of semiconductor nanoparticles and heterojunction composites, and considering the bandgap energy, is essential for enhancing the photo-current response and photo-resistance in photovoltaic devices. These considerations contribute to the design of more efficient photo-current and light-sensitive devices in optoelectronics.

2.3 I-V Characteristics

A voltage-current (I-V) characteristic curve, also known as the current-voltage characteristic or simply I-V curve, is a graphical representation of the relationship between the current (I) passing through a device or material and the voltage (V) applied across it. It is a fundamental tool used to study and understand the behavior of various electronic components, devices, and materials.

The I-V curve provides valuable information about the electrical properties and behavior of a device or material. It helps to analyze and understand various aspects. Firstly, it allows us to verify if the device or material follows Ohm's Law, which states that the current passing through a conductor is directly proportional to the voltage applied across it, given the resistance remains constant [97]. Secondly, for many devices and materials, the I-V curve exhibits nonlinear behavior, which is crucial in understanding the operation of diodes, transistors,

and other semiconductor devices [98]. Thirdly, the I-V curve helps identify the threshold voltage at which semiconductor devices like diodes and transistors start conducting (turn on) or stop conducting (turn off). This behavior is discussed by Jing, Chen, and Feng [99].

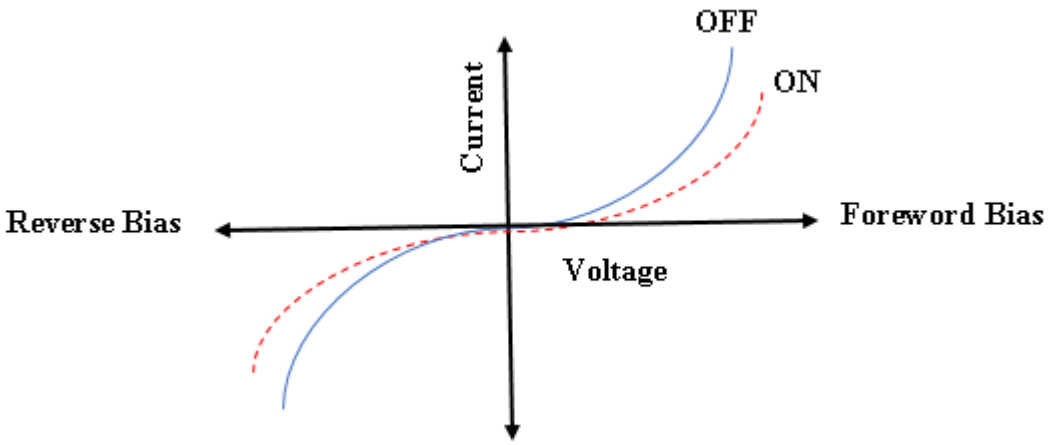

Figure 2.2 Schematic diagram of I-V curve at ON-OFF states.

2.4 Thermal Dependence Conductivity

The electrical conductivity of a material changes with temperature due to thermal excitation of charge carriers. For semiconductors, increased temperature leads to higher carrier concentration, leading to enhanced electrical conductivity. However, temperature also affects recombination processes, potentially degrading the performance of photovoltaic devices[100].

Understanding the temperature dependence of conductivity is crucial for optimizing device operation and predicting its behavior under varying environmental conditions [101].

The Arrhenius equation is a mathematical relationship that describes the temperature dependence of various chemical and physical processes, including the electrical conductivity of materials [102] . In the context of electrical conductivity, the Arrhenius equation relates the conductivity (σ) of a material to the temperature (T) and activation energy (E_a) involved in charge carrier movement through the material.

Arrhenius Equation for Electrical Conductivity: The Arrhenius equation for electrical conductivity is given by [103-104]:

$$\sigma = \sigma_o \, e^{\frac{E_a}{(K_B * T)}} \qquad (2.7)$$

where: σ = Electrical conductivity of the material (in $(\Omega.m)^{-1}$). σ_o= Pre-exponential factor, a constant representing the electrical conductivity at a reference temperature (usually at room temperature or another specified temperature). It is a scaling factor for the conductivity. E_a = Activation energy, which is the energy required for charge carriers (electrons or holes) to overcome the energy barrier and participate in conduction. It is measured in joules (eV). T = Temperature of the material in Kelvin (K). K_B = Boltzmann constant, approximately equal to 8.617×10^{-5} eV/K. The Arrhenius equation plays an important part in understanding the temperature dependence of electrical conductivity in semiconductors. The equation is of significant importance for several reasons [103-104].

The mobility of these charge carriers can be described by the Arrhenius equation, which provides insights into how easily they can move through the crystal lattice as the temperature changes. This equation helps to determine the activation energy required for the charge carriers to participate in conduction. The mobility is defined as the rate at which the charge carriers move in response to an applied electric field, which is usually measured in units of $(m^2/(V.s))$. A higher mobility value indicates that the charge carriers can move more freely, resulting in enhanced electrical conductivity[105].

The mobility of the charge carriers in semiconductors is greatly affected by temperature. As the temperature rises, the lattice vibrations in the semiconductor crystal become more pronounced, leading to changes in the movement of the charge carriers. At higher temperatures, the lattice vibrations can scatter the

charge carriers, causing a decrease in mobility. However, the thermal energy can also provide charge carriers with additional kinetic energy, making them move faster, which can increase mobility. Additionally, the increase in charge carrier concentration due to thermal generation can also impact mobility.

The Arrhenius equation relates the mobility of charge carriers to the temperature and an activation energy involved in their movement. It is expressed as [106]:

$$\mu = \mu_o e^{\frac{-E_a}{(K_B * T)}} \tag{2.8}$$

where μ represents charge carrier mobility, μ_o denotes the pre-exponential factor representing mobility at a reference temperature. The temperature dependence of charge carrier mobility is important for optimizing the design and performance of semiconductor devices.

2.5 Photoresistance

Photoresistance refers to the change in electrical resistance of a material in response to light exposure. In photoresistive materials, the conductivity is altered by the generation and recombination of charge carriers when exposed to light. The photoresistance of a material depends on its properties, such as bandgap, trap states, and defect concentrations. Control photoresistance is valuable for designing light-sensitive devices and assessing their performance in different lighting conditions [107].

In the case of semiconductors, the determination of photoresistance involves examining the time-varying photocurrent response. This response can be classified into two categories. The first category involves applying a voltage across two electrodes on the semiconductor material, which accelerates and separates electron-hole pairs, leading to photocurrent generation. The second category, known as photovoltaic, involves setting the source voltage to zero and

evaluating the semiconductor's resistance to light-induced electric current generation [108].

Under illumination, the presence of oppositely charged carriers creates an inherent electric field, resulting in measurable electric current generation. By studying the time-varying photocurrent response under different arrangements, Photoresistance provides useful information about a material's ability to resist the creation of an electric current as well as how it reacts to the transfer of electrons caused by light [109].

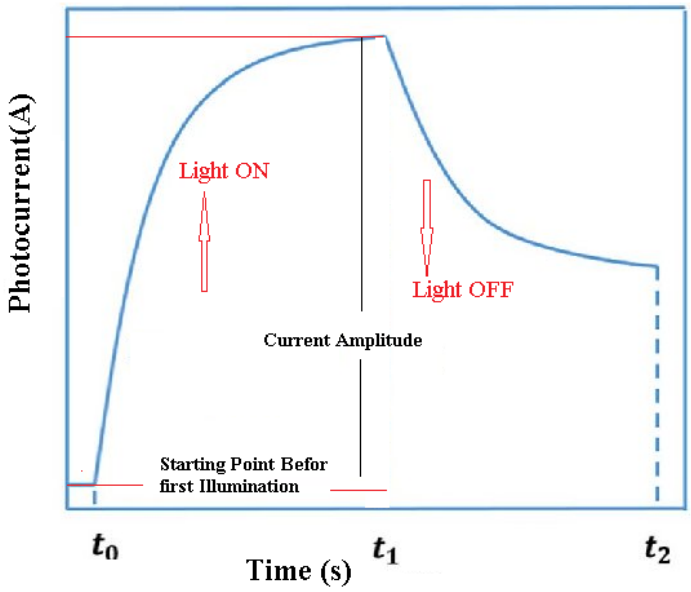

Figure 2.3 Modificated typicla plot of time dependant photocurrent response[110].

According to Figure 2.3, there are four main measurements:

1- Response time or rise time (R.T.) is a crucial metric used in the study of semiconductors and materials in general, as it provides valuable information into their interaction with light. It is defined as the time taken for the current to reach 90% of its maximum value, starting from the moment of illumination onset and ending when the illumination ceases[111].

In the field of optoelectronics and photonics, understanding the response time is essential to assess the performance and efficiency of various devices, such as photodiodes, solar cells, and light-emitting diodes (LEDs). The semiconductor's ability to rapidly respond to incoming light directly affects its functionality and suitability for specific applications.

Response time measurements often used to evaluate the speed at which a semiconductor material can switch between its conducting and non-conducting states under light exposure. The faster the response time, the more suitable the material may be for high-speed optoelectronic applications like optical communication or ultrafast photodetectors [112] .

Moreover, the response time is a key parameter in evaluating the suitability of a material for light-sensitive applications, like image sensors or photovoltaic cells. A shorter response time allows these devices to capture rapid changes in light intensity accurately, making them more efficient in capturing and converting light into electrical signals photodetectors [112] .

2- Recovery time or fall time (F.T.) refers to the duration it takes for the current to return to a specified baseline level after the illumination is removed.

Understanding the recovery time is important for assessing the ability of a semiconductor or material to revert to its initial state once the light source is switched off or blocked. This parameter is particularly relevant in applications where rapid switching or modulation of light sensitivity is required [113].

In devices like photodetectors and image sensors, the recovery time directly influences their performance during repeated exposure to light pulses or varying light intensities. A shorter recovery time allows these devices to quickly adapt to changes in illumination levels, enabling faster image capturing and better sensitivity to varying light conditions. On the other hand, in certain optoelectronic applications, a longer recovery time might be desirable. For instance, in certain

photodiodes used for high-speed communication, a slightly longer recovery time can act as a natural filter, ensuring that the device responds consistently to a specific frequency range of light signals.

Both response time and recovery time are critical parameters for the design and optimization of optoelectronic devices. The interplay between these two characteristics defines the device's ability to sense and respond to light effectively, making them key factors in material selection and device engineering.

3- The steady current region, where the current remains stable even with the lighting on, is primarily due to the specific characteristics of the semiconductor material used in the device. Semiconductors possess unique electrical properties that allow them to conduct electricity under certain conditions, such as exposure to light.

In the steady current region, the semiconductor material is operating in a state where the generated electron-hole pairs (electrons and corresponding positively charged holes) are efficiently collected and contribute to a constant flow of electric current. When light illuminates the semiconductor, it excites electrons, promoting them to higher energy levels, and creates electron-hole pairs. These charge carriers can either recombine (return to their original states), get trapped in the material, or be collected at the contacts of the device to form a current.

The stable current flow in the steady current region occurs because the rate of electron-hole pair generation due to the incident light is balanced with the rate of recombination and collection of these carriers. This balance ensures a steady state of current flow, even under continuous illumination [114].

The characteristics that influence the steady current region include the bandgap of the semiconductor material, the type and concentration of impurities, and the structure of the device.

The bandgap determines the energy required to promote electrons from the valence band to the conduction band, and the impurities (dopants) affect the number of charge carriers available for conduction.

Moreover, the device's structure, such as the design of the junctions and contacts, plays a crucial role in facilitating the efficient collection and transportation of charge carriers. A well-designed structure ensures that the generated charge carriers are directed toward the external circuit to contribute to a stable current flow.

Optimizing of the steady current region, leading to better-performing optoelectronic devices like photodiodes, solar cells, and light sensors.

The time rate of change of current, represented as dI/dt, is a valuable tool used to investigate the photocurrent trend in optoelectronic devices. It provides crucial information about how the current responds dynamically to changes in illumination or light exposure [115].

In optoelectronics, devices such as photodiodes, solar cells, and photoconductors generate a photocurrent when they are exposed to light. This photocurrent is the result of the excitation of charge carriers (electrons and holes) within the semiconductor material by incident photons. The generated charge carriers contribute to the flow of current in the external circuit.

4- The time rate of change of current (dI/dt), insights into the speed and magnitude of the photocurrent response to varying light conditions can be gained through the analysis of the time rate of change of current (dI/dt). Here are some key points to consider:

a. Dynamic behavior: The dI/dt value reflects the current's responsiveness to rapid changes in illumination. A high dI/dt indicates that the photocurrent can quickly follow fluctuations in light intensity, making the device

suitable for high-speed applications such as optical communication or high-frequency light detection.

b. Time constants: The time rate of change of current is related to the characteristic time constants of the device. Time constants represent the time required for the photocurrent to reach certain fractions of its steady-state value after a sudden change in light intensity. By analyzing these time constants, researchers can better understand the underlying charge transport and recombination processes within the semiconductor material.

c. Responsivity and sensitivity: The dI/dt value is directly related to the device's responsivity and sensitivity. Responsivity refers to the photocurrent generated per unit of incident light power, while sensitivity describes how small changes in light intensity result in measurable changes in the photocurrent. A higher dI/dt generally indicates greater responsivity and sensitivity, which are desirable qualities in light-sensitive devices.

d. Transient behavior: The dI/dt value provides insights into the transient behavior of the photocurrent during light exposure and when the illumination is turned on or off. Understanding the transient response is essential for applications where fast and accurate detection of light pulses or rapid changes in light intensity is required.

The time rate of change of current (dI/dt) is a powerful tool for investigating the photocurrent trend in optoelectronic devices. It provides a deeper understanding of the dynamic behavior, responsivity, sensitivity, and transient response, all of which are crucial for optimizing device performance and advancing various light-sensitive applications [116] .

2.6 Heterojunction

A comprehensive examination of the theoretical foundation concerning heterojunctions reveals that a heterojunction represents an interface or junction

that occurs between two diverse materials or crystalline structures within the semiconductor domain. These materials possess unique electronic characteristics, such as bandgap energy, electron affinity, and conductivity. Upon contact, these materials establish a boundary possessing one-of-a-kind electronic traits, which subsequently give rise to a multitude of electrical and optical phenomena[117].

Heterojunctions can be categorized into various types based on the nature of the materials and their manner of interaction. Moreover, a single heterojunction is produced when two distinct semiconductor materials come into contact. These materials generally possess disparate bandgaps and electronic characteristics. Single heterojunctions find applications in optoelectronic devices such as light-emitting diodes (LEDs) and laser diodes [118].In a double heterojunction, there exist two heterojunctions in series, accompanied by an additional layer of an alternative semiconductor material that is interposed between the two [119].

This configuration is frequently employed in cutting-edge electronic and photonic devices to achieve superior regulation of charge carriers. The application of strain to semiconductor materials can induce a heterojunction, thereby modifying the electronic properties of the materials at the interface and resulting in distinctive device characteristics[118-119].

Numerous approaches can be utilized to augment the performance of heterojunctions. The selection of semiconductor materials with complementary properties is of utmost importance in attaining the desired device characteristics. This process involves the careful choice of materials with appropriate bandgaps, electron affinities, and crystal structures[120].

By deliberately doping semiconductor materials at the heterojunction interface, carrier concentrations and conductivity can be altered, thereby allowing for the optimization of device performance. The variation of layer thickness at the

heterojunction interface can significantly affect charge carrier transport and recombination, thus exerting an influence on device efficiency[120].

Tailoring the interface at the atomic or nanoscale level can enhance the properties of charge transfer and minimize defects, thereby leading to improved device performance. The application of strain to the materials can modify their electronic band structures, thus enabling precise control of device properties. In order to minimize surface defects and provide carrier lifetimes, surface passivation techniques can be applied to heterojunctions [121].

Controlled charge transport holds immense importance in the realm of hybrid heterojunctions as well as bilayer heterojunctions, and its influence on the efficacy of devices constructed using these heterojunctions is substantial[122].

2.6.1 Controlled Charge Transport in Hybrid Heterojunctions

In a hybrid heterojunction, such as TiO_2:ZnO, the alignment of energy bands at the interface emerges as a crucial aspect in regulating controlled charge transport. The relative positions of the conduction and valence bands of the constituent materials exert an influence on the motion of charge carriers, encompassing electrons and holes.

Hybrid heterojunctions are frequently engineered with the intention of fostering effective charge separation. Upon the excitation of the system by light or an external stimulus, electron-hole pairs materialize. The energy band alignment and electric fields present at the interface contribute to the segregation of these charge carriers, thereby thwarting recombination. The existence of an inherent electric field at the interface, engendered by the variations in electron affinity or work function between the materials, can instigate the occurrence of directional charge transport[123].

Electrons often gravitate towards one side of the interface, while holes migrate to the other side, thereby facilitating their collection. The attributes of hybrid

heterojunctions can frequently be fine-tuned through the manipulation of the composition, thickness, or doping of the materials, thereby enabling control over the characteristics of charge transport. Meticulous engineering of the heterojunction interface at either the atomic or nanoscale level can heighten the transfer properties of charge, diminish defects, and ameliorate the overall efficiency of charge transport [124].

2.6.2 Controlled Charge Transport in Bilayer Heterojunctions

In a bilayer heterojunction, two semiconductor layers that possess distinct electronic properties are vertically arranged. The band offset between these layers assumes a critical role in the regulation of charge transportation. The dissimilarity in energy levels at the interface has the capability to generate obstacles or reservoirs for charge carriers.

Bilayer heterojunctions commonly exploit the band offset in order to amplify the separation of charges. Electrons can be confined to one layer, whereas holes are restricted to the other layer, thereby minimizing recombination. The band alignment possesses the ability to form energy barriers that impede the motion of charge carriers in specific directions, as well as energy reservoirs that facilitate motion in alternative directions[125].

This effect can be utilized to accomplish specific functions within devices. The mobility of charge carriers in each layer, as well as the properties at the interface, substantially effect the manner in which charge carriers traverse the bilayer structure. Materials with elevated carrier mobility are frequently chosen to augment the efficiency of transport. The thickness of each layer within a bilayer heterojunction can be regulated to exert influence over the depth and configuration of energy barriers and reservoirs, consequently affecting the characteristics of charge transportation[126].

Both hybrid and bilayer heterojunctions present possibilities for precise regulation of charge transfer, which is crucial for a range of electronic and optoelectronic applications, such as solar cells, photodetectors, and light-emitting devices. The comprehension and enhancement of these charge transfer mechanisms are pivotal in enhancing the efficiency of these devices[127] .

2.7 Sol-Gel Method

The solution-gelation (sol-gel) method stands as a widely acknowledged synthetic strategy employed to create high-quality metal oxide nanoparticles (MONPs) and composite materials. This approach grants exceptional precision in tailoring material characteristics and surface attributes. Operating under a chemical framework, the sol-gel process serves as a gateway to crafting diverse nanostructures, particularly MONPs. The process unfolds with the dissolution of a molecular precursor, often a metal alkoxide, in a water or alcohol solution. The ensuing solution, shaped through hydrolysis or alcoholysis, bears a moist disposition. Subsequent drying, customized to the desired gel attributes, becomes essential. In the case of alcohol-based solutions, evaporation of alcohol comes into play[128].

The sol-gel methodology is notably cost-efficient and imparts direct control over product chemistry due to its operation at low reaction temperatures. Moreover, its utility extends to ceramics manufacturing, acting as both a shaping material and a bridge for metal oxide thin films in diverse applications. The products forged through the sol-gel technique find their footing across a spectrum of sectors, spanning optics, electronics, energy, surface engineering, biosensing, pharmaceuticals, and chromatographic separations. Embedded within this conventional and industrial methodology is the crux of converting homogeneous

sols into gels, followed by solvent removal and drying, a step where drying methods significantly influence the resultant properties[129].

The sol-gel approach has garnered widespread attention across scientific domains, primarily due to its capacity to yield diverse materials with broad applications. This wet chemistry-based synthesis technique offers a flexible route to novel and functional materials, encompassing glasses, ceramics, and organic-inorganic hybrids. It functions effectively at low temperatures and mild chemical conditions, resonating as an environmentally friendly and dynamic bottom-up synthesis avenue [130].

In diverse research realms, such as nanotechnology, optoelectronics, semiconductors, medicine, biotechnology, and separation science, the sol-gel technique holds steadfast as a reliable and compelling method. It epitomizes the fusion of precision, innovation, and environmentally conscious synthesis, driving progress in these multifaceted fields [129-130].

Chapter Three

Methodologies and Experimental Procedures

3.1 Overview

This chapter is employed to describe all the experimental procedures including; materials preparations using sol-gel method, thin film deposition, and the instrumentations that utilized to investigate all the properties of the prepared samples. The structure of photoresistance devices are also explained in this chapter.

3.2 Spray Pyrolysis

Spray pyrolysis has recently garnered significant attention as a prominent method for depositing a diverse range of thin films that find application in a wide range of devices[131]. This active processing approach is underpinned by its ability to generate films with varying thicknesses while maintaining simplicity [132]. Spray pyrolysis distinctly offers an accessible avenue to craft films with diverse compositions, thereby eliminating the necessity for high-end substrates or intricate chemical formulations. Furthermore, the adaptability of this method is underscored by its capacity to facilitate the creation of multi-layered films with remarkable ease[133].

The convenience and cost-effectiveness of spray pyrolysis set it apart from alternative film deposition methodologies, particularly concerning equipment investment. The fundamental components comprising spray pyrolysis equipment include an atomizer for droplet generation, a precursor solution housing the desired materials, a substrate heater to enable controlled thermal interactions, and a temperature controller to govern the deposition conditions. This comprehensive setup empowers researchers and practitioners alike to harness the potential of this technique in crafting films tailored to their specific requirements, and it is gaining prominence as a pragmatic solution for thin and thick film fabrication.

3.3 Precursor

Considering the chemical nature of the sol-gel process, the solvent, catalyst, and stabilizer used influence the choice of a precursor in the synthesis of sol-gel nanoparticles. To achieve the desired heterostructure growth and avoid unwanted chemical interactions, both types of nanoparticles treated with the same solvent (2-Methoxyethanol), catalyst (HCl), and stabilizer (Monoethanolamine). Zinc acetate (ZnAc) used to synthesize zinc oxide (ZnO) [134] , whereas titanium tetraisopropoxide (TTIP) used to synthesize titanium dioxide (TiO2) [135].

3.4 Devices

Lateral and sandwich behaviors refer to two different modes of current flow within semiconductor devices, particularly in the context of thin-film or nanostructured devices [136].

Sandwich behavior also known as vertical behavior, sandwich behavior involves the flow of current through the thickness or depth of a semiconductor material. This mode of operation is achieved through a layered structure of heterostructures or multilayer thin films, where each layer contributes to the overall device functionality. The current travels vertically from one layer of the material to another, typically passing through different layers with varying electronic properties. This behavior is more similar to the traditional concept of current flow in a semiconductor, where electrons move through the bulk of the material [137]. Precautionary measures are taken during device preparation to accommodate this behavior, resulting in sandwich device which classified into two subtypes based on the substrate used ITO coated glass or Si/SiO_2 substrate.

Lateral behavior pertains to the flow of current across the surface of a semiconductor material, typically in a horizontal direction. In devices exhibiting lateral behavior, current moves laterally along the surface, often guided by specific structures or patterns on the material's surface. This mode of operation is

often used in applications like sensors, thin-film transistors, and some types of photovoltaic devices. The gadget includes an interdigitated electrode for studying lateral behavior [138]. Precautions are also taken during device preparation to accommodate this behavior. Lateral devices are designed to measure or manipulate current flow across a surface rather than through the bulk of the material.

3.4.1 ITO Coated Glass Substrate

An ITO-coated glass substrate is a commonly utilized choice for the creation of transparent conductive layers in various optoelectronic apparatus [139]. These devices encompass solar cells, LEDs, and photoresistivity sensors. The function of the ITO layer is to act as a transparent electrode that enables light transmission while simultaneously ensuring a conductive surface for the flow of electrical current. Therefore, it is highly suitable for applications that require both optical transparency and electrical conductivity [140], Figure 3.1 shows the prepared sandwich ITO device.

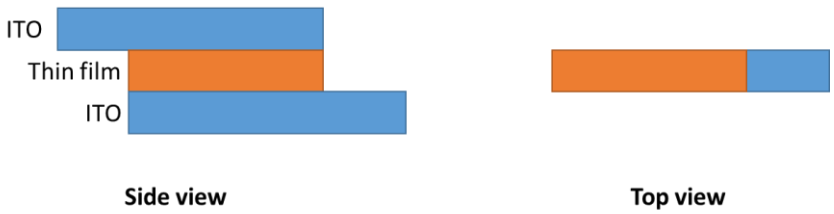

Figure 3.1 The prepared sandwich device(ITO) as Photoresistance.

3.4.2 Si/SiO_2 Substrate

Si/SiO_2 substrate composed of p-type silicon wafer coated with a layer of silicon dioxide is prominently utilized in diverse semiconductor applications due to its unique properties. This type of substrate exhibits a high degree of light absorption owing to the silicon material's exceptional photo-electronic properties, making it

a widely employed semiconductor material for various optoelectronic devices. Conversely, silicon dioxide (SiO_2) acts as an insulating material serving as a dielectric layer in multiple semiconductor devices. It offers electrical isolation between different components on the substrate and impedes unintended electrical interactions. Furthermore, SiO_2 indicates excellent chemical stability, rendering it resistant to most chemicals and solvents [141]. This substrate as illustrated in Figure 3.2 commonly exhibits high-quality surfaces with low roughness, making them suitable for processes such as thin-film deposition. It combines the desirable electrical and optical properties of silicon with the insulating characteristics of silicon dioxide, thus enabling the creation of complex semiconductor devices [142].

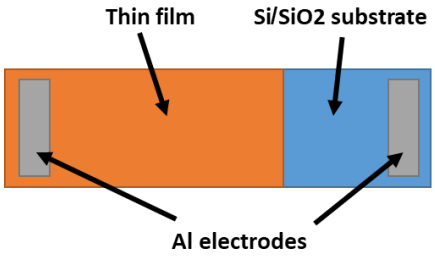

Figure 3.2 Top view of (Si/SiO_2) sandwich device as photoresistance.

3.4.3 Interdigitated Electrodes

Figure 3.3 shows the interdigitated electrode device. Interdigitated electrodes (IDEs) have proven to be useful substrates for studying the lateral dynamics of photocurrent responses. Because of its tightly spaced finger-like metal structures arrayed in a comb-like configuration, IDEs provide a large interaction area that excels at sensing changes in electrical properties such as impedance caused by substance interactions [100].

IDEs have particular advantages in the context of photocurrent lateral behavior. Their design maximizes surface area, making it easier to capture photo-generated charge carriers along the electrode's width. This tool allows you to investigate

how photo-current responsiveness varies throughout the surface of the electrode. IDEs allow for the measurement of spatial photo-generated current changes, which shed light on how different areas of the substrate react to input light.

IDEs are effective platforms for mapping and analyzing the lateral distribution of photocurrent, revealing vital information on material qualities, flaws, and performance differences. Their applications include optoelectronic devices, photodetectors, and solar cells, and they have made major contributions to the understanding and improvement of device efficiency and performance.

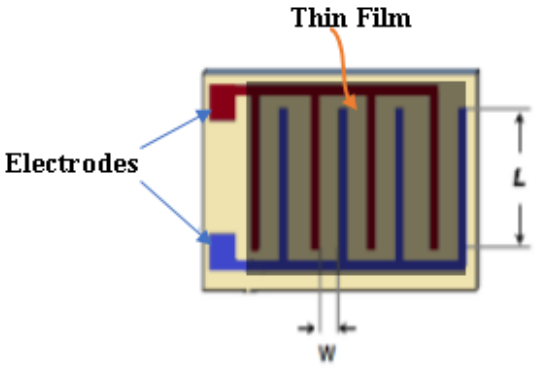

Figure 3.3 Top view of (IDEs) device as photoresistance.

3.5 Materials, and Synthesis Methods

3.5.1 TiO_2 Thin Film

A solution of TiO_2 was created by the addition of 3.23 ml of titanium tetraisopropoxide (Sigma-Aldrich, 205273, Germany), $Ti\{OCH(CH_3)_2\}_4$, to 40 ml of 2-methoxyethanol (MERCK, USA), ($C_3H_8O_2$) at 60±5°C, resulting in a molar concentration of 0.3 M. Stirring of the mixture for 30 minutes was followed by 24 hours of aging in the dark. The subsequent deposition process was conducted through the application of a spray pyrolysis method at 150°C on a hotplate. The thin film was formed through a total of ten sprays, with each spray

lasting one minute and allowing for moisture removal between layers. After 24 hours of aging, a 30-minute annealing step was performed at 600°C.

3.5.2 ZnO Thin Film

The synthesis of the ZnO thin film was conducted using a sol-gel approach similar to that previously employed in 3.5.1. The initial step involved combining 6.645g of zinc acetate dihydrate (HIMDIA, GRM 1434, India), $C_4H_5O_4Zn.2H_2O$, with 40 ml of 2-methoxyethanol at 60±5°C whilst stirring, resulting in a molar concentration of 0.3 M. Next, monoethanolamine (MEA) (THOMAS BAKER, India), $CH_2(OH)CH_2NH_2$, was slowly added as a stabilizing agent, and the solution was stirred for 30 minutes. The introduction of hydrochloric acid (HCl) expedited the reaction, which was allowed to continue for 60 minutes. Subsequently, the solution was shielded from light for 24 hours prior to the deposition process. Finally, the resulting ZnO thin film underwent annealing at 380°C for 30 minutes.

3.5.3 TiO_2:ZnO Hybrid Heterojunction

To create a TiO_2:ZnO hybrid heterostructure, the previously prepared ZnO and TiO_2 solutions were mixed in a 1:1 ratio under stirring for 30 minutes. The mixture was then aged for 24 hours and subsequently deposited using the spray pyrolysis method. A 30-minute annealing process at 380°C followed the deposition.

3.5.4 TiO_2/ZnO Bilayer Heterojunction

The sequential deposition process was executed for the bilayer structure of TiO_2/ZnO heterojunction. Firstly, the TiO_2 layer was subjected to deposition and annealing at an elevated temperature of 600°C. Subsequently, the deposition of the ZnO layer was carried out, followed by annealing at 380°C.

Photocurrent devices were fabricated by depositing the respective solutions onto clean Si/SiO_2, ITO, and interdigitated electrodes (IDEs) substrates, following the

aforementioned procedures. An aluminum (Al) contact layer was coated on the Si/SiO_2 device. For a visual representation, refer to Figure 3.4 in the provided work scheme flowchart.

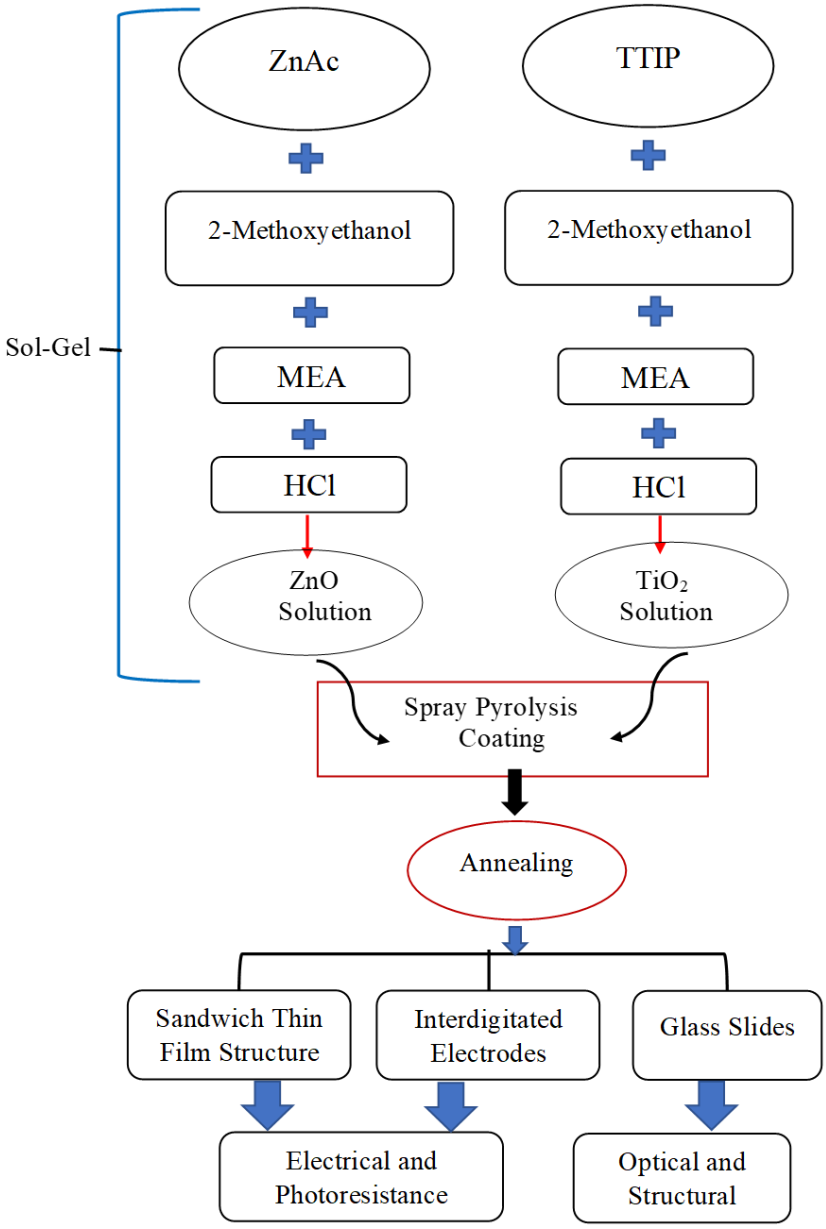

Figure 3.4 Work scheme of sol-gel synthesizing method of TiO_2 and ZnO nanoparticles.

3.6 Furnace and Annealing Procedure

The process of annealing facilitates the rearrangement and relaxation of atoms within the thin film, leading to the formation of a more ordered crystal structure

and thereby reducing defects while enhancing material properties. Thin films are often characterized by internal stresses due to differences in thermal expansion coefficients between the film and substrate. However, annealing can alleviate these stresses, thereby improving film integrity and reducing the likelihood of cracking or delamination. Moreover, annealing can modify the electrical conductivity and resistivity of thin films, making them more suitable for specific electronic and semiconductor applications, while also aiding in tuning the band gap of semiconductor materials [144].

The utilization of annealing can additionally facilitate improved adhesion between the thin film and substrate, thereby enhancing the overall stability and durability of the film-substrate interface. Furthermore, crystalline grains within the thin film can grow and coalesce during annealing, leading to larger and more ordered grains, thereby improving material properties such as mechanical strength and electrical conductivity. Annealing also enables the diffusion of atoms within the thin film, which can lead to alloying with the substrate or other layers, thereby making it an effective tool for creating multilayer structures with tailored properties [145].

The process of annealing can also aid in healing point defects, vacancies, and other crystal lattice imperfections, leading to improved material quality and performance. In the case of thin films employed in optical applications, annealing can modify the refractive index, transparency, and other optical properties, thereby enabling precise control over light interactions.

Annealing can also be employed to modify the microstructure of the thin film, thereby adjusting its mechanical properties such as hardness, elasticity, and resilience. Consequently, it provides researchers with the ability to study the influence of temperature and time on thin film properties, which is essential for understanding material behavior and developing new materials with enhanced characteristics. Finally, it can aid in achieving a more uniform composition

throughout the thin film, thereby reducing compositional variations that might have occurred during the deposition process [146].

The process conditions for the annealing procedure are illustrated in Figure 3.5, which shows a schematic diagram of the temperature vs. time program process. The annealing furnace employed in this study was the KSL-1600X model developed by MTI Corporation. This furnace was specifically programmed to regulate the temperature as a function of time, wherein the temperature was gradually increased in increments of 10 °C per minute. In order to achieve the desired temperature profile for the annealing process, the temperature was initially set at 20 °C and gradually increased until it reached half of the maximum temperature required. Subsequently, the furnace was maintained at this temperature for a duration equal to half of the maximum time required for the process. Following this, the furnace was reheated to reach the maximum temperature required and subsequently held at this level for the desired duration

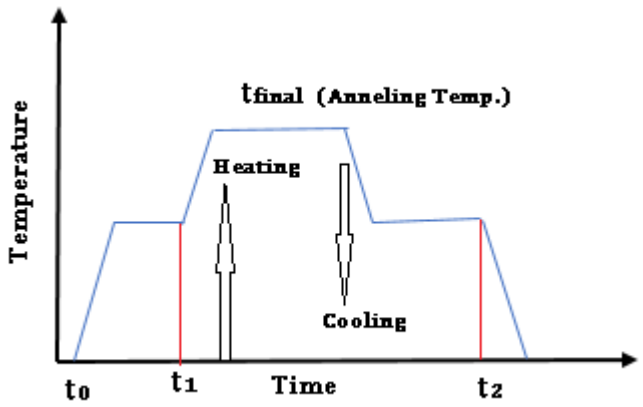

Figure 3.5 Schematic diagram of the temperature vs. time program process.

3.7 X-Ray Diffraction

X-ray diffraction has emerged as a widely used technique in various fields such as materials science, chemistry, physics, geology, and other disciplines where comprehending the atomic arrangement in crystalline materials is crucial. X-ray

diffraction, also known as XRD, is an experimental method that has demonstrated to be a potent instrument for the determination of the crystal structure of materials.

The procedure involves the application of X-rays onto a crystalline sample and subsequently analyzing the diffraction pattern that emerges to extract information about the arrangement of atoms within the crystal lattice. X-rays are generated using a high-energy source, typically an X-ray tube that produces a focused beam of X-rays with a well-defined wavelength.

Upon interaction with the crystal lattice, the X-rays will interact with the regularly spaced atoms. As per Bragg's law, the X-rays will be diffracted at specific angles when the path difference between the rays scattered by adjacent atomic planes is a multiple of the X-ray wavelength [147].

Bragg's law establishes the conditions for observing diffracted beams. When parallel X-rays at an angle of incidence penetrate a set of parallel lattice planes with indices h, k, l, and spacing d (as shown in Figure 3.6; Bragg's law reflection principle used In XRD), these lattice planes operate as mirrors. The path difference must be aligned with multiples of the wavelength in order for a diffracted beam to emerge by constructive interference, as described by equation 3.1:

$$2d_{hkl}sin\theta = n\lambda \qquad 3.1$$

Bragg's equation is represented by equation 3.1. diffracted beams that fail to meet this requirement will experience destructive interference. The value of n in this equation denotes the 'order' of diffraction [147].

This results in constructive interference, which produces a diffraction pattern that is unique to the crystal structure of the material. The processed data will show a series of peaks corresponding to the diffracted X-rays. Each peak represents a specific set of crystal planes that satisfied Bragg's law.

These peaks are subsequently utilized to determine the lattice spacing and other structural information. By analyzing the positions and intensities of the peaks, along with known crystallographic data, researchers are capable of determining the crystal structure of the material. This includes parameters such as lattice constants, unit cell dimensions, and atomic positions. If there exist databases of known crystal structures, one can compare the observed diffraction pattern with them to identify the material or confirm its known structure. In case the material is novel, the diffraction pattern can help determine its unique crystal structure. Once the crystal structure is determined, researchers can analyze its properties and behavior in relation to its atomic arrangement. This information is pivotal for comprehending the material's properties and potential applications.

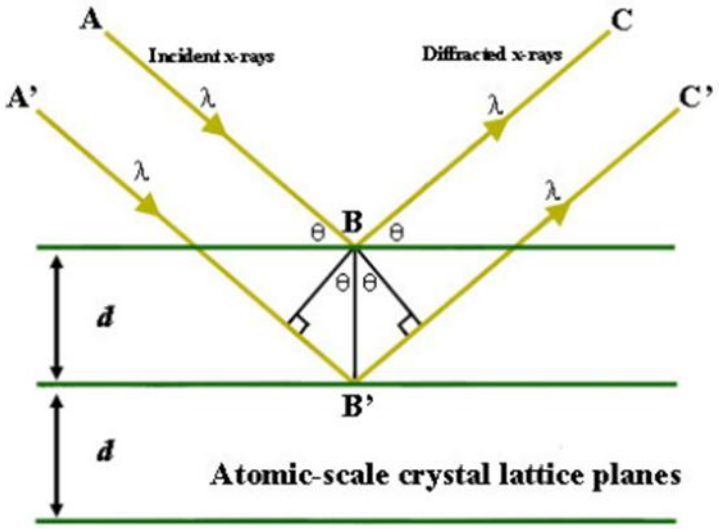

Figure 3.6 Bragg's Law Reflection Principle Used In X-Ray Diffraction[148].

3.8 UV-Vis. Spectrophotometer

A double beam UV-Visible spectroscopy is used to estimate the absorption characteristics of the studied thin films. The process of absorption may transpire as light travels through the sample or as it reflects off the sample surface. The determination of accurate absorbance is based on the incident and transmitted light as revealed by equation 3.2 which is Lambert's law of absorption.

$$I_T = I_o e^{-\alpha t} \qquad 3.2$$

Where I_o is the incident intensity of light, I_T the transmitted light intensity, α absorption coefficient, and t the thickness of sample Figure 3.7 illustrates the incident- transmitted intensities .

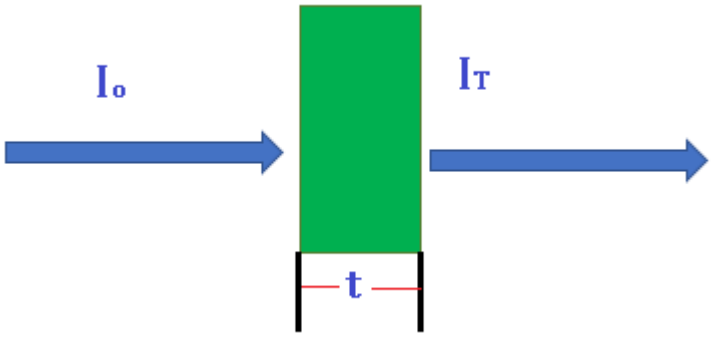

Figure 3.7 Typical plot of incident and transmitted light .

As atoms or molecules absorbed energy, electrons transfer from the ground state to an excited state. The energy absorption occurs discretely in quanta, which is equivalent to the difference in energy between the ground and excited states.

As analyte concentration rises, light absorption increases linearly, and light transmission decreases exponentially. A photon can induce a transition in energy levels if its energy matches the energy difference. Nanoparticles have distinct optical properties due to their size, known as surface plasmon polariton resonances. These resonances occur when nanoparticles interact with radiation, affecting the refractive index near their surface. This enables effective UV-Vis spectroscopic analysis of nanomaterials, which are sensitive to size, shape, aggregation, structure, and concentration changes, even at low concentrations [148].

Absorption spectroscopy covers electromagnetic radiation from 190 to 800 nm, ultraviolet (190-400 nm) and visible (400-800 nm) regions. This technique is

valuable for experimental analysis. The absorbance, transmittance, and reflectance as shown in Figure 3.8, are illustrated mathematically by equation 3.3 as follows :

$$A + T + R = 1 \qquad 3.3$$

Where A is the absorbance, T is the transmittance, and R represents the reflectance.

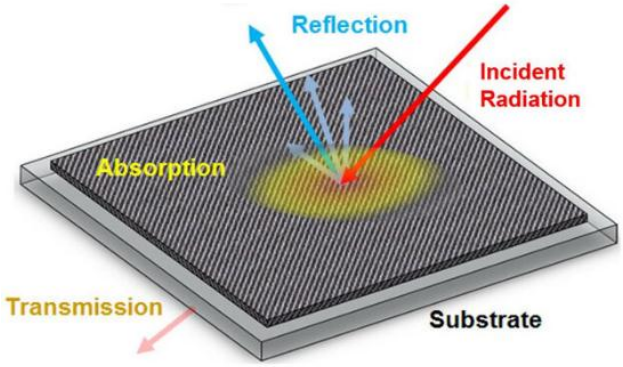

Figure 3.8 Schematic showing the absorption, transmission and reflection[149].

3.9 Keithly Instrument

Keithly 2400, was employed to conduct I-V characteristic of the samples in the ON and OFF states, which were induced by light illumination. This specific technique is highly suitable for measuring the resistivity of samples. As illustrated in Figure 3.9, the resistivity can be obtained by determining the voltage (V) and current (I) utilizing the following formula:

$$\rho = \frac{V}{I} * \frac{w*l}{t} \qquad 3.4$$

Additionally, the dimensions of the film, namely width, length, and thickness, are denoted by w, l, and t, respectively as in Figure 3.10.

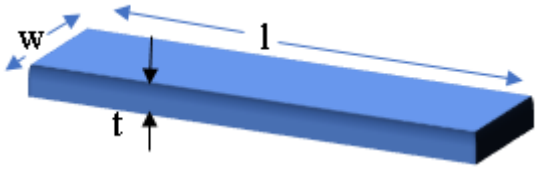

Figure 3.9 Typical plot of the thin film dimensions.

Moreover, the Keithly instrument was utilized to determine the time-dependent current by varying the light illumination between ON and OFF states. This method enables the current versus time to transition from an increasing behavior due to charge transitions until reaching a steady-state current. Subsequently, the light was turned off, causing the current to decay until it reached the steady-state once again.

3.10 Photoresistance System

The photoresistance system utilized in this , as depicted in Figure 3.10, was contained within a box made of medium-density fiberboard (MDF) wood, measuring 30 cm × 30 cm × 20 cm. This design choice ensured that the influence of light on the experiments was minimized. The setup also allowed for easy insertion and removal of samples, thereby enabling precise control over their positioning to optimize light exposure. To provide the necessary visible light for the experiments, an 80-watt tungsten laboratory lamp was securely positioned at a distance of 35 cm from the sample. To avoid excessive heat generation, the lamp was fastened using a holder and connected to a regulator, which stabilized the light intensity and prevented electrical fluctuations during operation.

At the heart of the system was a thin film device that seamlessly integrated with a computerized system from Keithley. This integration allowed for precise measurement and analysis of the photoresistance properties of the samples. A specially designed opening at the top of the box served as a controlled passage for

light, enabling the experimental conditions to be switched between the ON and OFF states.

In addition, a dedicated power supply unit ensured that consistent and regulated power was distributed to all components of the system. This guarantee of reliable and reproducible experimental outcomes was crucial. The sophisticated integration of the Keithley instrument facilitated the accurate capture and analysis of intricate variations in the photoresistance behavior of the thin film under different experimental conditions.

The seamless integration of a sophisticated computer system within the setup streamlined the acquisition, processing, and analysis of data. It served as a central hub for real-time monitoring and meticulous record-keeping of experimental parameters and results. The meticulously designed configuration and dimensions of the photoresistance system were optimized to ensure precise and controlled experimental conditions. This optimization allowed for in-depth investigations into the nuanced photoresistance properties of the thin film material. Such investigations have important implications for advancements in optoelectronics, semiconductor research, and material science.

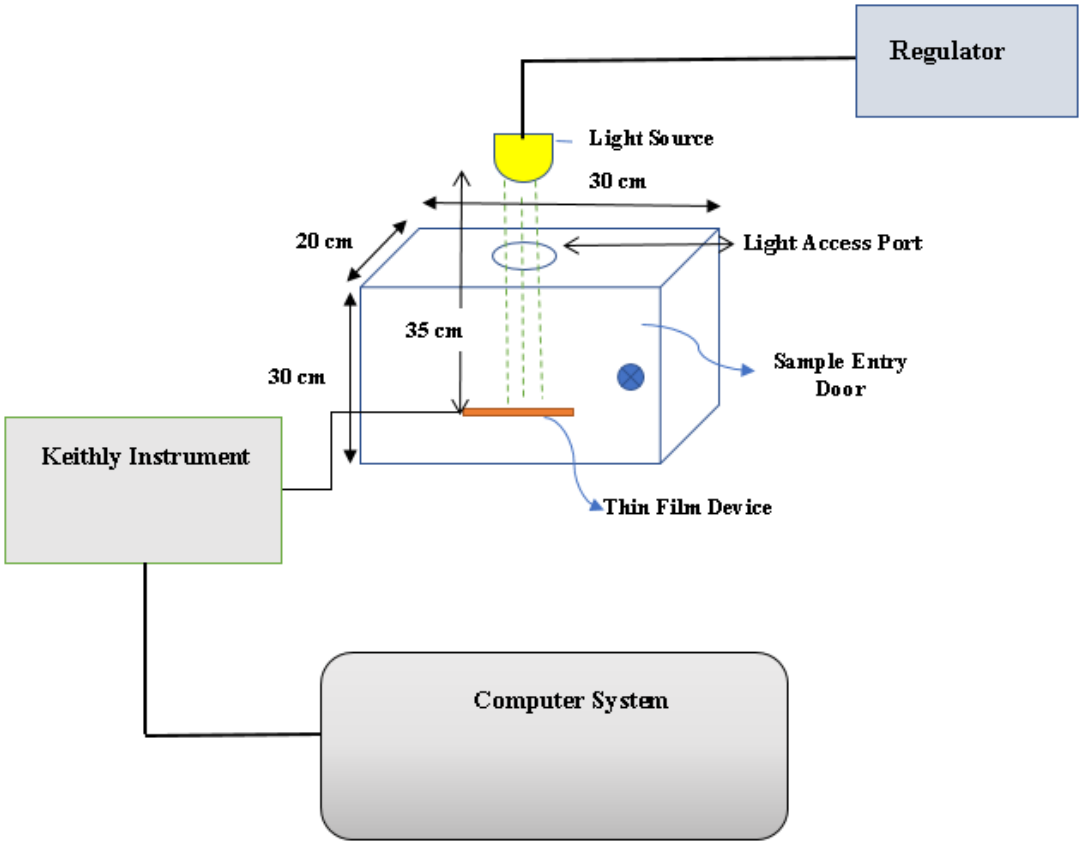

Figure 3.10 Schematic of the photoresistance system.

Chapter Four

Results and Discussion

4.1 Overview

This chapter extensively analyzes thin film materials for potential applications. It explores optical properties, confirms film thickness with a Lambda Reflectometer, and uncovers structural and electrical characteristics through X-ray Diffraction (XRD), Scanning Electron Microscopy (SEM), and current-voltage (I-V) measurements. Significance is placed on the photoresistive properties for optoelectronic use, with correlations contributing to broader technological insights. All films undergo analysis using X-ray diffraction, SEM, and UV-Vis spectroscopy, including deposition on glass slides.

4.2 X-ray Diffraction

4.2.1 Titanium Dioxide (TiO_2)

The X-ray diffraction (XRD) peaks (JCPDS 00-001-0562)[150], as shown in Figure 4-1, observed in the TiO_2 thin film at specific 2θ angles are significant as they correspond to crystallographic planes of the Anatase phase.

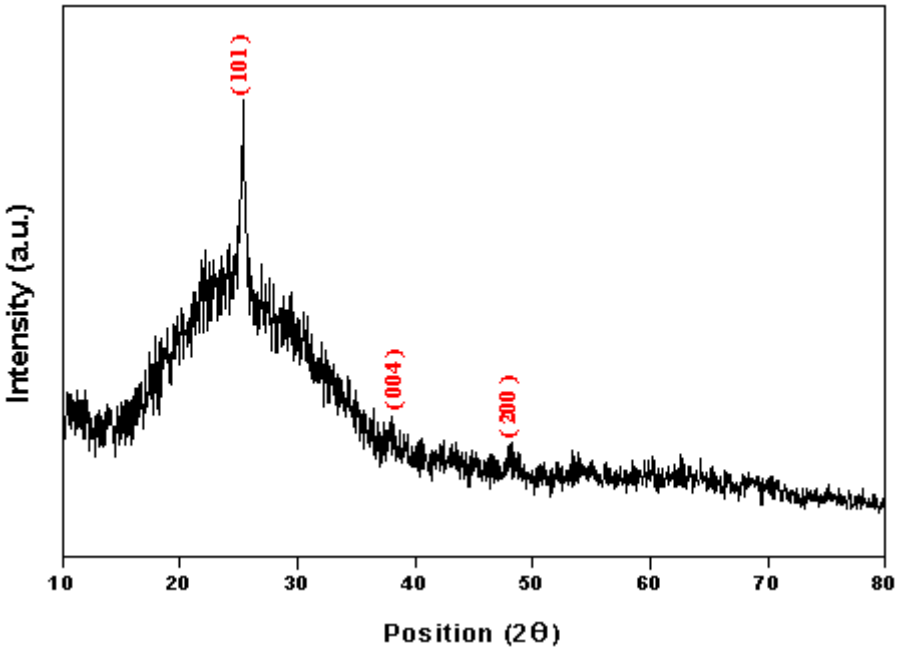

Figure 4.1 XRD Pattern of TiO_2.

This is crucial as different polymorphs of TiO_2 exhibit distinct XRD patterns due to their unique crystal structures.

Table 4-1 presents XRD analysis data for the TiO2 thin film, revealing crucial information about its crystal structure. The indexed (h k l) values denote crystallographic planes, while K represents the relative intensity factor. λ is the wavelength, β is the Bragg angle, and 2θ is the diffraction angle. D denotes the crystallite size, measured in nanometers. Lattice strain, indicative of structural distortion, is also provided. The observed peaks at (101), (004), and (200) positions align with Anatase phase crystallographic planes, confirming the predominant crystal structure.

The associated K values indicate the relative intensity of these planes. The calculated crystallite sizes (D) range from 25.394 to 48.073 nm, providing insight into the dimensions of the crystalline domains in nanoscale. The lattice strain values suggest minimal structural distortion.

***Table 4-1**: XRD Analysis Data for TiO_2 Thin Film*

h k l	K	λ(nm)	β(°)	2θ(°)	D(nm) (measured)	Lattice Strain
101	0.9	0.15406	0.59	25.394	14	0.011
004	0.9	0.15406	0.69	37.821	12.3	0.009
200	0.9	0.15406	0.72	48.073	12.2	0.007

4.2.2 Zinc Oxide (ZnO)

The wurtzite crystal structure of ZnO is confirmed by comparing its XRD pattern in Figure 4.2 with JCPDS card 01-079-0205[151]. The analysis reveals that the ZnO thin film comprises nano-sized particles with a hexagonal wurtzite crystal structure. In the specific context of ZnO, the diffraction peaks are identified by

their respective Miller indices (hkl) and the position (2θ), which represent the scattering angles.

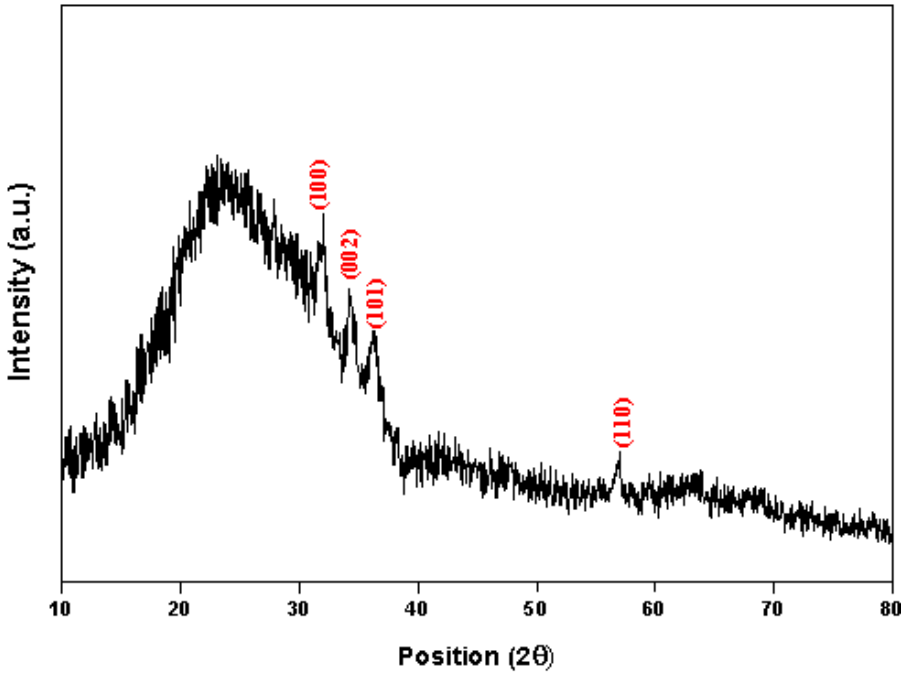

Figure 4.2 XRD Pattern of ZnO.

Table 4-2 presents a variety of parameters pertaining to the diffraction peaks and the associated calculations.

The Miller indices denote the crystallographic planes, specifically the (100), (002), (101), and (110) planes. The lattice strain values were relatively minor, indicating that the crystal lattice was under a comparatively low level of strain.

Table 4-2: XRD Analysis Data for ZnO Thin Film

h k l	**K**	**λ(nm)**	**β(°)**	**2θ(°)**	**D(nm) (measured)**	**Lattice Strain**
100	0.9	0.15406	0.394	32.047	21.4	0.006
002	0.9	0.15406	0.59	34.349	14.3	0.008
101	0.9	0.15406	0.689	36.371	12.3	0.009
110	0.9	0.15406	0.72	56.762	12.7	0.006

4.2.3 Hybrid Heterojunction ($ZnO:TiO_2$)

In Figure 4-3, the main point is the X-ray diffraction (XRD) pattern of the mixed hybrid. This pattern shows a mixing of TiO_2 and ZnO in an exact 1:1 ratio. The pattern seems to be more like ZnO.

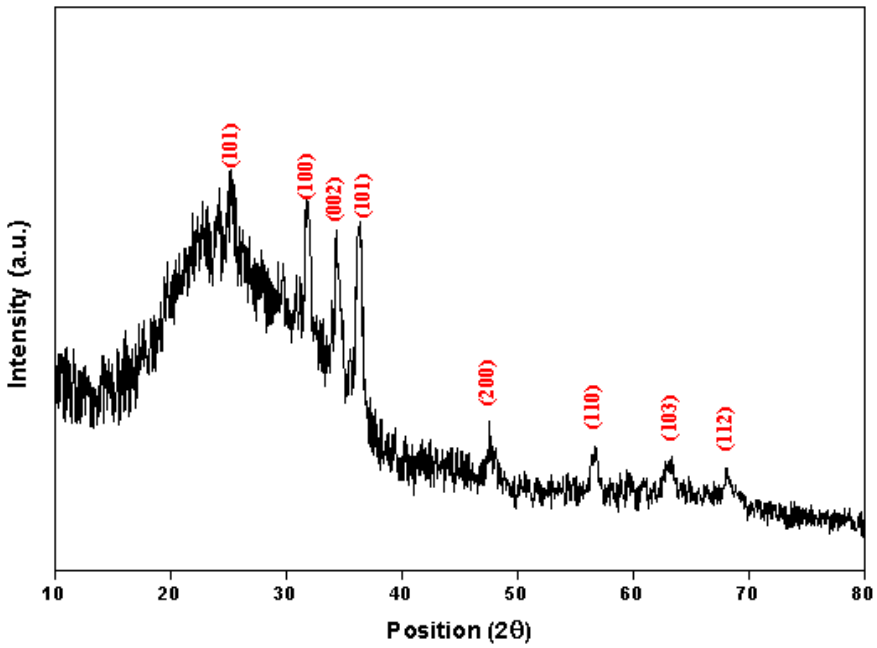

Figure 4.3 XRD Pattern of hybrid heterojunction.

Within the intricate field of the hybrid heterostructure, an intriguing alignment surfaces: all eight discernible peaks harmoniously correspond to the JCPDS card 01-076-0704 [152], unequivocally signifying the pronounced presence of the hallmark hexagonal ZnO structure. However, peaks found at distinct angular orientations, which are 25.28°, 47.76°, and 63.12°. These peaks converge in alignment with a specific reference code, JCPDS card 00-001-0562 [150], closely associated with the anatase phase of TiO_2. Table 4-3: gives an indication of the heterostructure nanoscale and lattice strain . The coexistence of ZnO and TiO_2 structures suggests an interface between these two materials. From the researcher's perspective, this interface may give rise to new peaks or a distinct diffraction pattern, indicative of the synergistic effects and potential novel properties resulting from the interaction between the two different structures.

Table 4-3: XRD analysis data of TiO_2:ZnO

h k l	K	λ(nm)	β(°)	2θ(°)	D(nm) (measured)	Lattice Strain
101	0.9	0.15406	0.85	25.28 TiO_2	9.7	0.017
100	0.9	0.15406	0.492	31.834 ZnO	17.1	0.008
002	0.9	0.15406	0.492	34.412 ZnO	17.2	0.007
101	0.9	0.15406	0.492	36.345 ZnO	17.3	0.007
100	0.9	0.15406	0.787	47.765 TiO_2	11.2	0.008
110	0.9	0.15406	0.59	56.695 ZnO	15.5	0.005
103	0.9	0.15406	0.96	63.121 TiO_2	9.8	0.007
112	0.9	0.15406	0.9	68.125 ZnO	10.8	0.006

4.2.4 Bilayer Heterojunction (TiO_2 / ZnO)

Layer heterostructure XRD pattern shows only one peak at position 36.203° that matched with reference code:01-076-0704 ZnO [153], and Reference code: 00-029-1361 TiO_2 [154],as shown in Figure 4-4.

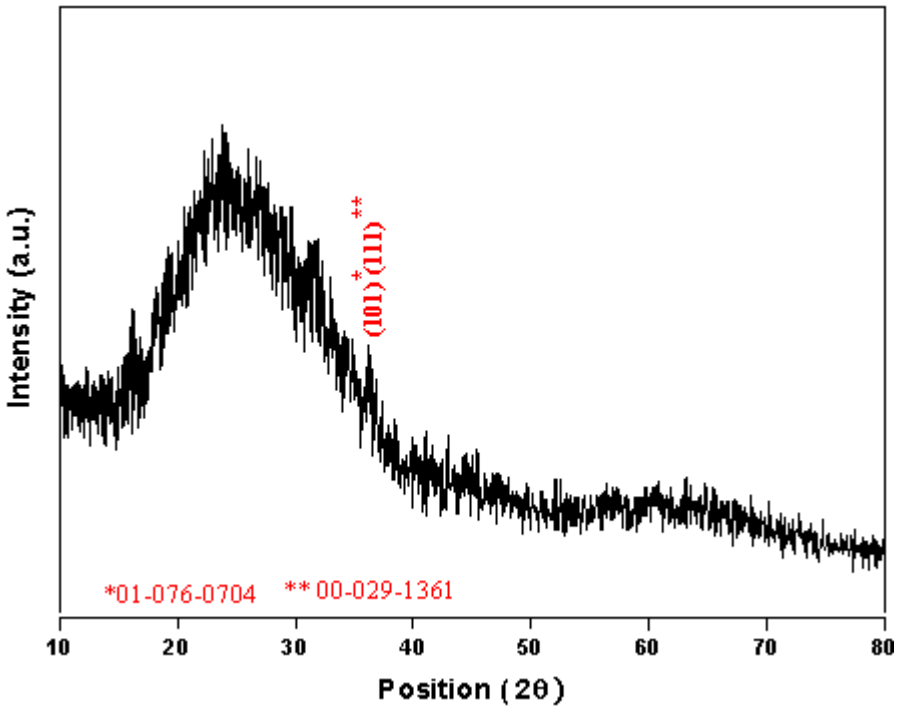

Figure 4.4; XRD Pattern of bilayer heterojunction

This peak intensity is more matched with reference code: 01-076-0704 ZnO, so this mean that the ZnO layer is more effective than that of TiO_2.

4.3 Morphological Properties (SEM)

In the pursuit of conducting a comprehensive morphological analysis of thin films, the methodology employed was Scanning Electron Microscopy (SEM). The selection of two distinct image scales was carefully considered within this approach. The initial image scale, with dimensions of 10 μm, was chosen to facilitate a panoramic examination of the thin film distribution. This broader view enabled the assessment of various characteristics, including surface roughness, the presence of cracks, and the identification of potential structural damages.

At the same time, a smaller 200 nm scale was carefully chosen for another image. The aim was to observe the sizes of crystal grains in the thin films more clearly. This resulted in a better understanding of how the grains were arranged and their sizes, granting us more insight into the structure of the films.

4.3.1 TiO_2

Through an investigation of the morphology of titanium dioxide (TiO_2) using scanning electron microscopy (SEM), noteworthy observations were made. Specifically, the study focused on the uniformity of the distribution of the thin film and the presence of clusters on its surface. The methodology adopted for depositing the TiO_2 thin film in multiple layers involved spray pyrolysis, which resulted in the outermost layer serving as a protective shield for the underlying TiO_2 material [155].

Figure 4-5 (TA) provided a visual representation of the TiO_2 thin film. The image showed that the distribution of the film was uniform, but clusters on the surface were observed, which were attributed to the rigorous annealing process [156]. Figure 4-5 (TB) presented SEM images of TiO_2, emphasizing nanoribbon-like structures.

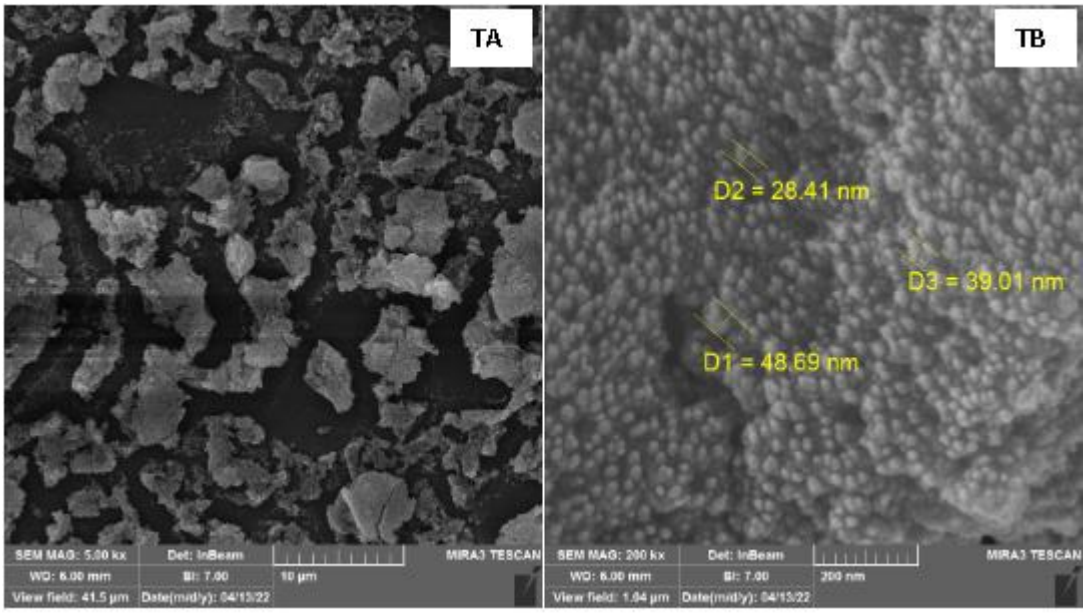

Figure 4.5 SEM images of TiO_2 thin film (TA) 10 μm scale, (TB) 200 nm scale.

These structures exhibited elongated and ribbon-like characteristics, manifesting a remarkable homeotropic alignment, indicative of a preferential orientation. Importantly, the synthesis process and annealing temperature played pivotal roles in altering the shape of the thin film particles. It should be noted that the reported bulk sizes of the TiO_2 material ranged from 28 to 48 nm. These dimensions, while significant, did not precisely correspond to individual nanoparticles (NPs). Instead, they represented aggregations of several NPs coming together to form these bulk-sized particles [157].

This comprehensive morphological analysis has shed light on the intricate behavior of TiO_2 thin films, revealing how synthesis techniques and annealing conditions could significantly impact their structural properties.

4.3.2 ZnO

The SEM images ZA and ZB in Figure 4-6 highlight the particle morphology of ZnO by revealing its spherical-like forms. This finding suggests that ZnO particles tend to form spherical shapes. The bulk diameters of the ZnO material were found to range from 44 to 166 nm. Furthermore, the thin film's dispersion shows that ZnO is consistently distributed, with no fractures or flakes on its outer shell. This

homogeneous distribution indicates that the annealing temperature was properly maintained, resulting in a uniform film distribution system[158].

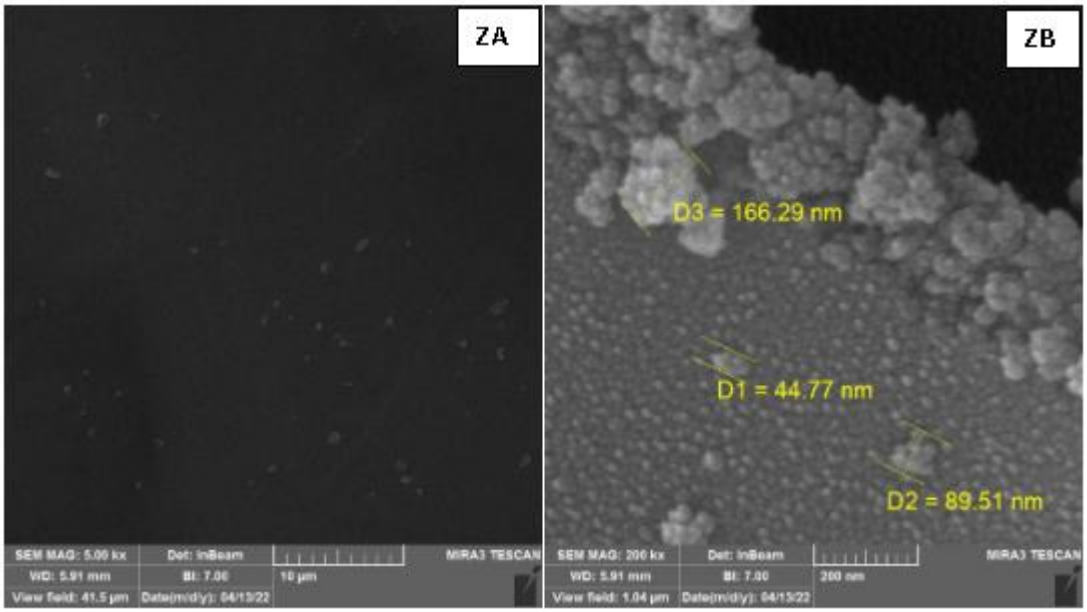

Figure 4.6 SEM images of ZnO thin film (ZA) 10 μm scale, (ZB) 200 nm scale.

4.3.3 Hybrid Heterojunction ZnO:TiO_2

The SEM images displayed in Figure 4-7 present the heterojunction mixture of the hybrid through a combination of ZnO and TiO_2 at a 1:1 ratio. It is noteworthy that the distribution observed in this mixture was found to have a uniform pattern. The image of the thin film structure of the hybrid presents an interesting overlap between the two structures of ZnO and TiO_2. This particular overlap creates an impression of the two structures blending together.

The process of synthesis and annealing temperature are significant factors that played a crucial role in the reshaping of the thin film particles. Subsequently, the bulk sizes of the hybrid material were measured to be within the range of 67-221 nm [159].

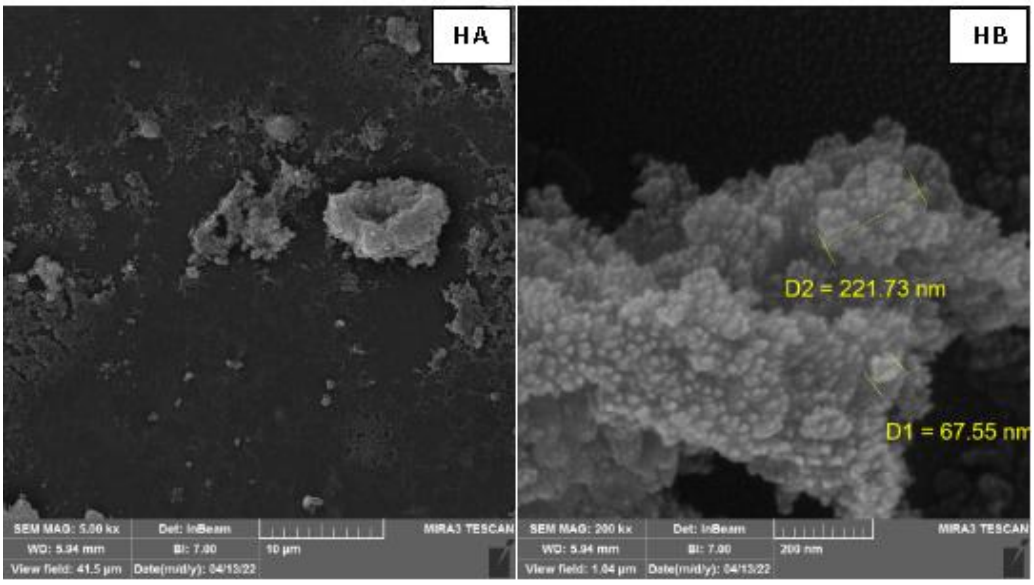

Figure 4.7 SEM images of hybrid thin film (HA) 10 μm scale, (HB) 200 nm scale.

4.3.4 Bilayer Heterojunction TiO_2/ZnO

Figure 4-8 (LA, and LB) shows a SEM image of the layered thin film that clearly shows a definite distinction between the two materials, forming a well-defined layered structure. The ZnO and TiO_2 layers are clearly distinct, indicating a layered structure. The bulk diameters of the layer were measured to be between 139 and 267 nm [160].

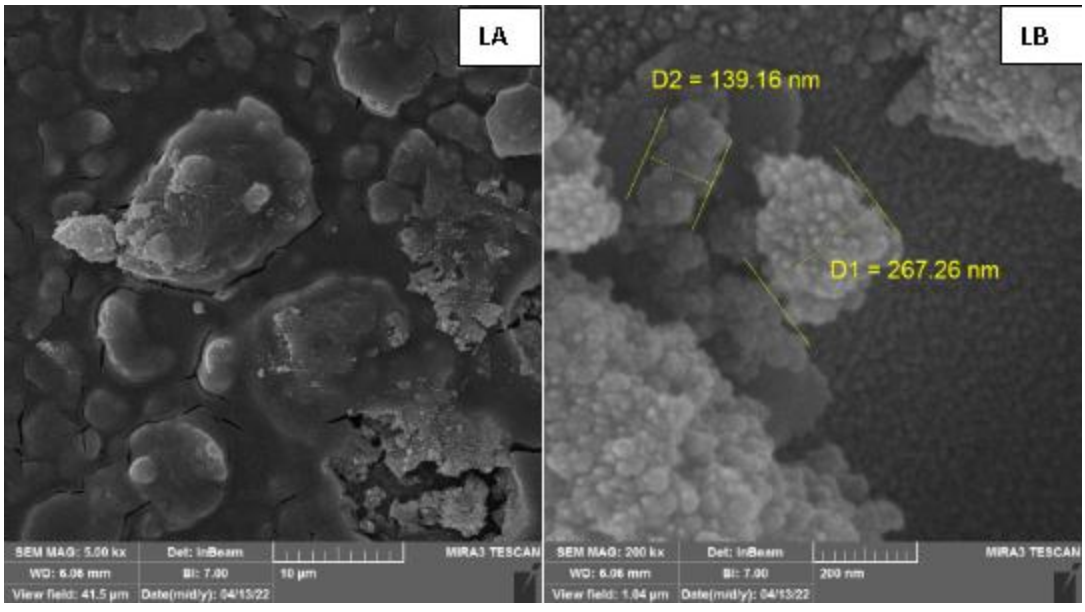

Figure 4.8 SEM images of Bilayer thin film (LA) 10 μm scale, (LB) 200 nm scale.

4.4 Optical Properties

The investigation of the optical properties was carried out through absorption spectra within the range of wavelengths from 200 to 800nm. From the absorption spectra represented in Figure 4-9, it was observed that the ZnO sample exhibited an absorption shoulder ranged from 350nm to 380nm, which was also evident in the bilayer. In contrast, the TiO_2 and hybrid thin films demonstrated clear absorption edges around 300-320nm.

Typically, ZnO and TiO_2 display optical absorption within the UV region below 400nm. The strong absorption in the UV region suggests that the photon energy is used for electron excitation from valence band to conduction band. This implies that light with photon energy that is higher or equal to the optical band gap absorbed by the semiconductor is required to enable the electron to have suitable energy to jump from the valence band to the conduction band [161].

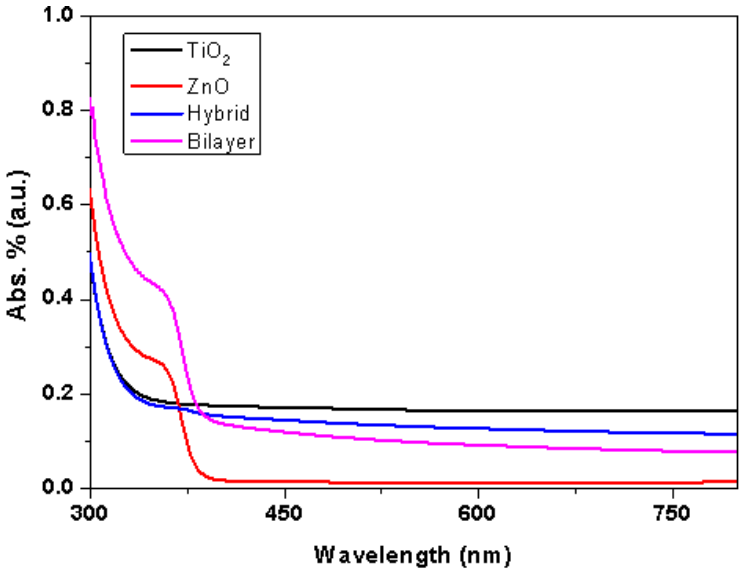

Figure 4.9 Absorption Spectrum of Thin Films .

The estimation of the optical band gap energy (Eg) was carried out using the Tauc equation [161]:

$$(\alpha hv) = C(hv - E_g)^{n} \qquad 4.3$$

Where α is the absorption coefficient, $hv(eV)$ is the photon energy, C an energy dependent constant, E_g is the optical band gap, and n is a constant depending on the band gap nature usually $n = 1/2$, 2 for allowed direct or indirect transition, respectively. The extrapolation of the linear part of the curve represents a value of Eg as shown in Figure 4.10. Band gap of the ZnO is found to be 3.3eV while the band gap of the TiO_2 is 3.75eV. On the other hand, ZnO/TiO_2 layer has exhibited a band gap of 3.23eV and the heterostructure ZnO:TiO_2 has shown a band gap of 3.57 eV.

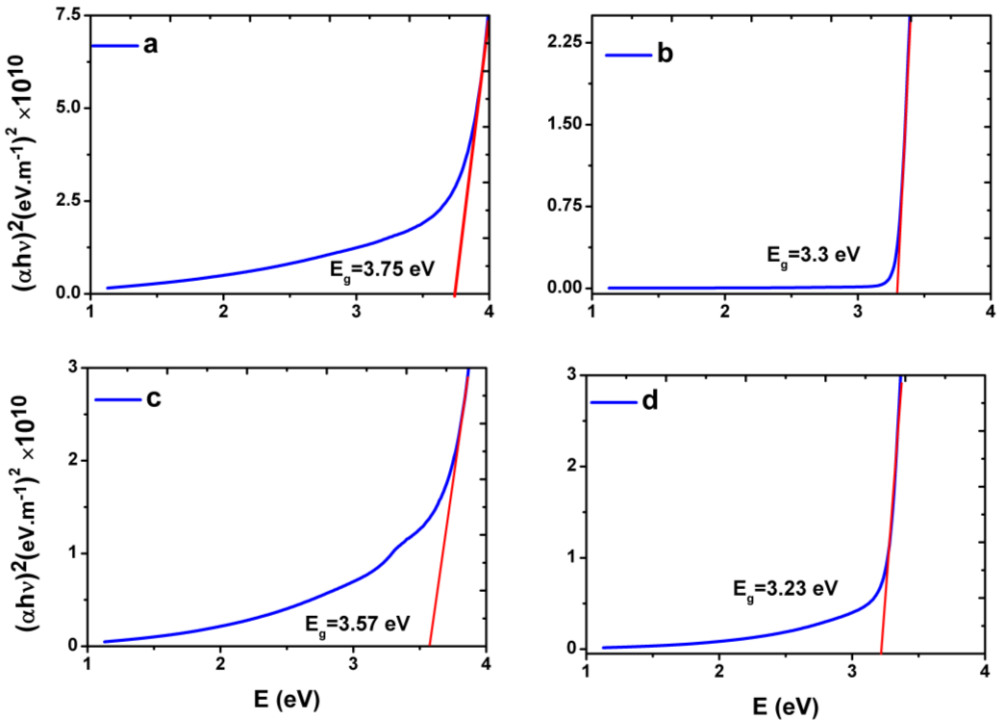

Figure 4.10 Energy gap of samples under study, a)TiO_2, b) ZnO, c)Hybrid, and d) Bilayer.

In addition, the thickness of the thin films was measured using optical thin measurements LIMF-10 (Lambda Scientific). The energy gap values and thin films thickness are presented in Table 4-4.

Table 4-4: Energy band gap measurements and thickness of investigated thin films

Thin Film Structure	**Energy gap (eV)**	**Thickness (nm)**
TiO_2	3.75	108
ZnO	3.3	100
TiO_2:ZnO (hybrid)	3.57	125
TiO_2/ZnO (bilayer)	3.23	144

4.5 Hall Measurements

According to the measurements by Hall instrument, the carrier concentration and carrier mobilities are listed in Table 4-5. All of the samples in this study have a negative carrier concentration, indicating an overabundance of electrons within the materials. This surplus of electrons is a common feature of n-type semiconductors, where electrons are the majority charge carriers [162].

Table4-5: Carrier Concentration and Mobility of Thin Film Materials

Thin Film	**Carrier Concentration N_b (cm^{-3}) $\times 10^{11}$**	**Carrier Mobility μ ($cm^2/V.s$) $\times 10^2$**
TiO_2	-1.20	2.48
ZnO	-0.969	4.65
Hybrid	-22.0	2.22
Bilayer	-1.60	2.54

TiO_2 has a carrier concentration of about -1.20×10^{11} cm^{-3}, indicating a moderate concentration of charge carriers. The related carrier mobility value for TiO_2 is roughly 2.48×10^{2} $cm^2/(V.s)$, indicating that the material had a moderate rate of charge carrier mobility.

In comparison, ZnO has a carrier concentration of roughly -9.69×10^{10} cm^{-3}, indicating a lower charge carrier concentration than TiO_2. The carrier mobility for ZnO is relatively high, at around 4.65×10^{2} $cm^2/(V.s)$. ZnO has a high carrier mobility.

When compared to the individual TiO_2 and ZnO materials, the hybrid sample, a combination of TiO_2 and ZnO, had a significantly different carrier concentration of around -2.20×10^{11} cm^3. This different carrier concentration reflects the changed electrical characteristics that can occur in composite materials.

Similarly, the bilayer sample, composed of TiO_2 and ZnO in a layered structure, had a carrier concentration of about -1.60×10^{11} cm^3. The carrier concentrations of the different TiO_2 and ZnO compounds varied.

The bilayer sample has a carrier mobility of around 2.54×10^{2} $cm^2/V.s$, indicating excellent charge transfer inside the layered structure. The carrier concentration and mobility numbers stress the possibility of tailoring electrical characteristics in heterojunctions and composite devices even further.

Carrier concentration and mobility are critical characteristics in semiconductor device design and optimization. The differences in these values discovered across different materials and their composites illustrate the fascinating electrical features that can emerge at interfaces and in composite structures [163].

Carrier mobility, a fundamental characteristic for understanding charge transfer inside materials, differs throughout the samples tested. Notably, the ZnO sample

has the maximum carrier mobility, followed by the TiO_2 sample, the bilayer sample, and finally the hybrid sample.

It is critical to emphasize the importance of carrier concentration and mobility values in understanding the electrical behavior of these materials. These values provide information about the efficiency of charge carrier transport within each material, which has practical significance for device applications and a better knowledge of their electrical properties [164].

4.6 I-V Characteristics

The purpose of this study is to look at the direct current resistance derived from the current-voltage characteristics of thin films such as TiO_2, ZnO, Hybrid, and bilayer formed on various substrates such as ITO-coated glass, Si/SiO_2, and interdigitated electrodes (ID). Resistance values, specifically resistance in the dark (R_{OFF}) and resistance under illumination (R_{ON}), as well as R_{OFF}/R_{ON} ratios, were examined to provide insight into how different substrates influence the resistive behavior of these materials.

Figures 4-11, 4-12, and 4-13 depict the I-V characteristics of the ITO, Si/SiO_2, and IDEs substrates, respectively. It is evident that the behavior of the I-V curve varies depending on the type of substrate employed in the investigation.

In the specific case of the ITO substrate, the I-V characteristic exhibits a consistent pattern in both the forward and reverse bias directions. This regularity is attributed to the transparent nature of the ITO substrate which permits a significant amount of light to pass through it from the top. Furthermore, the sandwich structure of the thin film can be analogized to a parallel connection of resistors. Since ITO is a conductive material with low resistance, the I-V behavior remains uniform [165]. Detailed values of these resistances can be found in Table 4-6.

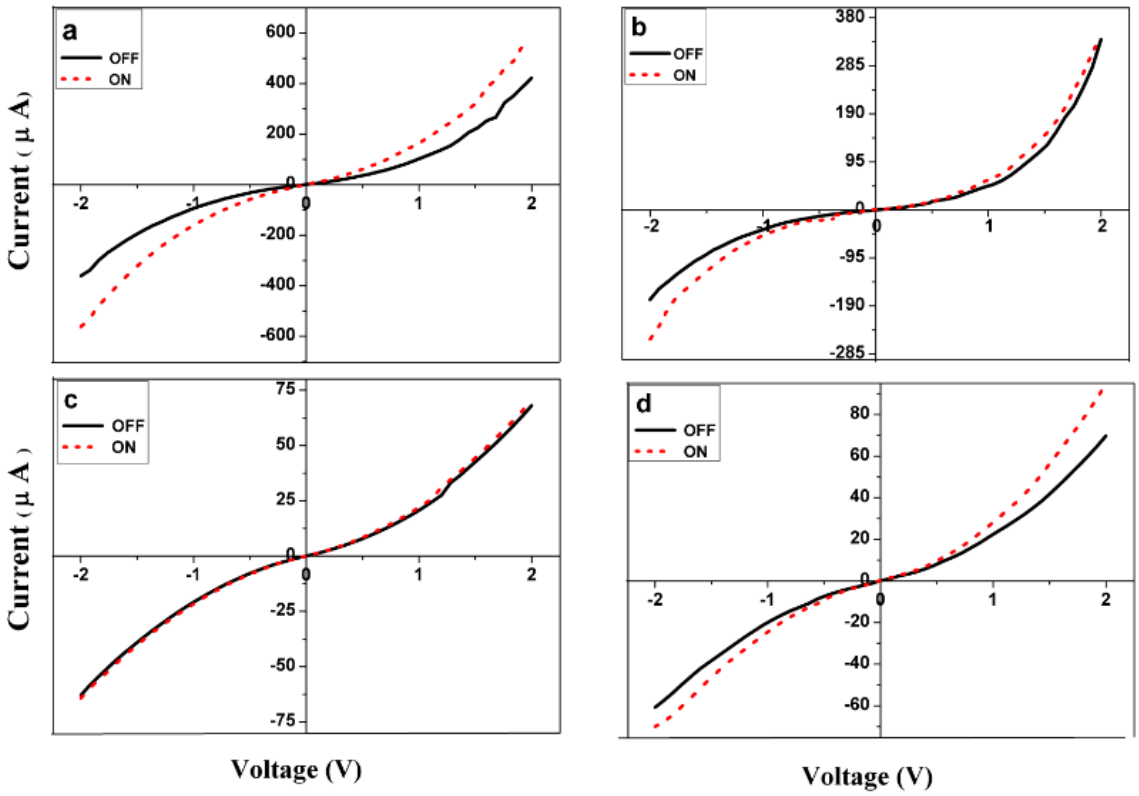

Figure 4.11 I-V ON-OFF ITO substrate behavior of (a)TiO_2, (b) ZnO, (c) Hybrid, and (d) Bilayer.

TiO_2 demonstrated resistance values of R_{OFF} and R_{ON} at 15.94 kΩ and 8.91 kΩ, respectively, resulting in an R_{OFF}/R_{ON} ratio of 1.79. This indicates that TiO_2 on ITO exhibits a photoresistive response of moderate magnitude.

ZnO, exhibited higher resistance values, with R_{OFF} and R_{ON} at 38.88 kΩ and 31.23 kΩ, respectively, resulting in an R_{OFF}/R_{ON} ratio of 1.24. The photoresistive behavior of ZnO on ITO is less pronounced in comparison to TiO_2 [166].

The R_{OFF}/R_{ON} ratios of hybrid and bilayer thin films on ITO were 1.06 and 1.36, respectively. These materials displayed varying degrees of photoresistive behavior on the ITO substrate, with hybrid demonstrating a slightly weaker response than bilayer.

Table 4-6:Resistance values of thin films ITO substrateat ON-OFF state.

Structure	**R_{OFF} (kΩ)**	**R_{ON}(kΩ)**	**R_{OFF}/R_{ON}**
TiO_2	15.94	8.91	1.79
ZnO	38.88	31.23	1.24
Hybrid	68.19	64.5	1.06
Bilayer	69.28	50.81	1.36

The Si/SiO_2 substrate shown in Figure 4-12 exhibits distinctive I-V behavior in the thin film structures, particularly in the forward bias region. Upon exposure to light, all structures demonstrate reduced resistance and increased current flow. However, in the reverse bias region, all structures align closely with the x-axis, indicating limited current flow[167].

Among the individual films, TiO_2 displays a resistance of 2.79×10^5 Ω with the light off, which decreases to 1.90×10^5 Ω with the light on, resulting in an R_{ON}/R_{OFF} ratio of 0.68. ZnO exhibits even lower resistance values, measuring 1.65×10^5 Ω with the light off and 1.37×10^5 Ω with the light on, corresponding to an R_{ON}/R_{OFF} ratio of 0.83.

Interestingly, the hybrid structure demonstrates higher resistance, registering 8.38×10^5 Ω with the light off and 1.60×10^5 Ω with the light on. This substantial reduction in resistance results in a notably low RON/ROFF ratio of 0.19, signifying efficient utilization of the generated photocurrent. Similarly, the bilayer structure exhibits a resistance of 3.46×10^6 Ω with the light off, which decreases to 1.70×10^6 Ω with the light on, resulting in an R_{ON}/R_{OFF} ratio of 0.49.

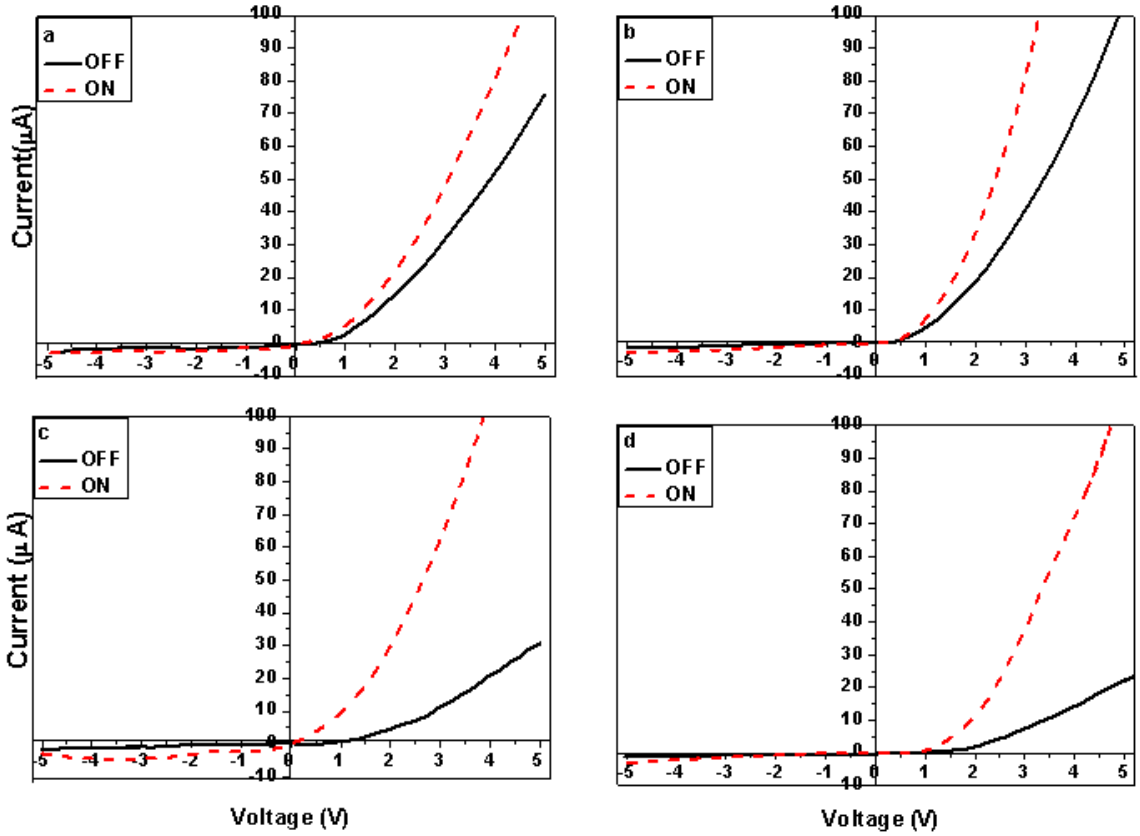

Figure 4.12 I-V ON-OFF Si/SiO_2 substrate behavior of (a)TiO_2, (b) ZnO, (c) Hybrid, and (d) Bilayer.

These observed resistance characteristics imply an enhancement in the conductivity of the thin film structures under light illumination, attributed to improved charge carrier generation, transport, and collection mechanisms. The variations in resistance values among the structures underscore the importance of material composition and structural design in determining conductivity and photoresponse [168].

The I-V behavior and resistance characteristics have been thoroughly analyzed for TiO_2, ZnO, hybrid, and bilayer thin film structures, particularly in the context of photovoltaic applications. The forward bias behavior clearly indicates increased current flow under light illumination, signifying improved conductivity. Conversely, in the reverse bias region, all structures exhibit alignment with the x-axis, indicating restricted current flow.

Significantly, the measured resistance values reveal a consistent reduction in resistance for all structures under light illumination. Among these structures, the hybrid structure demonstrates the most substantial decrease in resistance, highlighting its efficient photoconductive response. Furthermore, it is noteworthy that ZnO on Si/SiO_2 exhibits heightened sensitivity to light, characterized by an R_{OFF}/R_{ON} ratio of 4.49. Additionally, hybrid and bilayer thin films on Si/SiO_2 display R_{OFF}/R_{ON} ratios of 5.28 and 4.72, respectively, underscoring their substantial photoresistive responses when placed on Si/SiO_2.

Table 4-7: Resistance values of thin films Si/SiO_2 substrate at ON-OFF state.

Structure	**R_{OFF}(kΩ)**	**R_{ON}(kΩ)**	**R_{OFF}/ R_{ON}**
TiO_2	75	30.2	2.48
ZnO	30.2	6.72	4.49
Hybrid	102	19.3	5.28
Bilayer	136	28.8	4.72

It is worth mentioning that Si/SiO_2 is a p-type semiconductor, falling within the resistance range typical of semiconductors. This property suggests that this substrate may act as a potential heterojunction for the thin films deposited on it, facilitating intriguing semiconductor behavior and interactions.

Examining the I-V properties of thin films placed on an ID substrate, as shown in Figure 4-13, provides unique insights into lateral behavior. When working with TiO_2, it is clear that its behavior remains mostly unchanged at low applied voltage levels. However, as the voltage exceeds 150 volts, the behavior changes. This means that TiO_2 does not exhibit lateral behavior, demonstrating its resistance to electron transport. This behavior can be linked to two essential components. For starters, the tiny particle size of TiO_2 increases charge carrier confinement. Second, TiO_2 has a greater electron-hall density because of its huge energy gap and tiny crystal size. This increased density, in turn, increases the resistance to

electron transport inside the material. While it is observed that ZnO behaves somewhat ohmic, which means that the increase in the relationship between voltage and current remains mostly constant in this type of behavior [169-170].

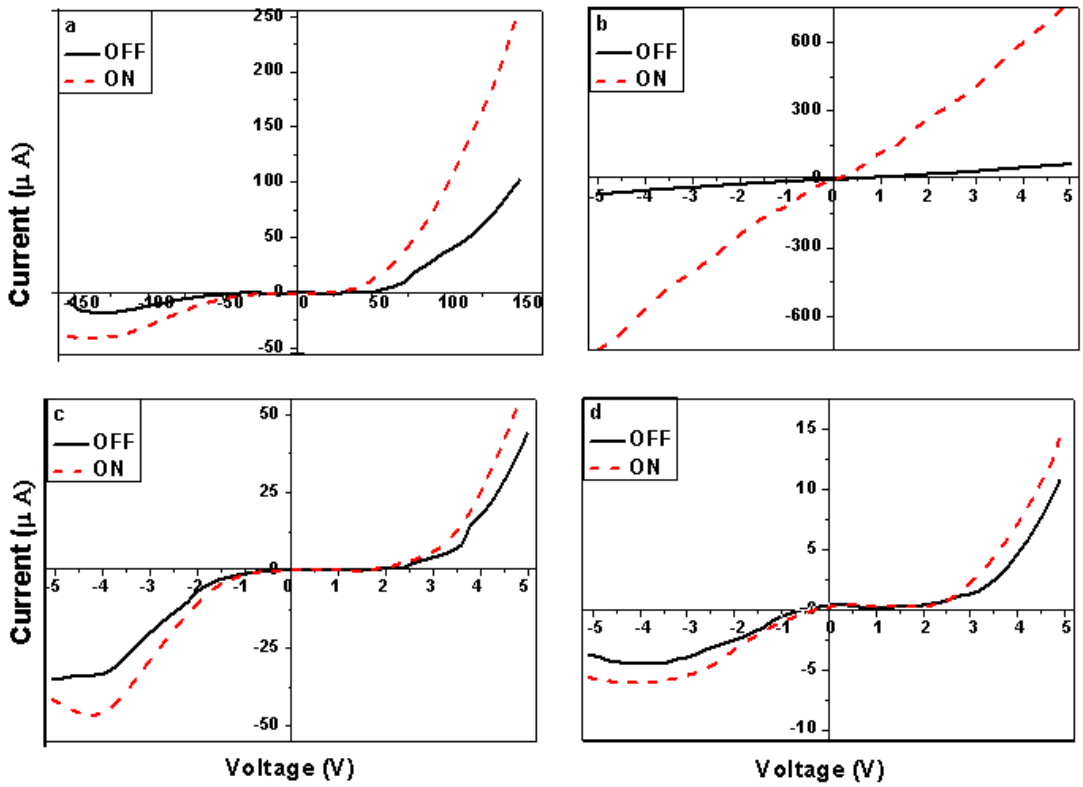

Figure 4.13 I-V ON-OFF interdigitated electrode substrate behavior of (a)TiO_2, (b) ZnO, (c) Hybrid, and (d) Bilayer.

When deposited on the IDE substrate, TiO_2 exhibited an R_{OFF}/R_{ON} ratio of 3.84, indicating moderate photoresistance. ZnO on the IDE substrate displayed a notably high R_{OFF}/R_{ON} ratio of 10.91, underscoring its exceptional sensitivity to lateral illumination. Hybrid and bilayer thin films on IDE showed R_{OFF}/R_{ON} ratios of 2.46 and 3.90, respectively, signifying their unique photoresistive characteristics in this lateral configuration [171-172].

Table 4-8: Resistance values of thin films interdigitated electrode substrate at ON-OFF state.

Structure	**R_{OFF}(kΩ)**	**R_{ON}(kΩ)**	**R_{OFF}/R_{ON}**
TiO_2	2×10^4	5.2×10^3	3.84
ZnO	96.2	88.1	10.91
Hybrid	1430	580	2.46
Bilayer	1500	384	3.90

This study reveals that the photoresistive behavior of thin films, including TiO_2, ZnO, hybrid, and bilayer, is significantly influenced by the choice of substrate. Si/SiO_2 substrates amplify the photoresistive response of these materials, with ZnO demonstrating particularly high sensitivity. On the other hand, IDEs substrates result in distinct lateral photoresistive behaviors, with ZnO exhibiting exceptional sensitivity [173].

The variation in resistance values observed between different substrates can be ascribed to a multitude of factors, encompassing the intrinsic characteristics of the materials, the nature of the substrates, and the interactions between the thin films and substrates. There exist various potential explanations for these observed disparities. Diverse substrates possess unique chemical compositions and surface properties, thereby leading to dissimilarities. Moreover, the interaction between the thin film and the substrate has the capacity to exert an influence on the electronic and structural properties of the thin film, consequently impacting its photoresistive behavior.

The overall electrical behavior of the thin film is significantly influenced by the conductivity of the substrate. Substrates with different conductivities can directly affect the charge transport mechanisms within the thin film, thereby causing variations in resistance values[174].

The orientation and crystal structure of the thin film may be influenced by the substrate. Modifications in the crystal structure have the potential to alter the electronic properties of the material, thereby impacting its conductivity and response to light [175].

The transparency of the substrate, particularly in the case of ITO, has an impact on the amount of incident light that reaches the thin film. This, in turn, can affect the photoresistive behavior, as the availability of light to induce changes in resistance may be either increased or decreased. The interfaces between the thin film and the substrate can introduce additional electronic states or defects, thereby influencing the dynamics of charge carriers and, consequently, the photoresistive response.

Disparities in the composition and thickness of the thin film across different substrates can result in differences in the density of charge carriers and their mobility, thereby affecting the overall resistance.

In the case of hybrid and bilayer structures involving the combination of TiO_2 and ZnO, the synergistic effects and interactions between these materials may vary depending on the substrate, thereby leading to differences in the photoresistive behavior.

In the case of interdigitated electrodes, the unique configuration can enhance the sensitivity of the thin film to light. The design of the electrodes may introduce localized variations in the strength of the electric field, thereby impacting the photoresistive response [176].

4.7 D.C. Thermal Conductivity

The Arrhenius equation serves as a powerful tool for understanding the relationship between reaction rates and temperature. To investigate the thermal dependence of conductivity, the activation energy (E_a) was calculated using the

Arrhenius equation [131] . Figure 4-13; shows three proposed regions covering a temperature range of 290 K to 490 K.

The acquired activation energy (E_a) values offer valuable insights into the stability and thermal sensitivity of these materials. The activation energy values provide a glimpse into the stability of diverse structures. Lower activation energy values indicate greater stability, as they suggest that a lower energy barrier must be overcome for reactions or processes to occur[132].

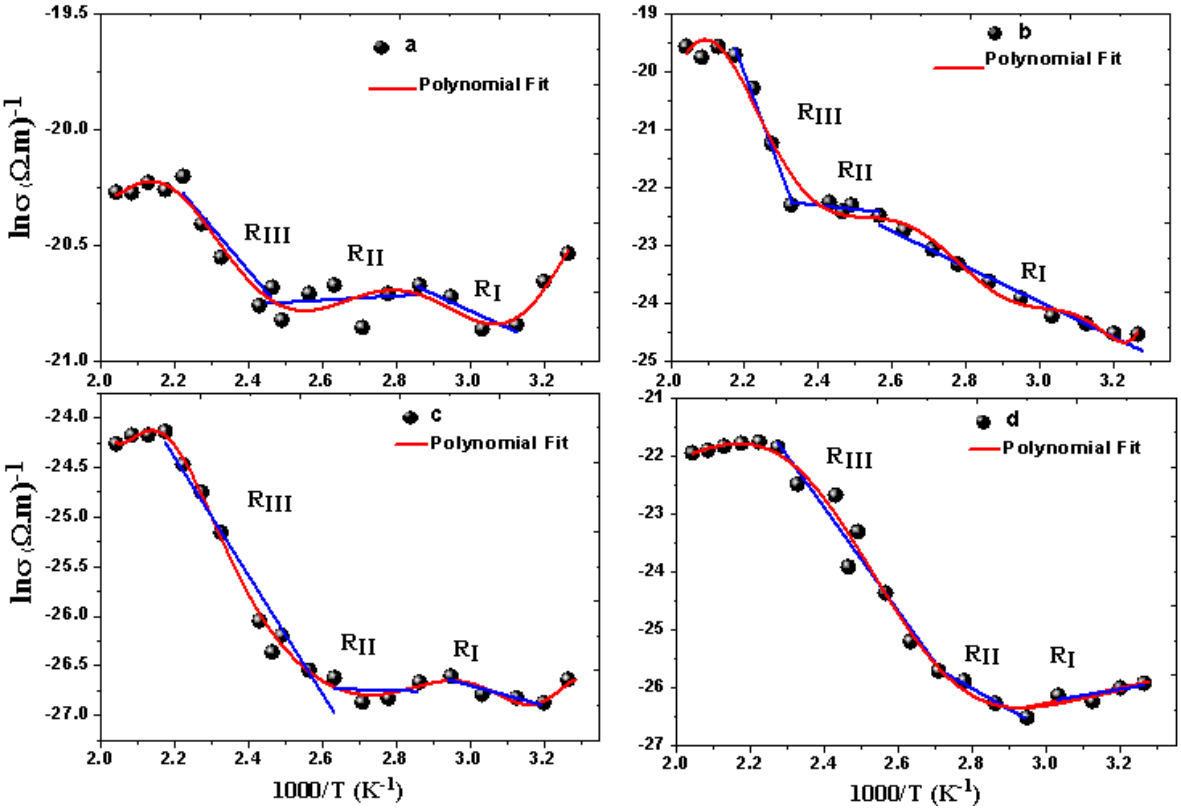

Figure 4.14 D.C. Thermal behavior, a) TiO_2, b) ZnO, c) ZnO: TiO_2, and d) TiO_2/ZnO.

TiO_2 is the most stable structure, with the lowest activation energy values across all regions, consistent with its proven role as a stable and dependable material in various applications. The significant difference in activation energy values between TiO_2 and the other structures in all regions highlights the remarkable temperature resilience of TiO_2. This behavior can be attributed to its robust crystal structure, strong chemical bonds, and inherent thermal stability. As the

temperature increases, the relative stability of TiO_2 becomes even more apparent, making it an ideal choice for applications that demand uniform performance across a broad temperature range [133].

In contrast, ZnO exhibits relatively higher activation energy values, indicating increased sensitivity to temperature changes. This characteristic can be attributed to the nature of its crystal lattice and weaker interatomic bonds. The increasing activation energy with temperature implies that the structural changes or reaction rates within ZnO are more prone to thermal fluctuations. This aspect could influence the behavior of the material in high-temperature environments, where degradation or altered performance might occur more readily[134].

Comparison of the two heterostructures, bilayer and hybrid, reveals intriguing differences in their temperature response. The lower activation energy value of hybrid indicates its greater stability compared to bilayer. This discrepancy can be attributed to the hybrid nature, where the close interaction between the two materials might impart unique thermal properties that shield it from temperature-induced changes to a greater extent.

The observed behaviors have implications for the practical application of these structures. TiO_2's stability makes it an attractive candidate for use in high-temperature environments, such as catalytic processes or electronic components in harsh conditions. On the other hand, the temperature sensitivity of ZnO might be harnessed for certain sensing applications, where its response to temperature variations could provide useful information. The distinct characteristics of the heterostructures offer opportunities for tailoring materials with specific thermal properties, enabling innovative design in nanotechnology and materials engineering [135].

Table 4-9: The activation energy of the four structures according to the region.

Thin film Structure	Region I	Region II	Region III
	E_a (eV)	E_a (eV)	E_a (eV)
TiO_2	0.062	0.0078	0.162
ZnO	0.248	0.0598	1.494
Hybrid	0.0866	0.009	0.514
Bilayer	0.113	0.309	0.768

The activation energy values obtained through the Arrhenius equation reveal significant insights into the stability and temperature sensitivity of TiO_2, ZnO, and their heterostructures. TiO_2's remarkable temperature resilience, ZnO's temperature sensitivity, and the unique behavior of the heterostructures open avenues for designing materials with tailored thermal properties.

4.8 Photoresistance

The results section focuses on photoresistance as a crucial metric to assess a material's response to light. Photoresistance, indicative of changes in electrical properties under illumination, offers insights into the material's behavior in sensors and optoelectronic devices. The experimental setup involved stabilizing samples under continuous visible light, and three substrates (ITO-coated glass, Si/SiO_2, and IDEs) were used to investigate various behaviors. The discussion covers key aspects such as starting position, photoresponse time, photodecay time, average current amplitude, and total illumination time, providing a comprehensive understanding of both pure thin film and heterojunction behavior.

4.8.1 ITO substrate

Examining Figure 4-15, and starting from the initial position prior to the start of the initial illumination period, it is clear that each thin layer does not begin at zero, but rather at a different higher value. This number varies from thin film to thin film, demonstrating that the phenomena of dark current affects all thin films. The

current that flows through the detector in the absence of incident photon flux is referred to as dark current. The importance of dark current resides in its ability to identify the fundamental current level that photocurrent must exceed in order to be detected.

It is apparent that TiO_2 reacts to light, albeit slowly, and that when the light is turned off, it responds slowly again but is unable to recover to the initial illumination value. This pattern is repeated for each of the three light times. While the beginning value of ZnO's illumination falls below the preceding value. While the first value of ZnO illumination is lower than the previous value, this trend is replicated across all illumination times. TiO_2 primarily shows the electron scavengers effect due to adsorbed oxygen at the surface [141].

Because oxygen is the most reactive gas in air, it can be adsorbed on the surface of TiO_2. Adsorbed oxygen molecules act as electron scavengers and are reduced to, increasing the photoresistance of TiO_2 during the illumination time. Furthermore, because the energy gap is larger than that of ZnO, this affects how quickly electrons flow from the valence band to the conduction band [142-143].

The trapping process is linked to the long fall time. Because of the prolonged illumination time, the increased electron density in the conduction band will enhance the rate of recombination. For the reasons stated above, when the light is turned on, the material resists photoconductivity and has an effect on the recovery of electrons, resulting in a discrepancy between the initial starting value and the other starting values [144].

ZnO thin film acts completely differently from TiO_2, which could be ascribed to less oxygen on the surface, resulting in a depletion area [145]. Under continuous illumination, holes grow and act as states that capture air, causing the surface to lose oxygen. As a result, the depletion layer would be smaller than before. The photoconductivity responses of the hybrid, and bilayer heterojunction and, which

are essentially equal to TiO_2 and ZnO, respectively. TiO_2 has a stronger effect in ZnO: TiO_2, which may suggest that TiO_2 overlaps with ZnO and has twice as many oxygen molecules as ZnO [146-147].

Furthermore, TiO_2 has a larger energy band gap than ZnO. When ZnO is deposited over a TiO_2 layer in a TiO_2/ ZnO heterostructure, the behavior is more akin to ZnO, resulting in ZnO being dominant and delaying rise and fall times due to the absence of TiO_2 [148].

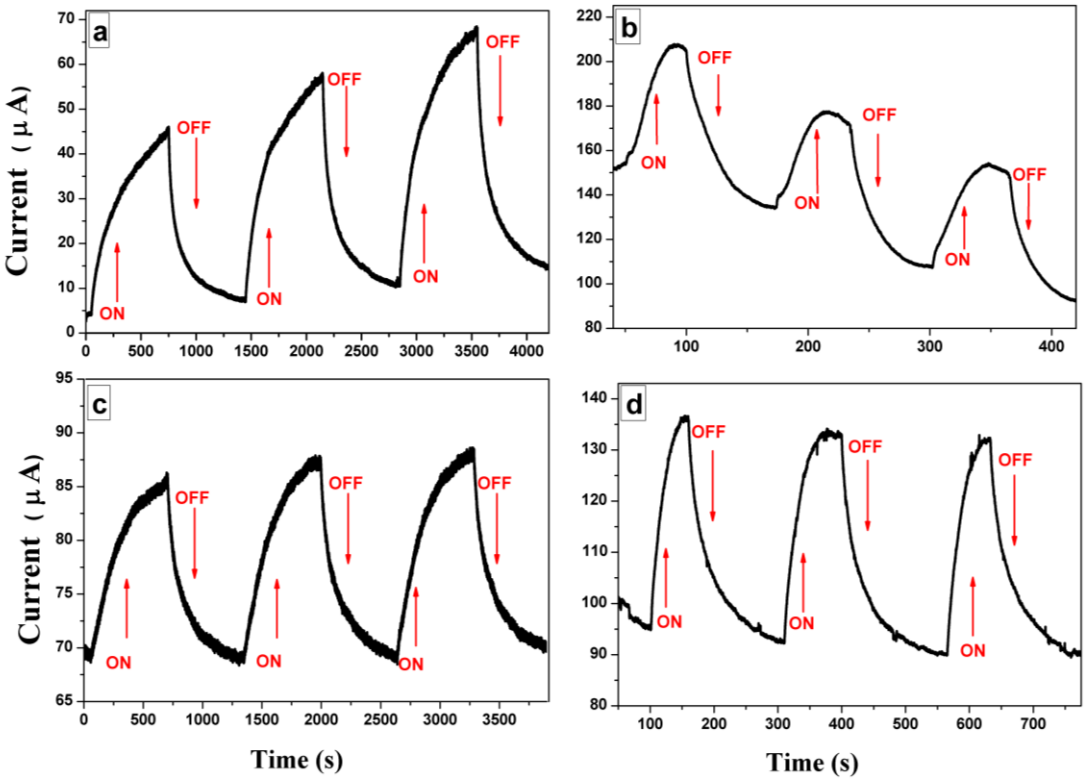

Figure 4.15 Photocurrent behavior using ITO substrate for a)TiO_2, b)ZnO, c)Hybrid, and d) Bilayer.

In both illustrated cases of heterojunctions, as shown in Figure 14-4 (c, and d), there exists a propensity towards regular patterns. The energy gap of both heterojunctions closely approximates that of TiO_2 and ZnO, correspondingly. This implies that in both cases, the presence of electron scavengers and electron traps is significantly diminished, leading to a more uniform and predictable behavior [149]. Although TiO_2 and ZnO may individually display inclinations towards

being influenced by electron scavengers and traps, the combination of these materials is able to mitigate these effects. The electron scavengers that may potentially impact TiO_2 can be rendered less effective due to the existence of ZnO, and vice versa for electron traps in ZnO. This combination is capable of establishing a harmonious environment where the adverse effects are minimized [150].

Table 4-10: Photoresistance characteristics of thin films on ITO substrate.

Thin Film	S.T. (μ A)	I_{ph} (μA)	I.P. (s)	R.T. (s)	F.T. (s)	$R_{ph}\times10^5$ (Ω)	$\rho_{ph}\times10^9$ (Ω.m)
TiO_2	4.2	11.03	750	459	258	4.53	1.57
ZnO	1.5	43.01	100	25	37	1.16	0.436
Hybrid	70.0	18.72	750	347	305	2.67	0.801
Bilayer	100.0	203.45	150	34	47	0.246	0.0640

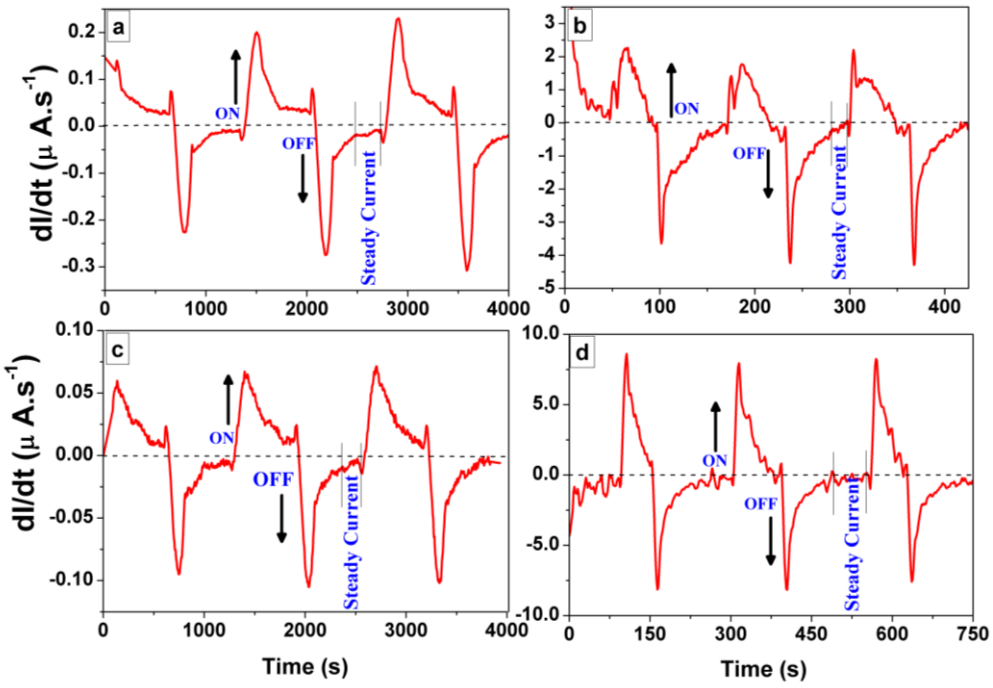

Figure 4-16 First deravitive of photocurrent behavior using ITO substrate for a)TiO_2, b)ZnO, c) hybrid, and d) bilayer.

In order to enhance the clarity of the behavior, the temporal behavior of the photocurrent in Figure 4-15 was subjected to the first derivative. It is indicated that upon activation of the light source, the initial derivative of the current with respect to time (dI/dt) reaches its maximum height and subsequently decreases until it attains a state of stability[151].

This occurrence can be elucidated as follows: Upon activation of the light source, electron-hole pairs are generated within the ZnO:TiO_2 thin films. This signifies that electrons are excited from the valence band to the conduction band, thereby leaving behind holes in the valence band. The initial surge of electron-hole pairs precipitates an increase in photocurrent [152].

Consequently, dI/dt experiences a rapid initial rise, culminating in its maximum value. In the aftermath of the initial surge of electron-hole pairs, a fraction of these carriers recombine, leading to a decrease in the photocurrent. This transient response is characterized by the decay in the rate of change of current, as manifested by the diminishing dI/dt [153].

Throughout this phase, carriers are still being generated and recombined, albeit the rate of recombination gradually attains equilibrium with the rate of carrier generation, thereby instigating the decrease in dI/dt. Ultimately, a state of stability is attained. In this state of stability, the rate of carrier generation resulting from the incident light is counterbalanced by the rate of carrier recombination. At this juncture, the system attains a dynamic equilibrium and the photocurrent remains relatively constant. dI/dt plateaus, suggestive of the stabilization of the rate of change of current, signifying that the system is no longer undergoing rapid changes [154].

Table 4-11: dI/dt values at ON-OFF states for thin films on ITO.

Thin Film	(dI/dt) ON ($\mu A.s^{-1}$)	(dI/dt) OFF ($\mu A.s^{-1}$)
TiO_2	0.165	-0.265
ZnO	8.21	-4.04
Hybrid	0.065	-0.23
Bilayer	8.13	-7.8

This behavior is frequently observed in photocurrent measurements conducted on semiconductor materials under illumination. The initial ascent in dI/dt followed by the subsequent decay, prior to reaching a state of stability, mirror the transient response of the material upon the abrupt introduction of light and the establishment of an equilibrium between carrier generation and recombination.

In addition, it can be observed from Figure 4-15 that the behavior of hybrid and bilayer heterojunction thin films is characterized by regularity. This implies that the presence of heterojunctions contributes to a consistent behavior in the photocurrent. Additionally, it is noteworthy that the photoresistance is minimized in the case of bilayer heterojunctions, while it is maximized in the presence of TiO_2.

4.8.2 Si/SiO_2 Substrate

Thin films of TiO_2 and ZnO, as well as the consequent heterojunction, display regular behavior with a relatively small initial reaction when deposited on a Si/SiO_2 substrate. Figure 4-16; depicts this regular pattern, specifically the time-dependent rise in current during illumination. Several important elements contribute to this consistency. For starters, the Si/SiO_2 substrate has a strong light-absorption capability, leading in a poor transmittance. As a result, a considerable part of incident light is transformed into light energy efficiently. This phenomenon has a considerable impact on the photocurrent's behavior in the system [155].

Furthermore, Si/SiO_2 is a p-type semiconductor with a tiny energy band gap. This characteristic allows charge carriers to pass from the valence level to the conduction level within the substrate. The n-type thin films placed on the Si/SiO_2 substrate form a heterojunction. In this structure, the interaction of the positive and negative charge carriers results in a relatively tiny depletion area, allowing for easy charge transfer [156].

The starting photocurrent values, which are 0.18 μA for TiO_2, 2.58 μA for ZnO, 1.25 μA for the hybrid configuration, and 0.84 μA for the bilayer, are notably low and can be considered close to zero. These low initial values serve as strong indicators of the photocurrent response's efficiency, which, in turn, signifies a desirable behavior in these thin films.

Another crucial aspect to consider in evaluating this behavior is the illumination time and response time, both of which are elucidated in Table 4-12. The uniform illumination period of 10 seconds across all thin films is indicative of their consistent and regular response to incident light. However, it's imperative to delve into the response time (R.T.), which denotes how rapidly the photocurrent rises upon illumination[157-158].

In this context, the TiO_2 thin film demonstrates a response time of 0.061 seconds, ZnO exhibits 0.141 seconds, the hybrid thin film showcases 0.383 seconds, and the bilayer film reveals 3.423 seconds. Interestingly, the bilayer film demonstrates the longest response time among the films.

To gain deeper insights into the efficiency and dynamics of the photocurrent response, it is valuable to consider the relationship between photocurrent amplitude and response time. Dividing the photocurrent amplitude by the response time yields values of 93 $\mu A \cdot s^{-1}$ for TiO_2, 538 $\mu A \cdot s^{-1}$ for ZnO, 221 $\mu A \cdot s^{-1}$ for the hybrid, and 674 $\mu A \cdot s^{-1}$ for the bilayer configuration. These results underscore how the photocurrent amplitude increases over time.

It is important to note that while a shorter response time might intuitively appear preferable, these results reveal that the efficiency of the behavior cannot be solely assessed based on response time. Instead, when considering both the photocurrent amplitude and response time, it becomes apparent that the bilayer heterojunction stands out with the highest value, indicating its excellent performance in this context

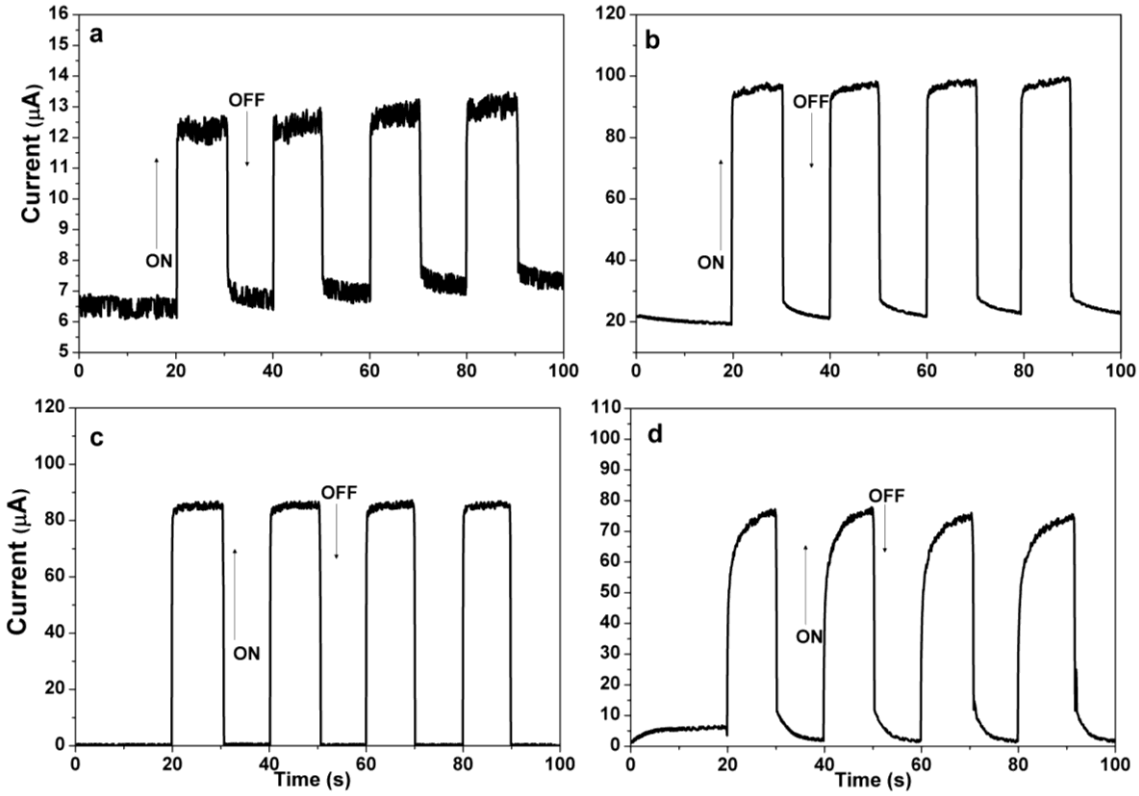

Figure 4.17 Photocurrent behavior using Si/SiO_2 substrate for a)TiO2, b)ZnO, c)Hybrid, and d) Bilayer.

The photoresistance and, consequently, the photoresistivity of these thin films, as depicted in Table 4-12, demonstrate an interesting trend. Specifically, the photoresistivity values of the heterojunctions, namely the hybrid and bilayer configurations, are notably the lowest among the thin films. This observation holds significant implications, suggesting that the heterojunctions exhibit enhanced photoresistive properties when deposited on a Si/SiO_2 substrate.

In other words, the hybrid and bilayer heterojunctions, when interfaced with the Si/SiO_2 substrate, showcase a heightened sensitivity to changes in resistance induced by incident light. This enhanced photoresistive behavior can be attributed to the intricate interplay of materials and the substrate's influence. It signifies their potential utility in applications where precise control of resistance in response to varying light conditions is required, such as in photodetectors and optoelectronic devices.

Table 4-12: Photoresistance characteristics of thin films on Si/SiO_2 substrate.

Thin Film	**S.T. (μ A)**	**I_{ph} (μA)**	**I.P. (s)**	**R.T.(s)**	**F.T. (s)**	**$R_{ph}\times10^5$ (Ω)**	**$\rho_{ph}\times10^7$ (Ω.m)**
TiO_2	0.18	5.65	10	0.061	0.077	8.85	123
ZnO	2.58	75.86	10	0.141	0.2216	0.659	9.89
Hybrid	1.25	84.47	10	0.383	0.3826	0.592	7.10
Bilayer	0.84	74.14	10	0.11	1.001	0.674	7.02

Figure 4-17 provides a valuable insight into the photocurrent behavior of these thin films when utilizing a Si/SiO2 substrate. It depicts the first derivative of the photocurrent, showcasing a regular trend where the photocurrent rises and falls in a consistent manner without any significant decay. The behavior is characterized by reaching a maximum height and then maintaining a steady state, indicating the stable performance of these thin films.

Table 4-14 further illustrates the regularity and responsiveness of these thin films by presenting the average values of the first derivative of photocurrent, denoted as (dI/dt), for both the ON and OFF states. Notably, the data reveals that the fastest response is attributed to the hybrid heterostructure.

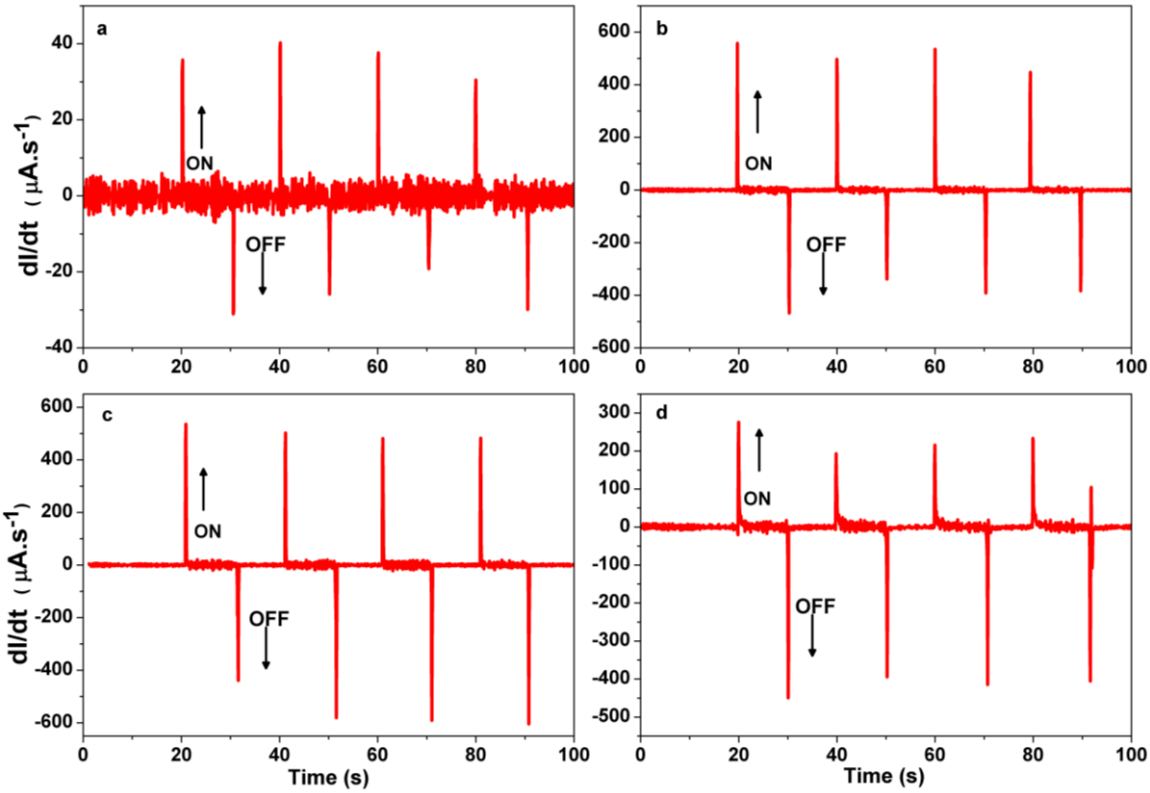

Figure 4-18 First derivative of photocurrent behavior using Si/SiO_2 substrate for a)TiO2, b)ZnO, c) hybrid, and d) bilayer.

These results clearly indicate that the hybrid heterostructure exhibits the fastest response in both the ON and OFF states, underscoring its excellent performance in terms of rapid changes in photocurrent.

Table 4-13: dI/dt values at ON-OFF states for thin films on Si/SiO_2.

Thin Film	**(dI/dt) ON ($\mu A.s^{-1}$)**	**(dI/dt) OFF ($\mu A.s^{-1}$)**
TiO2	35	-25
ZnO	502	-403
Hybrid	508	-521
Bilayer	190	-422

4.8.3 Interdigitated Electrode Substrate

The hybrid and bilayer structures, which incorporate both TiO_2 and ZnO constituents, exhibit distinguishable photocurrent responses that lie within the

range of behaviors observed in the individual materials. This intermediate behavior can be primarily ascribed to the distinctive amalgamation of structural properties and energy band gaps intrinsic to these heterojunction systems.

The complicated relationship between crystallite size and crystal structure remains relevant in these heterojunction systems, influencing their responses to photocurrent and resistance profiles [159].

While TiO_2 contributes smaller, more uniform crystallites as well as the anatase crystal structure, ZnO adds larger crystallites and the wurtzite crystal structure to the mix. Furthermore, the key component influencing the difference in photocurrent responsiveness between TiO_2 and ZnO on the IDE substrate remains their unique energy band gaps. TiO_2's larger band gap makes it less sensitive to visible light, resulting in a lower photocurrent. In contrast, ZnO's narrower band gap increases its sensitivity to light, resulting in a larger photocurrent [160].

The combination of TiO_2 and ZnO in the hybrid and bilayer structures yields band gaps that are intermediate in magnitude compared to those of the individual materials [161]. The observation -as shown in Figure 4-18- that the lateral behavior of TiO_2 is not significantly influenced by incident light and exhibits a very weak impact can likely be attributed to the specific configuration and geometry of the interdigitated electrodes (IDEs) substrate, especially when compared to an alternative setup, such as the sandwich configuration.

In an IDE substrate, the electrodes are arranged in a comb-like fashion, featuring closely spaced fingers. When a thin film, like TiO_2, is deposited on this type of substrate, the lateral behavior primarily involves the movement of charge carriers, such as electrons or holes, between adjacent electrodes. The spacing and design of the IDE structure can impose limitations on the lateral motion of charge carriers, restricting their ability to contribute to a detectable photocurrent.

Consequently, the lateral response to incident light in this setup may manifest as weak or even negligible.

In contrast, the behavior of ZnO is characterized as regular and evident, indicating a higher sensitivity to light. This heightened sensitivity is observed in both types of heterojunctions. The non-sensitive nature of TiO_2, when juxtaposed with the high sensitivity of ZnO, leads to a clear distinction in the behavior of both heterojunctions. They initiate with low responses and then gradually increase after the second illumination time-period [162].

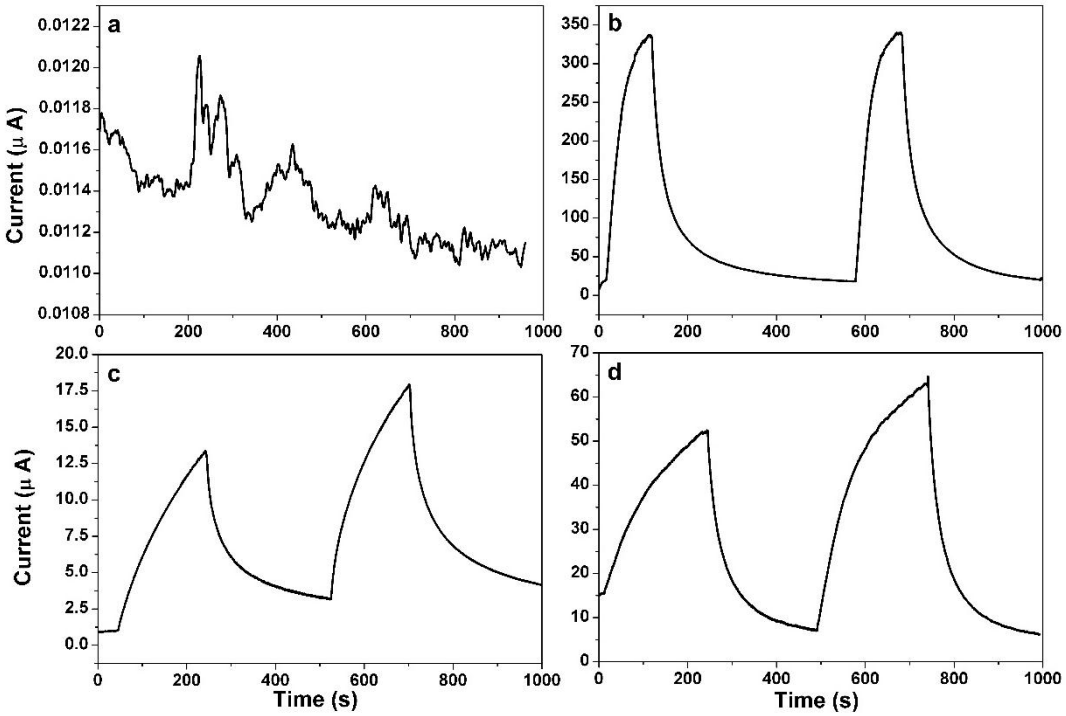

Figure 4-19 Photocurrent behavior using IDEs substrate for a)TiO_2, b)ZnO, c)Hybrid, and d) Bilayer.

The photoresistance characteristics of thin films coated on an Interdigitated Electrode (IDEs) substrate are shown in Table 4-14. The photoresistance and resistivity values provide information on how the materials' resistance varies under illumination. ZnO has an extremely low resistance (R_{ph}) and photoresistivity (ρ_{ph}), showing a considerable drop in resistance when exposed to

light. Higher R_{ph} and ρ_{ph} values are seen in TiO_2 which that the TiO_2 has very low sensitivity when it behaves as lateral. The hybrid structure, and the bilayer structure, indicating a less dramatic drop in resistance. Demonstrates that ZnO is the most light-sensitive material tested on the IDEs substrate, with strong photocurrent, quick reaction, and low photoresistance values. TiO2, on the other hand, has minimal light sensitivity, with low photocurrent and photoresistance values. With extended response times and moderate photoresistance levels, hybrid and bilayer materials exhibit intermediate properties.

Table 4-14: Photoresistance characteristics of thin films on IDE substrate.

Thin Film	**S.T. (μ A)**	**I_{ph} (μA)**	**I.P. (s)**	**R.T.(s)**	**F.T. (s)**	**$R_{ph}\times10^5$ (Ω)**	**$\rho_{ph}\times10^3$ (Ω.m)**
TiO_2	0.012	/	200	/	/	/	/
ZnO	10	333	200	50.4	67	0.15	0.254
Hybrid	0.9	15	200	129	127	3.33	7.03
Bilayer	15	58	200	159	149	0.86	2.09

Based on the observations presented in Figure 4-19, it is evident that the photocurrent response over time varies significantly among the different thin film materials. TiO_2 exhibits a minimal and almost negligible response to the applied light stimulus, indicating its limited sensitivity in generating photocurrent. ZnO, on the other hand, displays a consistent and regular response pattern over time.

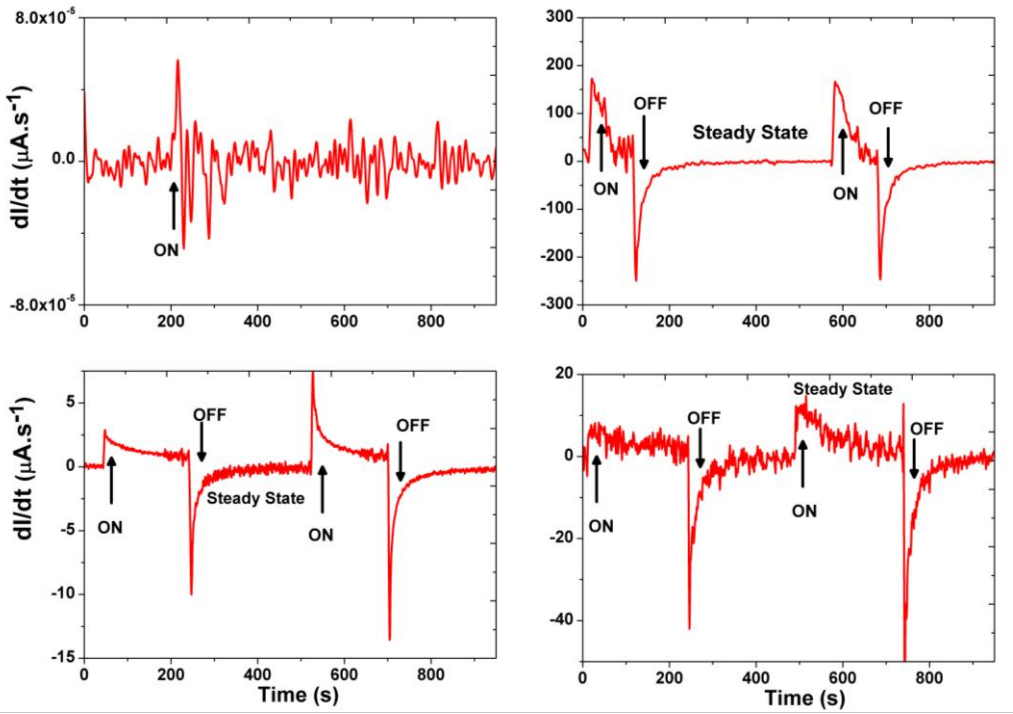

Figure 4.20 First derivative of photocurrent behavior using IDE substrate for a)TiO_2, b)ZnO, c) hybrid, and d) bilayer.

The photocurrent generated by ZnO demonstrates a steady increase when subjected to light. In the case of the heterojunctions, both the hybrid and bilayer structures, their initial responses are relatively small but notable. However, the significant finding is that after the second light illumination, the photocurrent response becomes much more pronounced, suggesting a cumulative effect or enhanced sensitivity in these heterojunctions upon repeated light exposure.

Table 4-15: dI/dt values at ON-OFF states for Thin Films on IDE.

Thin Film	**(dI/dt) ON ($\mu A.s^{-1}$)**	**(dI/dt) OFF ($\mu A.s^{-1}$)**
TiO_2	5.49×10^{-05}	-4.86×10^{-05}
ZnO	165	-249
Hybrid	5.58	-11.5
Bilayer	9.95	- 44

Table 4-16; further quantifies these observations by presenting the values of the first derivative of photocurrent, dI/dt, at both the ON and OFF states for the

various thin film materials on the IDEs substrate. TiO_2 exhibits very low dI/dt values, both in the ON and OFF states, emphasizing its weak photocurrent response. ZnO displays significantly higher dI/dt values in the ON state, indicating its strong and consistent photocurrent generation. In the OFF state, it shows a notable negative value, signifying a decrease in current after light exposure.

The hybrid structure demonstrates moderate dI/dt values in the ON state, indicating a reasonable photocurrent response. In the OFF state, it displays a negative value but of smaller magnitude, indicating a less dramatic reduction in current compared to ZnO. The bilayer structure exhibits even higher dI/dt values in the ON state, surpassing both TiO_2 and the hybrid structure, showcasing a more significant initial photocurrent response. However, it also demonstrates a noTable negative value in the OFF state, indicating a considerable reduction in current after light exposure.

Table 4-16: Photoresistance values across different substrates.

Thin Film	**Photoresistivity ITO (Ω.m)**	**Photoresistivity Si/SiO_2 (Ω.m)**	**Photoresistivity ID (Ω.m)**
TiO_2	1.87×10^8	1.20×10^9	/
ZnO	2.30×10^8	1.00×10^8	2.38×10^7
Hybrid	4.42×10^8	7.10×10^7	4.50×10^8
Bilayer	3.41×10^7	7.18×10^7	1.12×10^8

The photoresistivity values across different substrates for hybrid and bilayer structures, composed of TiO_2 and ZnO, reveal intriguing trends across various substrates. On ITO, the hybrid structure displays high photoresistance, indicating its potential for optoelectronic applications demanding higher resistance. However, on Si/SiO_2 and IDEs substrates, the hybrid structure exhibits lower photoresistance, making it suitable for applications requiring lower resistance.

The bilayer structure exhibits intermediate photoresistance values on all substrates, reflecting its mixed characteristics influenced by both TiO_2 and ZnO properties. These findings highlight the versatility of these heterostructures for diverse optoelectronic applications.

Chapter Five

Conclusions and Future Works

5-1 Conclusions

Based on the information presented in the fourth chapter on results and discussion, the following conclusions can be drawn:

1- The nanomaterials was synthesized via sol-gel method, which can be regarded as a good approach of synthesis.
2- XRD patterns confirm nano-scale structures with anatase (TiO_2) and wurtzite (ZnO) characteristics. Analysis of heterojunction XRD patterns highlights a combined structure, emphasizing the discernible impact on peak intensities from both TiO_2 and ZnO.
3- SEM images confirm successful morphology control, revealing ZnO thin films with uniform spherical shapes and TiO_2 thin films displaying nanoribbon-like morphology with elongated structures and homeotropic alignment.
4- The hybrid (ZnO:TiO_2) thin film structure revealed an intriguing overlap between the two constituent materials, ZnO and TiO_2.
5- The bilayer structure exhibited clear and distinct layers of the individual materials, providing further evidence of precise control over the deposition process.
6- Activation energy, crucial for charge carrier mobility, undergoes a significant change in heterojunctions, indicating the presence of interfaces between distinct materials. Lower activation energies in heterojunctions compared to individual materials suggest improved charge carrier transport, emphasizing the potential for enhanced mobility at the interface
7- The choice of substrate significantly influences the electrical behaviors of thin films (I-V). ITO substrate yields varying behaviors, with TiO_2 displaying lower resistance and moderate switching, while Si/SiO_2 substrate results in higher resistance and stronger switching. The IDEs substrate leads

to distinct behaviors, with TiO_2 showing very high resistance and ZnO exhibiting lower resistance with strong switching

8- Based on the photocurrent and time-dependent current change (dI/dt) characteristics of the thin films on different substrates:

a) **TiO_2 Thin Film:**

- On ITO substrates, the TiO_2 thin film exhibited a relatively gradual response in both photocurrent amplitude and dI/dt values, indicating a moderate switching behavior.
- On Si/SiO_2 substrates, the response was significantly faster with a higher dI/dt value during both ON and OFF states, suggesting pronounced switching ability.
- On IDEs substrates, the response was minimal, indicating minimal charge carrier mobility and limited switching behavior.

b) **ZnO Thin Film:**

- On ITO substrates, the ZnO thin film displayed a moderate response with respect to both photocurrent amplitude and dI/dt values, indicating moderate switching characteristics.
- On Si/SiO_2 substrates, the response was notably faster with significantly higher dI/dt values during both ON and OFF states, indicating strong switching capability.
- On IDEs substrates, the ZnO thin film exhibited a high response with respect to both photocurrent and dI/dt values, suggesting strong switchable behavior.

c) **Hybrid Thin Film (TiO_2:ZnO):**

- On ITO substrates, the hybrid thin film showed moderate responses in photocurrent amplitude and dI/dt values, indicating a decreased ability to switch compared to ZnO.
- On Si/SiO_2 substrates, the response was significantly faster, indicating pronounced switching characteristics.
- On IDE substrates, the response was substantial, reflecting a balanced electrical behavior influenced by both ZnO and TiO_2.

d) **Bilayer Thin Film (TiO_2/ZnO):**

- On ITO substrates, the bilayer thin film exhibited moderate switching behavior in both photocurrent amplitude and dI/dt values.
- On Si/SiO_2 substrates, the response was faster, indicating strong switching capability.
- On IDEs substrates, the bilayer thin film displayed a high response, suggesting potential for strong switchable behavior.

5-2 Future Works

As this investigation delves into the amalgamation, characterization, and electrical conduct of slim coatings on various substrates, it becomes evident that there exist numerous possibilities for further research and advancement. This section aims to pinpoint potential avenues of study as well as areas that warrant further investigation. Expanding upon the discoveries of the current study.

The discussion that follows indicates bright opportunities for future study in the fields of thin film materials and their applications in science and technology.. These proposed directions encompass both refining existing knowledge and delving into uncharted territories in the field of materials science and electronics.

1. Substrate Optimization for Thin Film Quality.
2. Enhancing Thin Film Behavior through Improved Heterojunction Design.
3. Thin Film Materials for Photovoltaic and Photocatalytic Applications.
4. Integration Strategies for Thin Film Devices: Fabrication and Practical Applications.
5. Tailoring Thin Film Properties through Doping and Alloying.
6. Multilayer thin films for Antenna applications.
7. Modeling and Simulation for Design Optimization of Thin Film Devices.

References

[1] Alberi, Kirstin, Marco Buongiorno Nardelli, Andriy Zakutayev, Lubos Mitas, Stefano Curtarolo, Anubhav Jain, Marco Fornari et al. "The 2019 materials by design roadmap." *Journal of Physics D: Applied Physics* 52, no. 1 (2018): 013001.

[2] Dobrzański, Leszek A., and Anna D. Dobrzańska-Danikiewicz. "Why are carbon-based materials important in civilization progress and especially in the industry 4.0 stage of the industrial revolution." *Materials Performance and Characterization* 8, no. 3 (2019): 337-370.

[3] Ali, Saleem H. "The materials science imperative in meeting the Sustainable Development Goals." *Nature Materials* 17, no. 12 (2018): 1052-1053.

[4] Aseev, Aleksander Leonidovich, Alexander Vasilevich Latyshev, and Anatoliy Vasilevich Dvurechenskii. "Semiconductor Nanostructures for Modern Electronics." Solid State Phenomena 310 (September 2020): 65–80.

[5] Winrich, Chuck. *Semiconductors and modern electronics*. Morgan & Claypool Publishers, 2019.

[6] Behera, Ajit, and Ajit Behera. "Advanced semiconductor/conductor materials." *Advanced Materials: An Introduction to Modern Materials Science* (2022): 557-596.

[7] Terna, Augustine D., Elias E. Elemike, Justina I. Mbonu, Omosede E. Osafile, and Rachael O. Ezeani. "The future of semiconductors nanoparticles: Synthesis, properties and applications." *Materials Science and Engineering: B* 272 (2021): 115363.

[8] Baig, Nadeem, Irshad Kammakakam, and Wail Falath. "Nanomaterials: A review of synthesis methods, properties, recent progress, and challenges." *Materials Advances* 2, no. 6 (2021): 1821-1871.

[9] Aseev, Aleksander Leonidovich, Alexander Vasilevich Latyshev, and Anatoliy Vasilevich Dvurechenskii. "Semiconductor nanostructures for modern electronics." *Solid State Phenomena* 310 (2020): 65-80.

[10] Joshi, Vedant A., Girish M. Joshi, and Sudheesh K. Shukla. "Synthesis, properties and applications of nanomaterials: A mini review." *Functionalized Nanomaterials Based Devices for Environmental Applications* (2021): 61-75.

[11] Stine, Keith J. "Special Issue “Materials Processing for Production of Nanostructured Thin Films”." *Processes* 9, no. 2 (2021): 298.

[12] Skowroński, Łukasz. "Optical and Microstructural Characterization of Thin Layers." *Crystals* 10, no. 9 (2020): 749.

[13] Kivisaari, Pyry, Mikko Partanen, Toufik Sadi, and Jani Oksanen. "Interplay of photons and charge carriers in thin-film devices." *Physical Review Applied* 16, no. 2 (2021): 024036.

[14] Jadkar, Sandesh R., Deepak Dubal, Dattatray Dhawale, Shoyebmohamad F. Shaikh, Ravindra Bulakhe, Ying Li, Qinglong Jiang, and Habib M. Pathan. "Thin Film Materials and Devices." *ES Mater. Manuf.* 10 (2020): 1-4.

[15] Kivisaari, Pyry, Mikko Partanen, Toufik Sadi, and Jani Oksanen. "Interplay of photons and charge carriers in thin-film devices." *Physical Review Applied* 16, no. 2 (2021): 024036.

[16] Kivisaari, Pyry, Mikko Partanen, Toufik Sadi, and Jani Oksanen. "Interplay of photons and charge carriers in thin-film devices." *Physical Review Applied* 16, no. 2 (2021): 024036.

[17] Pant, Rohit, Deependra Kumar Singh, Arun Malla Chowdhury, Basanta Roul, K. K. Nanda, and S. B. Krupanidhi. "Next-generation self-powered and ultrafast photodetectors based on III-nitride hybrid structures." *APL Materials* 8, no. 2 (2020).

[18] Rehman, Adeela, and Soo-Jin Park. "State of the art two-dimensional materials-based photodetectors: Prospects, challenges and future outlook." *Journal of Industrial and Engineering Chemistry* 89 (2020): 28-46.

[19] Zhu, Bin, Liangdong Fan, Naveed Mushtaq, Rizwan Raza, Muhammad Sajid, Yan Wu, Wenfeng Lin, Jung-Sik Kim, Peter D. Lund, and Sining Yun. "Semiconductor electrochemistry for clean energy conversion and storage." *Electrochemical Energy Reviews* (2021): 1-36.

[20] Kamalabadi, Mahdie, Kheibar Dashtian, Abbas Afkhami, Tayyebeh Madrakian, and Arash Ghoorchian. "Nanostructure Semiconductor Materials for Device Applications." In *Advances in Nanostructured Materials*, pp. 57-86. Singapore: Springer Singapore, 2022.

[21] De Colvenaer, Bert. "The future of power semiconductors: An EU perspecitve." In *2018 IEEE 30th International Symposium on Power Semiconductor Devices and ICs (ISPSD)*, pp. 15-23. IEEE, 2018.

[22] Frank, Michael P. "Throwing computing into reverse." *IEEE Spectrum* 54, no. 9 (2017): 32-37.

[23] Stanojevic, A. B. "Application of Photovoltaic Technology in the Use of Solar Energy." *Annals of Environmental Science and Toxicology* 5, no. 1 (2021): 094-098.

[24] Mitrašinović, Aleksandar M. "Photovoltaics advancements for transition from renewable to clean energy." *Energy* 237 (2021): 121510.

[25] Xu, Yalun, and Qianqian Lin. "Photodetectors based on solution-processable semiconductors: Recent advances and perspectives." *Applied Physics Reviews* 7, no. 1 (2020).

[26] Wang, M. J., S. Ren, K. K. Liang, H. H. Qin, and Y. P. Feng. "Photoelectric Characteristics and Applications of Quantum Effect Photodetector." *Integrated Ferroelectrics* 219, no. 1 (2021): 1-8.

[27] Zhou, Tianyi, and Kuan WA Chee. "Overcoming the Bandwidth-Quantum Efficiency Trade-Off in Conventional Photodetectors." In *Advances in Photodetectors-Research and Applications*. IntechOpen, 2019.

[28] Li, Yubo, and Zhen Pan. "Design of Photodiode Circuit Based on Signal Acquisition." *Optical Memory and Neural Networks* 28 (2019): 50-57.

[29] Young, Steve. "Bulk photovoltaic effect for next-generation light-sensitive devices." *SPIE Newsroom* (2016).

[30] - Lee, Seung-Hoon, Changjin Lee, Sung Cheol Yoon, and Yong-Young Noh. "Toward color-selective printed organic photodetectors for high-resolution image sensors: From fundamentals to potential commercialization." *Materials Science and Engineering: R: Reports* 147 (2022): 100660.

[31] Setya, W., A. Ramadhana, H. Restu Putri, A. Santoso, A. Malik, and M. M. Chusni. "Design and development of measurement of measuring light resistance using Light Dependent Resistance (LDR) sensors." In *Journal of Physics: Conference Series*, vol. 1402, no. 4, p. 044102. IOP Publishing, 2019.

[32] Wang, Lingbo. "Characteristics Test of Photoresistor and Its Application in Optical Control Switch." In *International Conference on Advances in Mechanical Engineering and Industrial Informatics (AMEII 2015)[26] Data sheet of the photo-light resistor*. 2015.

[33] Maini, Anil K. "Photo Sensors and Related Devices." (2018): 783-863.

[34] Regtien, P., and E. Dertien. "7—Optical Sensors." *Sensors for Mechatronics, 2nd ed.; Regtien, P., Dertien, E., Eds* (2018): 183-243.

[35] Denisov, B. N. "A photoresistor as a multifunctional optoelectronic element." *Journal of Communications Technology and Electronics* 52 (2007): 478-481.

[36] Hegde, Vindhya, T. S. Nivin, S. D. Sreeja, Sundararaman Gopalan, and C. O. Sreekala. "Photovoltaic studies of hybrid metal oxide semiconductors as photo anode in dye sensitized solar cells." In *AIP Conference Proceedings*, vol. 2162, no. 1. AIP Publishing, 2019.

[37] Noman, Muhammad Tayyab, Muhammad Azeem Ashraf, and Azam Ali. "Synthesis and applications of nano-TiO_2: A review." *Environmental Science and Pollution Research* 26 (2019): 3262-3291.

[38] Liao, D. L., Chadi A. Badour, and B. Q. Liao. "Preparation of nanosized TiO_2/ZnO composite catalyst and its photocatalytic activity for degradation of methyl orange." *Journal of Photochemistry and Photobiology A: Chemistry* 194, no. 1 (2008): 11-19.

[39] Nurfani, E., A. Lailani, W. A. P. Kesuma, M. S. Anrokhi, G. T. M. Kadja, and M. Rozana. "UV sensitivity enhancement in Fe-doped ZnO films grown by ultrafast spray pyrolysis." *Optical Materials* 112 (2021): 110768.

[40] Taghavi, Mahmoud, Masoumeh Tabatabaee, Mohammad Hasan Ehrampoush, Mohammad Taghi Ghaneian, Mojtaba Afsharnia, Ali Alami, and Jalal Mardaneh. "Synthesis, characterization and photocatalytic activity of TiO_2/ZnO-supported phosphomolybdic acid nanocomposites." *Journal of Molecular Liquids* 249 (2018): 546-553.

[41] Wang, Hai Ying, Yang, Xiang Li, Li Juan Li, and Ce Wang. "Preparation and characterization of porous TiO_2/ZnO composite nanofibers via electrospinning." *Chinese Chemical Letters* 21, no. 9 (2010): 1119-1123.

[42] Ghazali, Mohd Sabri Mohd, Wan Rafizah Wan Abdullah, Azmi Zakaria, Muhamad Azman Zulkifli, Mohd Hafiz Mohd Zaid, and Zahid Rizwan. "Effect of Co_3O_4 doping and sintering temperature on optical energy band gap properties in Zn-Bi-Ti-O varistor ceramics." In *AIP Conference Proceedings*, vol. 1885, no. 1. AIP Publishing, 2017.

[43] Sanchez, Clément, K. J. Shea, and S. Kitagawa. "Hybrid materials." *Chem. Soc. Rev* 40 (2011): 453-1152.

[44] Siwińska-Stefańska, Katarzyna, Adam Kubiak, Adam Piasecki, Anna Dobrowolska, Katarzyna Czaczyk, Mykhaylo Motylenko, David Rafaja, Hermann Ehrlich, and Teofil Jesionowski. "Hydrothermal synthesis of multifunctional TiO_2-ZnO oxide systems with desired antibacterial and photocatalytic properties." *Applied Surface Science* 463 (2019): 791-801.

[45] Li, Jian, Long Yan, Yufei Wang, Yuhong Kang, Chao Wang, and Shaobo Yang. "Fabrication of TiO_2/ZnO composite nanofibers with enhanced photocatalytic activity." *Journal of Materials Science: Materials in Electronics* 27 (2016): 7834-7838.

[46] Perednis, Dainius, and Ludwig J. Gauckler. "Thin film deposition using spray pyrolysis." *Journal of electroceramics* 14 (2005): 103-111.

[47] Onah, Emmanuel O., Jude N. Udeh, Sabastine Ezugwu, Assumpta C. Nwanya, and Fabian I. Ezema. "Recent Progress in Metal Oxide for Photovoltaic Application." *Chemically Deposited Nanocrystalline Metal Oxide Thin Films: Synthesis, Characterizations, and Applications* (2021): 99-145.

[48] Bajorowicz, Beata, Marek Kobylański, Anna Malankowska, Paweł Mazierski, Joanna Nadolna, Aleksandra Pieczyńska, and Adriana Zaleska-Medynska. "Application of metal oxide-based photocatalysis." (2018).

[49] Dikov, Hr, T. Ivanova, and P. Vitanov. "Oxide/metal/oxide nanolaminate structures for application of transparent electrodes." In *Journal of Physics: Conference Series*, vol. 764, no. 1, p. 012021. IOP Publishing, 2016.

[50] Kler, Rantej Singh. "Metal Oxide Nanomaterials and their Application in Solar Photoelectrolysis of Water." PhD diss., University of Sussex, 2014.

[51] Kim, Sungjun, Ki Chang Kwon, Jae Yong Park, Hyung Won Cho, Illhwan Lee, Soo Young Kim, and Jong-Lam Lee. "Challenge beyond graphene: metal oxide/graphene/metal oxide electrodes for optoelectronic devices." *ACS Applied Materials & Interfaces* 8, no. 20 (2016): 12932-12939.

[52] Mallampati, Bhargav, S. V. Nair, H. E. Ruda, and U. Philipose. "ZnO nanowire based photoconductor with high photoconductive gain." *MRS Online Proceedings Library (OPL)* 1805 (2015): mrss15-2135932.

[53] Phillips, J., W. Bowen, E. Cagin, and W. Wang. "Electronic and optoelectronic devices based on semiconducting zinc oxide." (2011): 101-127.

[54] Schimpf, Alina M., Carolyn E. Gunthardt, Jeffrey D. Rinehart, James M. Mayer, and Daniel R. Gamelin. "Controlling carrier densities in photochemically reduced colloidal ZnO nanocrystals: Size dependence and role of the hole quencher." *Journal of the American Chemical Society* 135, no. 44 (2013): 16569-16577.

[55] Virt, Ihor, Roman Gamernyk, Piotr Potera, Bogumił Cieniek, and Andrej Lozynsky. "Transient Photoconduction and Relaxation Photocurrent of ZnO Thin Films Produced by Pulsed Laser Deposition." *ECS Journal of Solid State Science and Technology* 11, no. 6 (2022): 063013.

[56] Mezzat, F., H. Zaari, A. El Kenz, and A. Benyoussef. "Effect of metal and non- metal doping of TiO_2 on photocatalytic activities: Ab initio calculations." *Optical and Quantum Electronics* 53 (2021): 1-14.

[57] El Rouby, Waleed MA, Ahmed Esmail A. Aboubakr, Sheng-Mu You, and Pierre Millet. "Role of photosensitizers in enhancing the performance of nanocrystalline TiO_2 for photoelectrochemical water splitting." In *Nanoscience*, pp. 181-212. 2021.

[58] Sabino, Fernando P., and Anderson Janotti. "Dramatic enhancement of visible-light absorption in TiO_2 by adding Bi." *arXiv preprint arXiv:2302.02461* (2023).

[59] Nair, Radhika V., Venkata Siva Gummaluri, Murukeshan Vadakke Matham, and C. Vijayan. "A review on optical bandgap engineering in TiO_2 nanostructures via doping and intrinsic vacancy modulation towards visible light applications." *Journal of Physics D: Applied Physics* 55, no. 31 (2022): 313003.

[60] Zhang, Wei, Haili He, Haoze Li, Linlin Duan, Lianhai Zu, Yunpu Zhai, Wei Li, Lianzhou Wang, Honggang Fu, and Dongyuan Zhao. "Visible-light responsive TiO_2-based materials for efficient solar energy utilization." *Advanced Energy Materials* 11, no. 15 (2021): 2003303.

[61] Chiou, Shang-Hau, Hsin-Chia Ho, Han-Ting Liao, Feng-Yu Tsai, Chun-Wen Tsao, Yung-Jung Hsu, and Chun-Hway Hsueh. "Plasmonic gold nanoplates-decorated ZnO branched nanorods@TiO_2 nanorods heterostructure photoanode for efficient photoelectrochemical water splitting." *Journal of Photochemistry and Photobiology A: Chemistry* 443 (2023): 114816.

[62] Kim, Byung Jun, Jun Hyung Jeong, Eui Young Jung, Tae Yeon Kim, Sungho Park, Jong-Am Hong, Kyu-Myung Lee, Woojin Jeon, Yongsup Park, and Seong Jun Kang. "A visible-light phototransistor based on the heterostructure of ZnO and TiO_2 with trap-assisted photocurrent generation." *RSC advances* 11, no. 20 (2021): 12051-12057.

[63] Arifin, Nurliyana Mohamad, Fariza Mohamad, Rosniza Hussin, Anis Zafirah Mohd Ismail, Shazleen Ahmad Ramli, Norazlina Ahmad, Nik Hisyamudin Muhd Nor, Mohd Zainizan Sahdan, Mohd Zamzuri Mohammad Zain, and Masanobu Izaki. "Development of homogenous n-TiO_2/ZnO bilayer/p-

Cu_2O heterostructure thin film." *Journal of Sol-Gel Science and Technology* 100 (2021): 224-231.

[64] Akhter, Parveen, Shahid Nawaz, Iqrash Shafiq, Arif Nazir, Sumeer Shafique, Farrukh Jamil, Young-Kwon Park, and Murid Hussain. "Efficient visible light assisted photocatalysis using ZnO/TiO_2 nanocomposites." *Molecular Catalysis* 535 (2023): 112896.

[65] Flory, F., Escoubas, L., & Berginc, G. "Optical properties of nanostructured materials: a review." *J. Nanophotonics* 5, no. 1 (2011): 052502-1-052502-22.

[66] Kim, Byung Jun, Jun Hyung Jeong, Eui Young Jung, Tae Yeon Kim, Sungho Park, Jong-Am Hong, Kyu-Myung Lee, Woojin Jeon, Yongsup Park, and Seong Jun Kang. "A visible-light phototransistor based on the heterostructure of ZnO and TiO_2 with trap-assisted photocurrent generation." *RSC advances* 11, no. 20 (2021): 12051-12057.

[67] Ng, Siowwoon, Petr Kuberský, Milos Krbal, Jan Prikryl, Viera Gärtnerová, Daniela Moravcová, Hanna Sopha et al. "ZnO coated anodic 1D TiO_2 nanotube layers: efficient photo-electrochemical and gas sensing heterojunction." *Advanced Engineering Materials* 20, no. 2 (2018): 1700589.

[68] Zhou, Ming, Bozhi Wu, Xueting Zhang, Shiquan Cao, Pengpeng Ma, Kaiping Wang, Zhengpeng Fan, and Maogen Su. "Preparation and UV photoelectric properties of aligned ZnO–TiO_2 and TiO_2–ZnO core–shell structured heterojunction nanotubes." *ACS applied materials & interfaces* 12, no. 34 (2020): 38490-38498.

[69] Zhu, Mei, Xiaochun Deng, Xin Lin, Li Zhang, Wei Zhang, Yaohong Lv, and Jiaqi Pan. "The carbon quantum dots modified ZnO/TiO_2 nanotube

heterojunction and its visible light photocatalysis enhancement." *Journal of Materials Science: Materials in Electronics* 29 (2018): 11449-11456.

[70] Kim, Byung Jun, Jun Hyung Jeong, Eui Young Jung, Tae Yeon Kim, Sungho Park, Jong-Am Hong, Kyu-Myung Lee, Woojin Jeon, Yongsup Park, and Seong Jun Kang. "A visible-light phototransistor based on the heterostructure of ZnO and TiO_2 with trap-assisted photocurrent generation." *RSC advances* 11, no. 20 (2021): 12051-12057.

[71] Navarro-Gázquez, Pedro José, Maria J. Muñoz-Portero, Encarna Blasco-Tamarit, Rita Sánchez-Tovar, and José García-Antón. "Synthesis and applications of TiO_2/ZnO hybrid nanostructures by ZnO deposition on TiO_2 nanotubes using electrochemical processes." *Reviews in Chemical Engineering* 39, no. 7 (2023): 1153-1186.

[72] Kim, Tea-Yon, Byung Su Kim, Jong Gyu Oh, Seul Chan Park, Jaeyoung Jang, Thomas W. Hamann, Young Soo Kang, Jin Ho Bang, Sixto Giménez, and Yong Soo Kang. "Interfacial Engineering at Quantum Dot-Sensitized TiO_2 Photoelectrodes for Ultrahigh Photocurrent Generation." *ACS Applied Materials & Interfaces* 13, no. 5 (2021): 6208-6218.

[73] Lawrence, Reece T., Mark P. Croxall, Cheng Lu, and M. Cynthia Goh. "TiO_2–NGQD composite photocatalysts with switchable photocurrent response." *Nanoscale* 15, no. 6 (2023): 2788-2797.

[74] Salau, Ayodeji Olalekan, Ademola Stanford Olufemi, Gabriel Oluleye, Victor Adewale Owoeye, and Isiaka Ismail. "Modeling and performance analysis of dye-sensitized solar cell based on ZnO compact layer and TiO_2 photoanode." *Materials Today: Proceedings* 51 (2022): 502-507.

[75] Marouf, Sara, Abdelkrim Beniaiche, Hocine Guessas, and Amor Azizi. "Morphological, structural and optical properties of ZnO thin films deposited by dip coating method." *Materials Research* 20 (2016): 88-95.

[76] Mote, V. D., Yp Purushotham, and B. N. Dole. "Williamson-Hall analysis in estimation of lattice strain in nanometer-sized ZnO particles." *Journal of theoretical and applied physics* 6 (2012): 1-8.

[77] Lavasani, Seyed Hosein, Mehdi Nasiri Sarvi, and Ebrahim Azimi. "Synthesis of Mesoporous Nanoparticles of TiO_2 in Anatase form from Ilmenite Concentrate."

[78] Senthil Kumari, S., W. Nirmala, Natarajan Chidhambaram, Arun Thirumurugan, and S. Gobalakrishnan. "Tailoring ultraviolet band absorption and emission features of ZnO nanoparticles through the crystallite size and lattice strain modulation: Role of yttrium ions." *physica status solidi (b)* 260, no. 3 (2023): 2200392.

[79] Duri, Inten Rafika, Heri Sutanto, and Eko Hidayanto. "Estimation Crystal Size and Lattice Strain of Nanocrystal Bi_2O_3 using the Scherrer and Size-Strain Plot Method." (2022).

[80] Mongkolsuttirat, K., and J. Buajarern. "Uncertainty evaluation of crystallite size measurements of nanoparticle using X-Ray Diffraction analysis (XRD)." *In Journal of Physics: Conference Series,* vol. 1719, no. 1, p. 012054. IOP Publishing, 2021.

[81] Xu, Ziyao, Yi Zhou, Chi Yung Yam, Lynn Groß, Antonietta De Sio, Thomas Frauenheim, Christoph Lienau, and Guanhua Chen. "Revealing generation, migration, and dissociation of electron-hole pairs and current emergence in an organic photovoltaic cell." *Science Advances* 7, no. 25 (2021): eabf7672.

[82] Burdov, Vladimir A., and Mikhail I. Vasilevskiy. "Exciton-photon interactions in semiconductor nanocrystals: Radiative transitions, non-radiative processes and environment effects." *Applied Sciences* 11, no. 2 (2021): 497.

[83] Sosna-Głębska, A., Szczecińska, N., Znajdek, K., & Sibiński, M. "Review on metallic oxide nanoparticles and their application in optoelectronic devices." *Acta Innovations* 30 (2019): 5-15.

[84] Mhetre, H. V., Kanse, Y. K., & Patil, S. S. "Nanomaterials: Applications in Electronics." 4, no. 6 (September 2021): 7–19.

[85] Georgakopoulos, T., Todorova, N., Pomoni, K., & Trapalis, C. "On the transient photoconductivity behavior of sol–gel TiO_2/ZnO composite thin films." *J. Non-Cryst. Solids* 410 (2015): 135-141.

[86] Li, X., Guo, Y., Ren, Y., Peng, J., Liu, J., Wang, C., & Zhang, H. "Narrow-bandgap materials for optoelectronics applications." *Frontiers of Physics* 17 (2022): 1-33.

[87] Sung, Y. M., Kim, T., Yun, D., Lim, M., Ko, D., Jung, C., Won, N., et al. "Increasing the Energy Gap between Band-Edge and Trap States Slows Down Picosecond Carrier Trapping in Highly Luminescent InP/ZnSe/ZnS Quantum Dots." *Small* 17, no. 52 (2021): 2102792.

[88] Zhang, C., Zhang, J., Ma, X., & Feng, Q. "High-Efficiency Semiconductor Photovoltaic Devices." In *Semiconductor Photovoltaic Cells* (2021), pp. 433-461.

[89] Wong, J., Omelchenko, S., & Atwater, H. A. "Impact of semiconductor band tails and band filling on photovoltaic efficiency limits." *ACS Energy Letters* 6, no. 1 (2020): 52-57.

[90] Han, T. "Optical Properties of Low Dimensional Semiconductor Materials." PhD diss., KTH, 2008.

[91] Neamen, D. "Semiconductor physics and devices." McGraw-Hill, Inc., 2002.

[92] Elliott, R. J., & Gibson, A. F. "An introduction to solid state physics and its applications." Barnes & Noble, 1974.

[93] Makuła, P., Pacia, M., & Macyk, W. "How to correctly determine the band gap energy of modified semiconductor photocatalysts based on UV–Vis spectra." *ACS Publications* (2018).

[94] Stenzel, O. "The physics of thin film optical spectra." *Springer Series in Surface Sciences* 978 (2015): 214-220.

[95] Bandyopadhyay, A., & Bhowmick, A. K. "Factors influencing the structure and properties of nanocomposites derived by sol-gel technique." *J. Polym. Eng.* 26, no. 8–9 (2006): 821–852.

[96] Kautz, R. L., & Martinis, J. M. "Noise-affected I-V curves in small hysteretic Josephson junctions." *Phys. Rev. B* 42, no. 16 (1990): 9903.

[97] Jing, J., Chen, Z., & Feng, C. "Using the photoinduced volt-ampere curves to study the p/n types of the corrosion products with semiconducting properties." *J. Electroanalytical Chemistry* 881 (2021): 114961.

[98] Orazem, M. E., & Tribollet, B. "A tutorial on electrochemical impedance spectroscopy." *ChemTexts* 6, no. 2 (2020): 12.

[99] Streetman, B. G., & Banerjee, S. "Solid state electronic devices." 4. New Jersey: Prentice hall, 2000.

[100] Hummel, Rolf E., and Rolf E. Hummel. "Electrical properties of materials." *Understanding Materials Science: History· Properties· Applications* (1998): 180-216.

[101] Singh, Surinder, Anumeet Kaur, Parwinder Kaur, and Lakhwant Singh. "High-temperature dielectric relaxation and electric conduction mechanisms in a $LaCoO_3$-modified $Na_0.5Bi_0.5TiO_3$ system." *ACS omega* 8, no. 28 (2023): 25623-25638.

[102] Sapunov, Valentin N., Eugene A. Saveljev, Mikhail S. Voronov, Markus Valtiner, and Wolfgang Linert. "The basic theorem of temperature-dependent processes." *Thermo* 1, no. 1 (2021): 45-60.

[103] Sze, S. M., Li, Y., & Ng, K. K. "Physics of semiconductor devices." John Wiley & Sons, 2021.

[104] Züfle, Simon, Stéphane Altazin, Alexander Hofmann, Lars Jäger, Martin T. Neukom, Wolfgang Brütting, and Beat Ruhstaller. "Determination of charge transport activation energy and injection barrier in organic semiconductor devices." *Journal of Applied Physics* 122, no. 11 (2017).

[105] Dufaux, T. "Nanoscale Organic/Inorganic Hybrid Photovoltaic Devices." PhD thesis, EPFL, 2012.

[106] Bai, R., Teh, Y., & Bhattacharya, K. "Collective behavior in the kinetics and equilibrium of solid-state photoreaction." *Extreme Mechanics Letters* 43 (2021): 101160.

[107] Lu, L., Jiang, X., Peng, H., Zeng, D., & Xie, C. "Quantitative characterization of the long-term charge storage of a ZnO-based nanorod array film through persistent photoconductance." *RSC advances* 8, no. 30 (2018): 16455-16463.

[108] Palomares, Emilio, Núria F. Montcada, María Méndez, Jesús Jiménez-López, Wenxing Yang, and Gerrit Boschloo. "Photovoltage/photocurrent transient techniques." In *Characterization Techniques for Perovskite Solar Cell Materials*, pp. 161-180. Elsevier, 2020.

[109] Hu, Laigui, Xian Liu, Simon Dalgleish, Michio M. Matsushita, Hirofumi Yoshikawa, and Kunio Awaga. "Organic optoelectronic interfaces with anomalous transient photocurrent." *Journal of Materials Chemistry C* 3, no. 20 (2015): 5122-5135.

[110] Di Liberto, Giovanni, Sergio Tosoni, and Gianfranco Pacchioni. "Role of heterojunction in charge carrier separation in coexposed anatase (001)–

(101) surfaces." *The journal of physical chemistry letters* 10, no. 10 (2019): 2372-2377.

[111] Barnes, Piers RF, Kati Miettunen, Xiaoe Li, Assaf Y. Anderson, Takeru Bessho, Michael Gratzel, and Brian C. O'Regan. "Interpretation of optoelectronic transient and charge extraction measurements in dye-sensitized solar cells." *Advanced materials* 25, no. 13 (2013): 1881-1922.

[112] Chetia, Anupam, Jayanta Bera, Atanu Betal, and Satyajit Sahu. "A brief review on photodetector performance based on zero dimensional and two dimensional materials and their hybrid structures." *Materials Today Communications* 30 (2022): 103224.

[113] Yang, Ming, Haoliang Chang, Jinhuan Chen, and Xinyu Zhu. "Multiplier Effects of Photodetectors—Source of Gain." *Coatings* 13, no. 6 (2023): 1088.

[114] Emeline, Alexei V., Aida V. Rudakova, Ruslan V. Mikhaylov, Kirill M. Bulanin, and Detlef W. Bahnemann. "Photoactive heterostructures: How they are made and explored." *Catalysts* 11, no. 2 (2021): 294.

[115] Ma, Ming-Yu, Dong Han, Nian-Ke Chen, Dan Wang, and Xian-Bin Li. "Recent progress in double-layer honeycomb structure: A new type of two-dimensional material." *Materials* 15, no. 21 (2022): 7715.

[116] Palomares, Emilio, Núria F. Montcada, María Méndez, Jesús Jiménez-López, Wenxing Yang, and Gerrit Boschloo. "Photovoltage/photocurrent transient techniques." In *Characterization Techniques for Perovskite Solar Cell Materials*, pp. 161-180. Elsevier, 2020.

[117] Velický, Matěj, and Peter S. Toth. "From two-dimensional materials to their heterostructures: An electrochemist's perspective." *Applied Materials Today* 8 (2017): 68-103.

[118] Sun, Bingqi, Jing Xu, Min Zhang, Longfei He, Hao Zhu, Lin Chen, Qingqing Sun, and David Wei Zhang. "Progress on crystal growth of two-dimensional semiconductors for optoelectronic applications." *Crystals* 8, no. 6 (2018): 252.

[119] Eshete, Mesfin, Xiyu Li, Li Yang, Xijun Wang, Jinxiao Zhang, Liyan Xie, Linjie Deng, Guozhen Zhang, and Jun Jiang. "Charge Steering in Heterojunction Photocatalysis: General Principles, Design, Construction, and Challenges." *Small Science* 3, no. 3 (2023): 2200041.

[120] Rai, Amritesh, Hema CP Movva, Anupam Roy, Deepyanti Taneja, Sayema Chowdhury, and Sanjay K. Banerjee. "Progress in contact, doping and mobility engineering of MoS2: an atomically thin 2D semiconductor." *Crystals* 8, no. 8 (2018): 316.

[121] Li, Ziqing, Tingting Yan, and Xiaosheng Fang. "Low-dimensional wide-bandgap semiconductors for UV photodetectors." *Nature Reviews Materials* 8, no. 9 (2023): 587-603.

[122] Li, Ziqing, Tingting Yan, and Xiaosheng Fang. "Low-dimensional wide-bandgap semiconductors for UV photodetectors." *Nature Reviews Materials* 8, no. 9 (2023): 587-603.

[123] Li, Chunmei, Jinyong Wang, Dongyang Li, Nasir Ilyas, Zhiqiang Yang, Kexin Chen, Peng Gu et al. "An oxide-based heterojunction optoelectronic synaptic device with wideband and rapid response performance." *Journal of Materials Science & Technology* 123 (2022): 159-167.

[124] Li, Chunmei, Jinyong Wang, Dongyang Li, Nasir Ilyas, Zhiqiang Yang, Kexin Chen, Peng Gu et al. "An oxide-based heterojunction optoelectronic synaptic device with wideband and rapid response performance." *Journal of Materials Science & Technology* 123 (2022): 159-167.

[125] Lee, Tack Ho, Song Yi Park, Xiaoyan Du, Sujung Park, Kaicheng Zhang, Ning Li, Shinuk Cho, Christoph J. Brabec, and Jin Young Kim. "Effects on Photovoltaic Characteristics by Organic Bilayer-and Bulk-Heterojunctions: Energy Losses, Carrier Recombination and Generation." *ACS Applied Materials & Interfaces* 12, no. 50 (2020): 55945-55953.

[126] Lee, Tack Ho, Song Yi Park, Xiaoyan Du, Sujung Park, Kaicheng Zhang, Ning Li, Shinuk Cho, Christoph J. Brabec, and Jin Young Kim. "Effects on Photovoltaic Characteristics by Organic Bilayer-and Bulk-Heterojunctions: Energy Losses, Carrier Recombination and Generation." *ACS Applied Materials & Interfaces* 12, no. 50 (2020): 55945-55953.

[127] Lee, Chia-Chen, Chih-I. Chen, Yu-Te Liao, Kevin C-W. Wu, and Chu-Chen Chueh. "Enhancing efficiency and stability of photovoltaic cells by using perovskite/Zr-MOF heterojunction including bilayer and hybrid structures." *Advanced Science* 6, no. 5 (2019): 1801715.

[128] Parashar, Mritunjaya, Vivek Kumar Shukla, and Ranbir Singh. "Metal oxides nanoparticles via sol–gel method: a review on synthesis, characterization and applications." *Journal of Materials Science: Materials in Electronics* 31 (2020): 3729-3749.

[129] Thiagarajan, Shrividhya, Anandhavelu Sanmugam, and Dhanasekaran Vikraman. "Facile methodology of sol-gel synthesis for metal oxide nanostructures." *Recent applications in sol-gel synthesis* (2017): 1-17.

[130] Parashar, Mritunjaya, Vivek Kumar Shukla, and Ranbir Singh. "Metal oxides nanoparticles via sol–gel method: a review on synthesis, characterization and applications." *Journal of Materials Science: Materials in Electronics* 31 (2020): 3729-3749.

[131] Vardelle, Armelle, Christian Moreau, Jun Akedo, Hossein Ashrafizadeh, Christopher C. Berndt, Jörg Oberste Berghaus, Maher Boulos et al. "The

2016 thermal spray roadmap." *Journal of thermal spray technology* 25 (2016): 1376-1440.

[132] Guild, Curtis, Sourav Biswas, Yongtao Meng, Tahereh Jafari, Anne M. Gaffney, and Steven L. Suib. "Perspectives of spray pyrolysis for facile synthesis of catalysts and thin films: An introduction and summary of recent directions." *Catalysis Today* 238 (2014): 87-94.

[133] Faisal, Nadimul Haque, Anil Prathuru, Rehan Ahmed, Vinooth Rajendran, Mamdud Hossain, Viswanathan Venkatachalapathy, Nirmal Kumar Katiyar et al. "Application of thermal spray coatings in electrolysers for hydrogen production: advances, challenges, and opportunities." *ChemNanoMat* 8, no. 12 (2022): e202200384.

[134] Foo, Kai Loong, Uda Hashim, Kashif Muhammad, and Chun Hong Voon. "Sol–gel synthesized zinc oxide nanorods and their structural and optical investigation for optoelectronic application." *Nanoscale research letters* 9 (2014): 1-10.

[135] Pabón, Elizabeth, Jaime Retuert, Raúl Quijada, and Antonio Zárate. "TiO_2–SiO_2 mixed oxides prepared by a combined sol–gel and polymer inclusion method." *Microporous and Mesoporous Materials* 67, no. 2-3 (2004): 195-203.

[136] Zheng, Yichu, Axel Fischer, Natalia Sergeeva, Sebastian Reineke, and Stefan CB Mannsfeld. "Exploiting lateral current flow due to doped layers in semiconductor devices having crossbar electrodes." *Organic Electronics* 65 (2019): 82-90.

[137] Asadi, Kamal. "Resistance switching in two-terminal ferroelectric-semiconductor lateral heterostructures." *Applied Physics Reviews* 7, no. 2 (2020).

[138] Lu, Jong-Hong, Jen-Wei Luo, Zong-Han Syu, and Hsuan-Chung Wu. "Optimizing the design of transparent conductive substrates." *Journal of Vacuum Science & Technology A* 33, no. 6 (2015).

[139] Asadi, Kamal. "Resistance switching in two-terminal ferroelectric-semiconductor lateral heterostructures." *Applied Physics Reviews* 7, no. 2 (2020).

[140] Morales-Masis, Monica, Stefaan De Wolf, Rachel Woods-Robinson, Joel W. Ager, and Christophe Ballif. "Transparent electrodes for efficient optoelectronics." *Advanced Electronic Materials* 3, no. 5 (2017): 1600529.

[141] Gao, Nan, Meng Chen, Hongtao Xu, Zhongying Xue, Nan Zhang, Lu Fei, and Xing Wei. "Fabrication of silicon-on-insulator with high uniform top Si for silicon photonics applications." *Materials Science in Semiconductor Processing* 117 (2020): 105159.

[142] Cabral, Cyril, Christian Lavoie, Conal Murray, Adam Pyzyna, and Ken Rodbell. "Thin film deposition research and its impact on microelectronics scaling." *Journal of Vacuum Science & Technology A* 38, no. 4 (2020).

[143] Kumar, A. Akshaya, and S. K. Kumar. "Fabrication of interdigitated electrodes (IDEs) modified with sensitive layers of ZnO nanorods and nanoflowers." In *AIP Conference Proceedings*, vol. 2162, no. 1. AIP Publishing, 2019.

[144] Al-Shomara, S. M., and W. R. Alahmad. "Annealing temperature effect on structural, optical and photocatalytic activity of nanocrystalline TiO_2 films prepared by sol-gel method used for solar cell application." *Dig J Nanomater Biostruct* 14 (2019): 617-625.

[145] Bui, Quang Chieu, Bassem Salem, Herve Roussel, Xavier Mescot, Youssouf Guerfi, Carmen Jiménez, Vincent Consonni, and Gustavo Ardila. "Effects of thermal annealing on the structural and electrical properties of

ZnO thin films for boosting their piezoelectric response." *Journal of Alloys and Compounds* 870 (2021): 159512.

[146] Liu, Wen-Jen, Yung-Huang Chang, Chia-Chin Chiang, Yuan-Tsung Chen, Pei-Xin Lu, Yu-Jie He, and Shih-Hung Lin. "Studying the Effects of Annealing and Surface Roughness on Both the Magnetic Property and Surface Energy of $Co_{60}Fe_{20}Sm_{20}$ Thin Films on Si(100) Substrate." *Coatings* 13, no. 10 (2023): 1783.

[147] Ali, Asif, Yi Wai Chiang, and Rafael M. Santos. "X-ray diffraction techniques for mineral characterization: A review for engineers of the fundamentals, applications, and research directions." *Minerals* 12, no. 2 (2022): 205.

[148] Kafle, Bhim Prasad. "Introduction to nanomaterials and application of UV–Visible spectroscopy for their characterization." *Chemical analysis and material characterization by spectrophotometry* 6 (2020): 147-198.

[149] Perkampus, Heinz-Helmut. *UV-VIS Spectroscopy and its Applications.* Springer Science & Business Media, 2013.

[150] Prabhu, C. Anantha, D. Silambarasan, R. Sarika, and V. Selvam. "Synthesis and characterization of TiO_2." *Materials Today: Proceedings* 64 (2022): 1793-1797.

[151] Dhoke, Shailesh K. "Synthesis of nano-ZnO by chemical method and its characterization." *Results in Chemistry* 5 (2023): 100771.

[152] Rajkumar, C. "Effect of annealing temperature on response time of ZnO photoconductor fabricated using thermal evaporation technique." *Physica Scripta* 97, no. 11 (2022): 115806.

[153] Albadarin, Nusayba A., Mohd Sobri Takriff, Mohd Nur Ikhmal Salehmin, Wong Wai Yin, Sin Tee Tan, Abdul Amir H. Kadhum, Lorna Jeffery Minggu, Aymen Alamarneh, and Eman Shqirat. "Hydrothermal synthesis

of Ag–ZnO nanostructures as an advanced material for photoelectrochemical applications." *International Journal of Electrochemical Science* 16, no. 8 (2021): 210848.

[154] Rodchanarowan, Aphichart, Pongpak Chiyasak, Phuri Kalnaowakul, Pattraporn Krajaisri, Rachakorn Puranasiri, Sakdipat Jaturapronperm, and Bhuwadol Thanathattakum. "Effect of Ni addition on magnetism and corrosion resistivity of Ti/Co/Ni nanocomposites by sol–gel methods." *Journal of Magnetism and Magnetic Materials* 555 (2022): 169338.

[155] Paramasivam, V., Radha Krishnan Beemaraj, Mathalai Sundaram, and Arun Prasath. "Investigate the characterization and synthesis process of Titanium dioxide nanoparticles." *Materials Today: Proceedings* 52 (2022): 1140-1142.

[156] Chávez-Mejía, A. C., P. I. Zaragoza-Sánchez, R. Magaña-López, C. E. Barrera-Díaz, and B. E. Jiménez-Cisneros. "Effect of the electrolyte chemical nature on the formation and characteristics of TiO2 nanotubes synthesized by anodic oxidation using a Ti cathode." *Journal of Materials Science: Materials in Electronics* 31, no. 18 (2020): 15907-15918.

[157] Abdulsada, Ali Hamid, Khudheir A. Mishjil, and Ahmad N. Abd. "Effect of thermal annealing on properties of polycrystalline Titanium dioxide (TiO_2) thin film prepared by simple chemical method." *In Journal of Physics: Conference Series*, vol. 1032, no. 1, p. 012037. IOP Publishing, 2018.

[158] Chaves, J. M., A. L. A. Escada, A. D. Rodrigues, and APR Alves Claro. "Characterization of the structure, thermal stability and wettability of the TiO_2 nanotubes growth on the Ti–7.5 Mo alloy surface." *Applied Surface Science* 370 (2016): 76-82.

[159] Tummapudi, Nagamalleswari, Sreenivasulu Modem, Nitchal Kiran Jaladi, Gsvrk Choudary, and Srinivasa Rao Kurapati. "Structural, morphological,

optical and mechanical studies of annealed ZnO nano particles." *Physica B: Condensed Matter* 597 (2020): 412401.

[160] Lu, Kathy. "Hybrid materials–a review on co-dispersion, processing, patterning, and properties." *International Materials Reviews* 65, no. 8 (2020): 463-501.

[161] Skowroński, Łukasz. "Optical and Microstructural Characterization of Thin Layers." *Crystals* 10, no. 9 (2020): 749.

[162] Mamat, M. H., M. Z. Sahdan, Z. Khusaimi, A. Zain Ahmed, S. Abdullah, and M. Rusop. "Influence of doping concentrations on the aluminum doped zinc oxide thin films properties for ultraviolet photoconductive sensor applications." *Optical materials* 32, no. 6 (2010): 696-699.

[163] Ye, H. G., Z. C. Su, F. Tang, G. D. Chen, Jian Wang, Ke Xu, and S. J. Xu. "Role of free electrons in phosphorescence in n-type wide bandgap semiconductors." *Physical Chemistry Chemical Physics* 19, no. 45 (2017): 30332-30338.

[164] Kadem, Burak Y., Mohammed J. Mohammed Ali, and Ameer F. Abdulameer. "The effects of Al-doped ZnO layer on the performance of organic solar cell." *In 2019 12th International Conference on Developments in eSystems Engineering (DeSE)*, pp. 741-746. IEEE, 2019.

[165] Romele, Paolo, Zsolt M. Kovács-Vajna, and Fabrizio Torricelli. "Electronic and ionic transport in organic materials and devices." In *Organic Flexible Electronics*, pp. 71-105. Woodhead Publishing, 2021.

[166] Gupta, K. M., Nishu Gupta, K. M. Gupta, and Nishu Gupta. "Excess Carriers in Semiconductors." *Advanced Semiconducting Materials and Devices* (2016): 145-189.

[167] Nunes de Carvalho, C., A. L. Luís, G. Lavareda, and A. Amaral. "Influence of different unheated substrates on the properties of ITO thin films deposited by rf-PERTE." *Key Engineering Materials* 230 (2002): 567-570.

[168] Venkatachalam, S., H. Nanjo, K. Kawasaki, H. Hayashi, T. Ebina, and D. Mangalaraj. "Optoelectronic properties of ZnSe, ITO, TiO_2 and ZnO thin films." In *Optoelectronics-Materials and Techniques*. Intech Open, (2011): 165-184.

[169] Kováč, Jaroslav, Martin Florovič, Andrej Vincze, Edmund Dobročka, Ivan Novotný, Miroslav Mikolášek, and Jaroslava Škriniarová. "Fabrication and characterization of Si/SiO/TiO/ZnO heterostructures from sputtered and oxidized Ti-film." *Journal of Electrical Engineering* 68, no. 7 (2017): 58-61.

[170] Wasapinyokul, Kamol, W. I. Milne, and D. P. Chu. "Photoresponse and saturation behavior of organic thin film transistors." *Journal of Applied Physics* 105, no. 2 (2009).

[171] Shim, Jae Hyuk, Quanli Hu, Mi Ra Park, Yawar Abbas, Chi Jung Kang, Jaewan Kim, and Tae-Sik Yoon. "Resistive switching characteristics of TiO_2 thin films with different electrodes." *Journal of the Korean Physical Society* 67 (2015): 936-940.

[172] Hajjaji, Anouar, Mosbah Amlouk, Mounir Gaidi, Brahim Bessais, and My Ali El Khakani. *Chromium doped TiO_2 sputtered thin films: synthesis, physical investigations and applications.* Springer, 2014.

[173] Jia, Baohua. "2D optical materials and the implications for photonics." *APL Photonics* 4, no. 8 (2019).

[174] Udachan, Shiva L., Narasimha H. Ayachit, and Lingappa A. Udachan. "Impact of substrates on the electrical properties of thin chromium films." *Ingeniería y Universidad* 23, no. 2 (2019).

[175] Yildiz, A., M. Irimia, M. Toma, I. Spulber, G. Zodieriu, M. Dobromir, D. Timpu, and F. Iacomi. "Effect of the substrate nature on electron transport in Ga doped ZnO thin films grown by RF sputtering." *Materials Today: Proceedings* 5, no. 8 (2018): 15888-15894.

[176] Cadatal-Raduban, Marilou, Tomoki Kato, Yusuke Horiuchi, Jiří Olejníček, Michal Kohout, Kohei Yamanoi, and Shingo Ono. "Effect of substrate and thickness on the photoconductivity of nanoparticle titanium dioxide thin film vacuum ultraviolet photoconductive detector." *Nanomaterials* 12, no. 1 (2021): 10.

[177] Zhuiykov, Serge, Toshikazu Kawaguchi, Zhenyin Hai, Mohammad Karbalaei Akbari, and Philippe M. Heynderickx. "Interfacial engineering of two-dimensional nano-structured materials by atomic layer deposition." *Applied Surface Science* 392 (2017): 231-243.

[178] Akazawa, Housei. "Substrate-dependent luminescent properties of thin-film phosphors: Comparative study of Eu3+-doped ZnO films deposited on SiO_2, Si, and sapphire substrates." *Thin Solid Films* 689 (2019): 137513.

[179] Nawaz, Muhammad, Muhammad Imran, and Mohsan Raza. "Variable thermal conductivity influence on micropolar nanofluid flow triggered by a stretchable disk with Arrhenius activation energy." *Heat Transfer* (2023).

[180] Alencar, Maria VS, Glauco VP Bezerra, Laís D. Silva, José F. Schneider, M. Jesus Pascual, and Aluísio A. Cabral. "Structure, glass stability and crystallization activation energy of SrO-CaO-B_2O_3-SiO_2 glasses doped with TiO_2." *Journal of Non-Crystalline Solids* 554 (2021): 120605.

[181] Serrapede, Mara, Umberto Savino, Micaela Castellino, Julia Amici, Silvia Bodoardo, Elena Tresso, and Angelica Chiodoni. "Li+ insertion in nanostructured TiO_2 for energy storage." *Materials* 13, no. 1 (2019): 21.

[182] Abate, Antonio. "Specialty Grand Challenges in Optoelectronics." *Frontiers in Electronics* 1 (2020): 579890.

[183] Brinkert, Katharina, Florian Le Formal, Xiaoe Li, James Durrant, A. William Rutherford, and Andrea Fantuzzi. "Photocurrents from photosystem II in a metal oxide hybrid system: Electron transfer pathways." *Biochimica et Biophysica Acta (BBA)-Bioenergetics* 1857, no. 9 (2016): 1497-1505.

[184] Georgakopoulos, T., N. Todorova, S. Karapati, K. Pomoni, and C. Trapalis. "Photoconductivity studies on surface modified TiO2 nanoparticles." *Materials Science in Semiconductor Processing* 99 (2019): 175-181.

[185] Li, Ye-Fei, Ulrich Aschauer, Jia Chen, and Annabella Selloni. "Adsorption and reactions of O_2 on anatase TiO_2." *Accounts of chemical research* 47, no. 11 (2014): 3361-3368.

[186] Nowotny, Janusz, Wenxian Li, and Tadeusz Bak. "Effect of oxygen activity on semiconducting properties of TiO_2 (rutile)." *Ionics* 21 (2015): 1399-1406.

[187] Wojcik, Peter M., Lyndon D. Bastatas, Negar Rajabi, Pavel V. Bakharev, and David N. McIlroy. "The effects of sub-bandgap transitions and the defect density of states on the photocurrent response of a single ZnO-coated silica nanospring." *Nanotechnology* 32, no. 3 (2020): 035202.

[188] Ma, Huizhong, Baofei Hao, Wentao Song, Jinpeng Guo, Mingyuan Li, and Lan Zhang. "A High-efficiency TiO_2/ZnO nano-film with surface oxygen vacancies for dye degradation." *Materials* 14, no. 12 (2021): 3299.

[189] Yuan, Sujun, Jiuke Mu, Ruiyi Mao, Yaogang Li, Qinghong Zhang, and Hongzhi Wang. "All-nanoparticle self-assembly ZnO/TiO_2 heterojunction thin films with remarkably enhanced photoelectrochemical activity." *ACS Applied Materials & Interfaces* 6, no. 8 (2014): 5719-5725.

[190] Shen, Kai, Kunjie Wu, and Deliang Wang. "Band alignment of ultra-thin hetero-structure ZnO/TiO_2 junction." *Materials Research Bulletin* 51 (2014): 141-144.

[191] Babaie-Aghdam, Samaneh, Naeimeh Sadat Peighambardoust, and Farzad Nasirpouri. "Morphological evolution of sol-electrophoretic deposited ZnO nanostructures on anodic TiO_2 nanotubes for back-side illuminated dye-sensitised solar cells." *Materials Research Bulletin* 160 (2023): 112134.

[192] Gowthaman, K., P. Gowthaman, M. Venkatachalam, M. Saroja, M. Kutraleeswaran, and S. Dhinesh. "Design and synthesis of TiO2/ZnO nanocomposite with enhanced oxygen vacancy: Better photocatalytic removal of MB dye under visible light-driven condition." *Inorganic Chemistry Communications* 146 (2022): 110197.

[193] Chiou, Shang-Hau, Hsin-Chia Ho, Han-Ting Liao, Feng-Yu Tsai, Chun-Wen Tsao, Yung-Jung Hsu, and Chun-Hway Hsueh. "Plasmonic gold nanoplates-decorated ZnO branched nanorods@TiO_2 nanorods heterostructure photoanode for efficient photoelectrochemical water splitting." *Journal of Photochemistry and Photobiology A: Chemistry* 443 (2023): 114816.

[194] Georgakopoulos, T., N. Todorova, K. Pomoni, and C. Trapalis. "On the transient photoconductivity behavior of sol–gel TiO_2/ZnO composite thin films." *Journal of Non-Crystalline Solids* 410 (2015): 135-141.

[195] Friedrich, D., L. Valldecabres, and M. Kunst. "Charge carrier kinetics in ZnO films and nanorods." *Chemical Physics Letters* 515, no. 1-3 (2011): 109-115.

[196] Pomoni, K., A. Vomvas, and Chr Trapalis. "Transient photoconductivity of nanocrystalline TiO_2 sol–gel thin films." *Thin Solid Films* 479, no. 1-2 (2005): 160-165.

[197] Sturman, Boris Itskhakovich. "Ballistic and shift currents in the bulk photovoltaic effect theory." *Physics-Uspekhi* 63, no. 4 (2020): 407.

[198] Liu, Wenfei. *Advances in Hybrid Nanolithography: Wafer-Scale Fabrication of 1D to 3D Micro-and Nanostructures.* University of California, Los Angeles, 2022.

[199] Jia, Lemin, Wei Zheng, and Feng Huang. "Observation of negative differential resistance in SiO_2/Si heterostructures." *Cell Reports Physical Science* 2, no. 11 (2021).

[200] Hedayati, Mohammad H., Jianjing Wang, Harry CP Dymond, Dawei Liu, and Bernard H. Stark. "Overtemperature protection circuit for GaN devices using a di/dt sensor." *IEEE Transactions on Power Electronics* 36, no. 7 (2020): 7417-7428.

[201] Mele, Paolo, Satoru Kaneko, and Tamio Endo. *Functional Oxide Thin Films and Nanostructures: Growth, Properties, and Applications*. MDPI, Basel, 2022.

[202] González, Sergio, Giovanni Vescio, Juan Luis Frieiro, Alina Hauser, Flavio Linardi, Julian López-Vidrier, Marek Oszajca, Sergi Hernández, Albert Cirera, and Blas Garrido. "Inkjet-Printed p-NiO/n-ZnO Heterojunction Diodes for Photodetection Applications." *Advanced Materials Interfaces* (2023): 2300035.

[203] Dwivedi, Shyam Murli Manohar Dhar, Avijit Dalal, Anupam Ghosh, Punam Murkute, Hemant Ghadi, Chiranjib Ghosh, Subhananda Chakrabarti, Satyaban Bhunia, and Aniruddha Mondal. "InN nanowires based near-infrared broadband optical detector." *IEEE Photonics Technology Letters* 31, no. 18 (2019): 1526-1529.

[204] Zheng, Zhi, Xiaotao Zu, Yong Zhang, and Weilie Zhou. "Rational design of type-II nano-heterojunctions for nanoscale optoelectronics." *Materials Today Physics* 15 (2020): 100262.

[205] Sharma, Vikas, Tapan Kumar Das, P. Ilaiyaraja, and C. Sudakar. "Oxygen non-stoichiometry in TiO_2 and ZnO nano rods: Effect on the photovoltaic properties of dye and Sb_2S_3 sensitized solar cells." *Solar Energy* 191 (2019): 400-409.

الخلاصة

تم تحضير أجهزة الأغشية الرقيقة من ثاني أكسيد التيتانيوم (TiO_2) وأكسيد الزنك (ZnO) وتوصيفها لتطبيقات المقاومة الضوئية. تم تصنيعه باستخدام طرق التجيل بالمحلول والرش على ركائز مختلفة لدراسة تأثير الركيزة على الأجهزة المحضرة.

كما تم إجراء الفحوصات التكميلية بما في ذلك؛ حيود الأشعة السينية، وقياسات فجوة الطاقة، وتركيزحاملات الشحنات، تحركية حاملات الشحنة، والخصائص المورفولوجية، والمشتقة الأولى للتيار فيما يتعلق بقيم الوقت (dI/dt) لحالات التشغيل والإيقاف.

تظهر نتائج فحص XRD أنماطًا بلورية مميزة ووجود أطوار TiO_2 (anatase) وZnO (wurtzite) في الأغشية الرقيقة. تظهر قياسات فجوة نطاق الطاقة تقلبات في قيم فجوة النطاق، مما يكشف عن معلومات حول الخصائص الإلكترونية البصرية للمواد. يتراوح مدى فجوة الطاقة لجميع العينات بين (3.23-3.75 eV) .

تكشف صور المجهر الإلكتروني الماسح (SEM) عن إدارة الشكل وحجم الجسيمات للأغشية الرقيقة من TiO_2 وZnO. تم تصميم المواد النانوية لأشكال وأحجام معينة من خلال السيطرة الدقيقة بإجراءات الإنتاج ودرجات حرارة التلدين، بدءًا من التراكيب الشبيهة بالكروية في ZnO إلى الأشكال الشبيهة بالشريط النانوي في TiO_2. يعرض الهيكل الهجين تداخلًا غير عادي بين المادتين، مما يعني إنشاء ترابط متغاير مع واجهة محددة جيدًا.

عند ترسيبه على ركائز أكسيد القصدير الإنديوم (ITO)، يظهر TiO_2 انخفاضًا في المقاومة وسلوك تبديل معتدل. على العكس من ذلك، تعرض ركائز Si/SiO_2 مقاومة أعلى وسلوك تبديل أكثر وضوحًا. علاوة على ذلك، يُظهر TiO_2 مقاومة عالية جدًا، بينما يُظهر ZnO مقاومة أقل مع سلوك تحويل قوي على ركائز الأقطاب الكهربائية المتداخلة (IDEs).

يُظهر الهجين ($ZnO:TiO_2$) سلوك تبديل معتدل نسبيًا على ركائز ITO، كما يتضح من نسبة المقاومة المنخفضة عندما يكون الضوء مطفأً عندما يكون الضوء مضاءً بنسبة (R_{OFF}/R_{ON}) تبلغ 1.06. على ركائز Si/SiO_2، يُظهر الغشاء الرقيق الهجين نسبة R_{OFF}/R_{ON} أعلى بكثير تبلغ 5.28، مما يشير إلى مقاومة أقوى وسلوك تبديل أكثر وضوحًا. وبالمثل، فإن نسبة R_{OFF}/R_{ON} للأغشية الرقيقة الهجينة على ركائز IDEs هي 2.46، مما يشير إلى استجابة معتدلة ولكنها مميزة للضوء.

وبالمثل، يعرض الفيلم الرقيق ثنائي الطبقة سلوك تبديل معتدل على ركائز ITO، مع نسبة R_{OFF}/R_{ON} تبلغ 1.36. على ركائز Si/SiO_2، يُظهر الغشاء الرقيق ثنائي الطبقة مقاومة كبيرة وسلوك تحويل قوي،

كما يتضح من نسبة R_{OFF}/R_{ON} البالغة 4.72. عند تطبيقها على ركائز IDEs، تبلغ نسبة R_{OFF}/R_{ON} للفيلم الرقيق ثنائي الطبقة 3.9، مما يدل على تفاعل معتدل ولكنه مهم للضوء.

تتضمن الدراسة أيضًا فحصًا شاملاً لخصائص المقاومة للضوء. يتمتع TiO_2 بأعلى قيم المقاومة الضوئية، والتي تتراوح من 1.57×10^{9} (Ω.m) على ITO إلى 123×10^{7} (Ω.m) على Si/SiO_2، بينما لا توجد استجابة على ركيزة IDEs. يمتلك ZnO قيم مقاومة ضوئية أقل تتراوح من 0.436×10^{9} (Ω.m) إلى 9.89×10^{7} (Ω.m) و 0.254×10^{3} (Ω.m). تتراوح المقاومة الضوئية للفيلم الرقيق الهجين من 0.801×10^{9} (Ω.m) إلى 7.1×10^{7} (Ω.m) و7.03×10^{3} (Ω.m) ، في حين تتراوح المقاومة الضوئية للفيلم الرقيق ثنائي الطبقة من $0.064\ 10^{9}$ (Ω.m) إلى 7.02×10^{7} (Ω.m) و 2.09×10^{3} (Ω.m) .
تشير القيمة الموجبة إلى الحركة أثناء التعرض للضوء، بينما تشير القيمة السالبة إلى التسارع من نطاق التوصيل إلى نطاق التكافؤ. تؤكد هذه العلاقة على الدور الحاسم لـ dI/dt في فهم حركية نقل الشحنة والمقاومة في المواد المقاومة للضوء، حيث تشير أدنى قيمة إلى أعلى مقاومة للضوء والعكس صحيح.

كانت قيم dI/dt مؤشرا على الأداء الأمثل لأنواع الأغشية الرقيقة الهجينة وثنائية الطبقة على ركائز مختلفة. على وجه الخصوص، عند ترسيبه على ركيزة ITO، يُظهر الفيلم الرقيق الهجين خصائص مواتية للغاية، مع قيم dI/dt تبلغ $0.065\ \mu A\ s^{-1}$ (ON) و$-0.23\ \mu A.s^{-1}$ (OFF). على الركيزة Si/SiO_2، أظهرت كل من الأغشية الرقيقة الهجينة وثنائية الطبقة قيمًا مثالية قابلة للمقارنة. يعرض الفيلم الرقيق الهجين قيم dI/dt تبلغ $508\ \mu A.s^{-1}$ (ON) و $-521\ \mu A.s^{-1}$ (OFF)، بينما يعرض الفيلم الرقيق ثنائي الطبقة قيم dI/dt تبلغ $190\ \mu A\ s^{-1}$ (ON) و$-422\ \mu A.s^{-1}$ (OFF). والجدير بالذكر أن أداء الطبقة الرقيقة ثنائية الطبقة كان أفضل على الركيزة IDEs، مع قيم dI/dt تبلغ $9.95\ A.s^{-1}$ (ON) و$-44\ A.s^{-1}$ (OFF). أظهرت النتائج ديناميكيات المعدل الحالي المتغيرة للأغشية الرقيقة المختلفة على ركائز متنوعة، مما يوفر رؤى قيمة حول سلوكياتها المقاومة للضوء وخصائصها الكهربائية.

جمهورية العراق
وزارة التعليم العالي والبحث العلمي
جامعة بابل
كلية العلوم ـ قسم الفيزياء

تحضير ودراسة خواص المقاومية الضوئية لوصلة اوكسيد الخارصين / ثنائي اوكسيد التيتانيوم النانوية

اطروحة

مقدمة الى مجلس كلية العلوم / قسم الفيزياء كجزء من متطلبات درجة دكتوراه الفلسفة في الفيزياء

من قبل

احمد عبدالله عودة علي

بكالوريوس/ جامعة النهرين (1994)

ماجستير/ جامعة النهرين (1997)

تحت اشراف

الاستاذ الدكتور
حكمت عدنان جواد

الاستاذ المساعد الدكتور
براق يحيى كاظم

1445 هـ

2023 م